KINETICS OF OXIDATION OF P-PHENYLENE DIAMINE BY 2,6-DICHLORO QUININE-4-CHLORO-IMIDE

Dr. Neeraja Valluru

Dept . of chemistry ,SRR &CVR Government Degree College (A) , Vijayawada.
Email: neeraja2812@gmail.com

Sailaja Valluru

Dept. of ChemsitryP.BSiddartha College of Arts & Science (A) Vijayawada.

Received: Jan. 2020 Accepted: Feb. 2020 Published: Feb. 2020

Abstract: Gibbs reagent 2,6-dichloroquinone -4-chloro-imide (DCQCI) has been utilised for the estimation of phenols and pyridoxine for a quite number of years. Para-phenylene diamine (p-PDA) having two (1,4)-diamino functions attached to a benzene nucleus is well known to undergo a variety of oxidation or oxidative hydrolytic reactions in the presence of electron acceptors.The investigation mainly deals with the oxidation of p-phenylene diamine in aqueous AcOH – $HClO_4$ mixtures by 2,6-dichloroquinone-4-chloro-imide. The reaction is found to be first order in oxidising agent. The reaction is found to be second order in substrate. The reaction rate decreases with increasing the concentration of perchloric acid.

The most probable mechanistic scheme envisaged is that precursor intermediate complex being formed between the oxidant species and a molecule of unprotonated substrate species which in a rate determining step condenses with another molecule of the substrate to give intermediate product which in fast step gives final product.

Introduction and Scope: Gibbs reagent 2,6-dichloroquinone -4-chloro-imide (DCQCI) has been utilised for the estimation of phenols and pyridoxine for a quite number of years. The main reaction has been a coupling process leading to colour changes and thus colorimetry was extensively used for the assay of these compounds.Para-phenylene diamine (p-PDA) having two (1,4)-diamino functions attached to a benzene nucleus is well known to undergo a variety of oxidation or oxidative hydrolytic reactions in the presence of electron acceptors. The actual products of the reaction depend upon the reaction conditions employed: concentration, the nature of the oxidant, the acidity of the medium, the solvent system besides the relative ratios of the oxidant and substrate concentrations. The reactions of para-phenylene diamine are very complicated due to the availability of two donar nitrogen sites, and due to the subsequent reactions of the intermediate products not to mention of the additional complication of electrophilic attack at the nitrogen sites and at the nucleus.

P-Phenylene Diamine: The investigation mainly deals with the oxidation of p-phenylene diamine in aqueous AcOH – $HClO_4$ mixtures by 2,6-dichloroquinone-4-chloro-imide.

a) Dependence on Oxidant: The reaction is found to be first order in oxidising agent. Plot of log(a-x) vs time is linear up to three half lives of the reaction indicating first order dependence on oxidising agent .The kinetic data is given in Table 1.

Table 1

[p–PDA] = 12.5 x 10^{-3} M $[H^+]$ = 0.1 M
AcOH – H_2O = 10% - 90%(v/v) Temp = 35°C

Variant	[Variant] x 10^4 M	k_1 x 10^2 min^{-1}
DCQCI	2.5	10.7
	5.0	9.2
	10.0	10.1

b) Dependence on Substrate: The reaction is found to be second order in substrate. Plot of log k_1 vs log [S] is linear with slope two indicating second order dependence. The observation that the plot of $\frac{[S]}{k_1}$ vs $\frac{1}{[S]}$ is linear and passes through origin also confirms the second order dependence on substrate. Such second order dependence has been observed in the oxidation of p-phenylene diamine with I_3^-. The kinetic data is given Table -2.

Table 2:

[DCQCl] = 5.0×10^{-4} M $[H^+]$ = 0.1 M
AcOH – H_2O = 10% - 90%(v/v) Temp = 35°C

Variant	[Variant] x 10^3 M	$k_1 \times 10^2$ min^{-1}
p-phenylene diamine	3.1	0.25
	6.2	1.56
	12.5	9.23
	25.0	47.74

c) Dependence on Acid Concentration: The reaction rate decreases with increasing the concentration of perchloric acid. The reaction is found to be inverse mixed order. Plot of log k_1 vs log$[H^+]$ is linear with a slope of 1.5 . Plot of k_1 $[H^+]$ vs $\frac{1}{[H^+]}$ gives an intercept and slope . The intercept corresponds to first order component and slope corresponds to second order component. This explains the observed mixed order kinetics. The combination of first order kinetics and second order kinetics giving inverse dependence on $[H^+]$ gives resultant inverse 1.5 order on H^+. The kinetic data is given in Table: 3.

Table 3:

[DCQCl] = 5.0×10^{-4} M [p-PDA] = 12.5×10^{-3}M
AcOH – H_2O = 10% - 90% (v/v) Temp = 35°C

Variant	[Variant] x 10^2 M	$k_1 \times 10^2$ min^{-1}
$HClO_4$	5.0	33.2
	10.0	9.2
	20.0	6.0
	40.0	1.6

Effect of Varying Solvent Composition: The reactions have been carried out at varying solvent compositions to find the effect of change in dielectric constant. The reaction rate decreases with increase in concentration of acetic acid. This reaction essentially involves $H_2O\overset{+}{C}l$ and the dipolar molecule of the amine. This requires an increase in rate with decrease in dielectric constant. But the observation is reverse. Thus specific solvent effects probably are causing this observation. Probably the following factors like solvation, acidic or basic nature of the solvent, effect of solvent on molecular dispersion, non random distribution of the component of mixed solvent are responsible. Plot of log k_1 vs $\frac{1}{D}$ is linear (Fig.6). The kinetic data is given in Table-4.

Table 4:

[DCQCl] = 5.0×10^{-4} M $[H^+]$ = 0.1 M
[p-PDA] = $12.5\ 10^{-3}$ M Temp = 35°C

Variant	% of Variant	$k_1 \times 10^2$ min^{-1}
AcOH	5	10.5
	10	9.2
	20	6.1
	40	4.5

Effect of Temperature: The reactions are carried out at three different temperatures i.e., 35°C, 45°C and 55°C to compute various activation parameters. Plot of log k_1 vs $\frac{1}{T}$ is linear (Fig.7). The kinetic data is given in Table-5.

Table 5:

$[DCQCI] = 5.0 \times 10^{-4}$ M $[H^+] = 0.1$ M

$[p\text{-}PDA] = 12.5 \times 10^{-3}$ M AcOH - H_2O = 10% - 90% (v/v)

Variant	Change in Variant °C	$k_1 \times 10^2$ min^{-1}
Temperature	35	9.2
	45	13.8
	55	29.0

The derived Arrhenius parameters are given in Table 6.

Table 6:

Arrhenius Parameters at 308°K:

Compound	$\Delta E^{\neq}$ KJ/mole	$\Delta H^{\neq}$ KJ/mole	$-\Delta S^{\neq}$ JK^{-1} / mole	$\log_{10} P_Z$	$\Delta G^{\neq}$ KJ/mole.
p-phenylene diamine	44.18	41.4	130.44	6.45	81.65

The kinetic features and net activation parameters do not provide any clue whether or not this reaction involves termolecular interactions.

In as much the oxidant DCQCI is well known to function as a two electron oxidant. It is reasonable to assume that this reaction does not go through step wise one electron transfer which would mean that this reaction should go through radical path way. It appears that this mechanistic speculation involving radicals would impose large energy barrier, since a large number of nuclei-rearrangement should be required for radical formation and hence it is most unlikely that this reaction would proceed through radical path way.

The possibility that the rapid electron transfer from one of the substrate species to the oxidant species followed by rate determining condensation of the redox intermediate thus produced with the second substrate species is also unlikely as this mechanistic supposition would involve too many ionic species in an equilibrium step, and there should be much larger retardation with increase in H^+ than what has been observed experimentally.

Mechanism and Rate Law: The most probable mechanistic scheme envisaged is that precursor intermediate complex being formed between the oxidant species and a molecule of unprotonated substrate species which in a rate determining step condenses with another molecule of the substrate to give intermediate product which in fast step gives final product.

The sequence of reactions may be represented as follows.

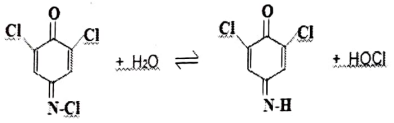

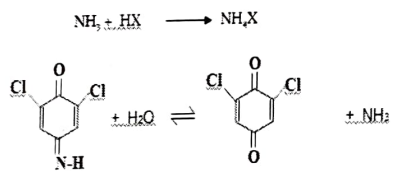

The most active species H_2OCl^+ produced in first hydrolytic step. The mechanistic path way involving the main oxidant species and substrate are given below.

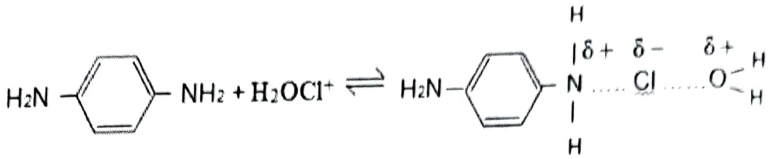

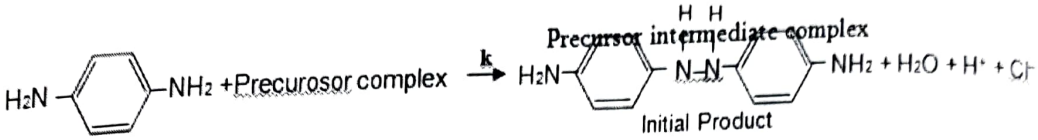

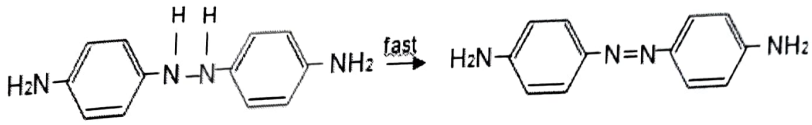

The relevant rate law is derived as follows. The sequence of reactions of hydrolysis of DCQCI are given below.

2-6-dichloroquionone-4-chloro-imide + $H_2O \underset{}{\overset{Kh_1}{\rightleftharpoons}}$ 2,6-dichloroquionone-imide + HOCl

$$H^+ + HOCl \overset{K_p}{\rightleftharpoons} H_2O\overset{+}{Cl}$$

$$S + H^+ \overset{K_1}{\rightleftharpoons} SH^+$$

$$SH^+ + H^+ \overset{K_2}{\rightleftharpoons} SH^{+2}$$

$$S + H_2O\overset{+}{Cl} \overset{KC_1}{\rightleftharpoons} \text{Complex}_1$$

$$\text{Complex}_1 + S \xrightarrow[\text{slow}]{k} \text{Products}$$

$$\therefore \text{Rate} = k\,[C_1]\,[S]$$

$$= k.KC_1.[S]\,[S]\,[H_2O\overset{+}{Cl}]$$

$$= k.KC_1.K_p\,[S]^2\,[H^+]\,[HOCl]$$

$$S_T = S + SH^+ + SH^{+2}$$

$$= S + K_1\,[S]\,[H^+] + K_1.K_2[S]\,[H^+]^2$$

$$= S\,[1 + K_1H^+] + K_1K_2\,[S]\,[H^+]^2$$

by neglecting Square terms

$$S_T = S\,[1 + K_1H^+]$$

$$\therefore \text{Rate} = \frac{kKC_1K_p[S_T]^2[HOCl][H^+]}{[1+K_1H^+]^2}$$

$$= \frac{kKC_1K_p[S_T]^2[HOCl][H^+]}{[1+2K_1H^+ + K_1H^{+^2}]}$$

$$= \frac{kKC_1K_p[S_T]^2[HOCl]_T[H^+]}{[1+2K_1H^+ + K_1H^{+^2}][1+K_pH^+]}$$

Replacing $[HOCl]_T$ by DCQCI

$$\therefore \text{Rate} = \frac{Kh_1kKC_1K_p[S_T]^2[DCQCl][H^+]}{\{1+2K_1H^+ + K_1H^{+2}\}\{1+K_pH^+\}}$$

If $1 < K_pH^+$ neglecting the second term in the denominator we get

$$\therefore \text{Rate} = \frac{kKC_1[S_T]^2[DCQCl]}{\{1+2K_1H^+ + K_1H^{+2}\}}$$

The rate law explains the observed first order in oxidant, second order in substrate, and a mixed order in H^+ involving both first order component of H^+ and second order component in H^+ resulting in inverse 1.5 order in H^+.

Stoichiometric Studies: The product studies under the given set of conditions were performed and worked up as follows. The ratio of substrate-oxidant was maintained as 1:10. The reactants were mixed and the mixture was allowed to react over night. It has been found that two oxidant species HOCl and 2,6-dichloro benzoquinone interact causing oxidation to the products in a ratio 2:1 indicating that both the species interact finally giving.

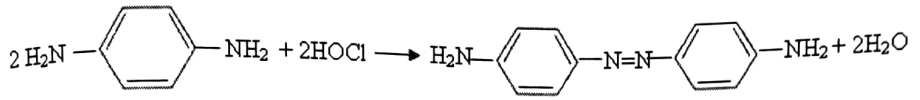

Similarly

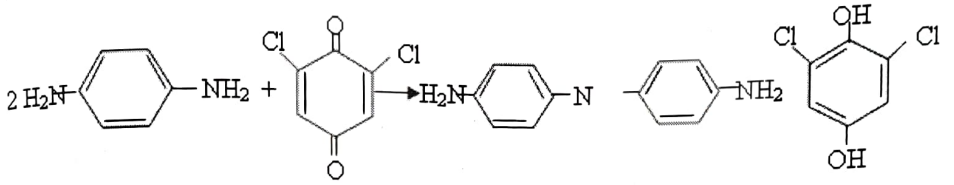

The experimental procedure is as follows.

The contents were treated with solid sodium bicarbonate until there was no evolution of carbon dioxide gas. The resultant mixture was extracted with diethyl ether, the solvent was evaporated from the ether layer and a minimum quantity of dilute HCl was added $(pH \sim 3)$.

The green colour solution was evaporated over a water bath to get a dirty green solid. This crude product was crystallized from absolute ethanol and filtered. The HCl from this salt was neutralized by treatment with a saturated solution of $NaHCO_3$, the green solid was filtered, washed well with water, recrystallised from absolute ethanol, vaccum-dried and desiccated.

References:

1. J.C. Panigrahy Ph.D.Thesis, Berhampur Univerity and references cited therein (1990)
2. L.N.Palo Ph.D.Thesis, Berhampur University and references cited therein (1990)
3. M.S.Ramachandran, T.S.Vivekanandam, N.R.Subbaratnam and N.Raja ram, Indian J.Chem., **22**, (1983) 895.
4. G.Grampp and W.Jaenicke, J.Chem.Soc., Faraday Trans-II **81**, (1985)1035.
5. A.Hunig and R.Richter, Chem Ber., **91**, (1958) 442; E.A.Burns, Anal.Chem., **32**, (1960) 1800; G.W.Ewing In '*Instrumental Methods of Chemical Analysis*'. 3rd ed., Mc.Graw Hill Kogakusha Ltd., Tokyo (1969) P.102.

***

Optik - International Journal for Light and Electron Optics 205 (2020) 164236

Contents lists available at ScienceDirect

Optik

journal homepage: www.elsevier.com/locate/ijleo

Original research article

Optical, electrical and photoluminescence studies on Al_2O_3 doped PVA capped ZnO nanoparticles for optoelectronic device application

Ravindranadh Koutavarapu[a], R.K.N.R. Manepalli[b], B.T.P. Madhav[c], T. Satyanarayana[d], G. Nagarjuna[e], Jaesool Shim[a,*], M.C. Rao[f,*]

[a] School of Mechanical Engineering, Yeungnam University, Gyeongsan, 712-749, Republic of Korea
[b] Department of Physics, The Hindu College, Machilipatnam, 521001, India
[c] LCRC-R&D, Department of ECE, Koneru Lakshmaiah Education Foundation, Guntur, 522502, India
[d] Department of EIE, Lakireddy Bali Reddy College of Engineering, Mylavaram, 521230, India
[e] Department of Physics, S.R.R. & C.V.R. Govt. Degree College, Vijayawada, 520004, India
[f] Department of Physics, Andhra Loyola College, Vijayawada, 520008, India

ARTICLE INFO

Keywords:
ZnO
Co-precipitation
XRD
SEM
Optical
DC conductivity
I-V
PL

ABSTRACT

ZnO is a significant I I-V I n-type direct bandgap semiconductor material which has shown great attention because of its applications in light-transmitting diodes and photograph detectors. In the present investigation, Al_2O_3 doped ZnO nanoparticles were prepared by co-precipitation technique utilizing PVA as a host polymer. X-ray diffraction studies revealed the cubic structure of nanoparticles. The determined normal crystallite size of Al_2O_3 doped PVA capped ZnO nanoparticles was around 12 nm. SEM image showed that the nanoparticles were distributed uniformly with small sized grains consisting of nano dots like tips due to the agglomeration of particles. FTIR demonstrated the trademark vibrational modes of constituent components in the host matrix. The optical studies of all samples displayed close band edge retention at 351 nm (3.26 eV). From the DC studies the conductivity was found to be 3.24×10^{-3} S/cm. EPR studies revealed the crystalline structure and coordination/neighbourhood site evenness of Al_2O_3 doped ZnO in the host lattice. Photoluminescence studies of Al_2O_3 doped PVA capped ZnO nanoparticles demonstrated two groups at 416 and 619 nm. The main band was seen in violet and other band in blue region. These studies revealed that the Al_2O_3 doped PVA capped ZnO nanoparticles materials can be used as LEDs, electroluminescence boards and plasma devices.

1. Introduction

Zinc oxide (ZnO) material possesses a large number of properties when compared to the IV group elements, because of wide energy bandgap of 3.37 eV. It has stable wurtzite structure. When compared to the other materials, ZnO has emerged an attractive material for its different kind of properties and flexible application like reflection coatings, anode materials, solar cells, optoelectronic devices, antibacterial specialist and sensor applications [1,2]. Silicon based transistors are used in many devices. But their energy bandgap is low. In order to fulfil the drawback, ZnO based materials are used as a thin film transistors (TFTs). Owing to its wide energy bandgap and high electrical properties, it is used in optoelectronic and photovoltaic devices. ZnO exhibits high UV

* Corresponding authors.
E-mail addresses: jshim@ynu.ac.kr (J. Shim), raomc72@gmail.com (M.C. Rao).

https://doi.org/10.1016/j.ijleo.2020.164236
Received 2 December 2019; Accepted 16 January 2020

transmitting radiation and gets more stabilized at room temperature, even when compared to the phosphorus and GaN [3]. By using ZnO nanopowders acoustic wave filters which are mostly used in audio and video frequency circuits have been developed [4]. A few creators have announced high photoluminescence efficiencies in ZnO nanostructures [5]. Additionally ZnO is a domain well disposed material, which is uniquely attractive for bio-applications.

Several techniques have been used to prepare the nanomaterials such as spin coating method, CVD technique, thermal decomposition, co-precipitation method etc. Among these co-precipitation method is chosen to prepare the nanoparticles, due to the cost effectiveness as well as the stability in environment conditions such as ambient temperatures, pressure variance etc [6]. Due to these properties, the prepared nanoparticles showed the tremendous change in their size, shapes as well as optical properties. Moreover, the properties can be additionally improved in nano-ZnO structures, nanoparticles, nanowires, which upgrade the exciton oscillator quality and quantum efficiency [7]. In optoelectronic applications, the ZnO particles demonstrated a wide unmistakable photoluminescence in the blue-green locale i.e. 470–550 nm. The obvious outflow is ascribed to deformities, for example, oxygen opening which are accepted to be situated close to the surface region [8]. The properties of ZnO can be customized for spintronic applications however doping diverse progress metal particles such as Co, Al, Mn, V, Fe, etc. into the ZnO lattice. Much exertion has been paid to the natural attractive trade collaborations of ZnO frameworks. So as to address the real instrument of attractive cooperation's in these frameworks, it is similarly critical to have an essential comprehension of various nanoscaled stage development and their outcomes on optical properties [9]. Size consistency and substance dependability in nanosized particles are the primary issues that influence attraction and are stayed to be a test in the field of weakened attractive semiconductors and optoelectronic applications [10].

In this present examination, Al_2O_3 doped PVA capped ZnO nanoparticles were prepared by co-precipitation method. The aim of this work is to prepare the nanosized particles which show a great influence on optoelectronic applications. Until now, based on these aluminium doped ZnO nanoparticles, no proper literature has been found on optoelectronic applications. Due to the insertion of aluminium oxide in the zinc oxide a large number of oxygen vacancies are generated. As a result a wide energy bandgap is obtained. It shows tremendous change on optical properties. The novelty of this present work is to prepare Al_2O_3 doped PVA capped ZnO nanoparticles with cost effective co-precipitation method. The prepared nanomaterials can be used for extensively obtaining the novel materials with different properties, because through this process nanosize grain particles have been deposited with high purity than those reported by other methods. The prepared nanoparticles can give the output which can be utilized in many applications like luminescence, optoelectronic and display devices.

2. Experimental

2.1. Preparation of Al_2O_3 doped PVA capped ZnO nanoparticles

Zinc Oxide (ZnO) and polyvinyl alcohol (PVA) with 98 % purity were obtained from Sigma Aldrich Ltd., India. Cleaned refined water was utilized as a dissolvable. In the present exploratory technique, 50 mL of two fold refined water was taken in a 100 mL of measuring flask. 2.6 g of PVA and 0.050 g of Zinc Oxide were included. The homogenous solution was left for 48 h at room temperature to swell. Later the arrangement was warmed up to 80 °C by steady working as long as 6 h until precipitate was formed. 1.5 mL of sodium hydrogen telluride (NaHTe) and 0.02 mol % nickel oxide were added drop wise to the arrangement. Following couple of minutes a straightforward arrangement was framed. The readied arrangement was thrown on level glass plate dishes and permitted to vanish the dissolvable followed by putting in tourist oven. Al_2O_3 doped PVA capped ZnO nanoparticles were obtained.

2.2. Characterization

XRD pattern was recorded on PANalytical X'Pert Pro X-beam powder diffractometer utilizing CuK_α (1.54060 Å) radiation. Size and morphology of nanoparticles were observed by using Hitachi S-3400 N Scanning electron microscope. FTIR spectrum of the sample was recorded on a Bruker-Alpha FTIR spectrophotometer. The optical transmission spectrum was measured on Hitachi Make UV-VIS spectrometer-3900 in the wavelength range $200-800$ nm. DC conductivity measurement was done by using standard four-probe technique. EPR spectrum of the sample was performed on JEOL JES-FA200 EPR spectrometer. I–V and surface resistance of the prepared nanoparticles were measured using Keithley 2400 Source-Meter. Photoluminescence spectra was recorded on Horiba Jobin-Yvon Fluorolog-3 spectrofluorimeter with Xe continuous (450 W) and pulsed (35 W) lamps as excitation sources. The CIE chromaticity was calculated by using Horiba Jobin-Yvon flouorolog-3 spectrofluorimeter.

3. Results and discussion

3.1. XRD analysis

XRD is utilized to decide the level of crystalline nature of Al_2O_3 doped PVA capped ZnO utilizing Debye-Scherrer's condition. As the particle size increases the intensity of XRD peaks decreases. As a result the FWHM of broadening peaks increases. The low intensity XRD peaks indicate that the films consist of coarsely fine grains (nanocrystalline) and/or are amorphous in nature. The diffraction peaks are observed close to $2\theta = 21.2^\circ, 38.2^\circ, 42.1^\circ$ and 53.6° are attributed to (1 1 0), (2 1 1), (3 2 0), and (4 1 0) planes, which are shown in Fig. 1. The obtained peaks are compared to the JCPDS card no. 80-0075. The films are highly oriented along (1 1 0) and (2 0 1) planes. The significant improvement in crystallinity is due to sintering of nanocrystals into effectively larger crystals after the annealed process [11]. The crystalline size data is acquired from FWHM and the normal crystalline size can be determined

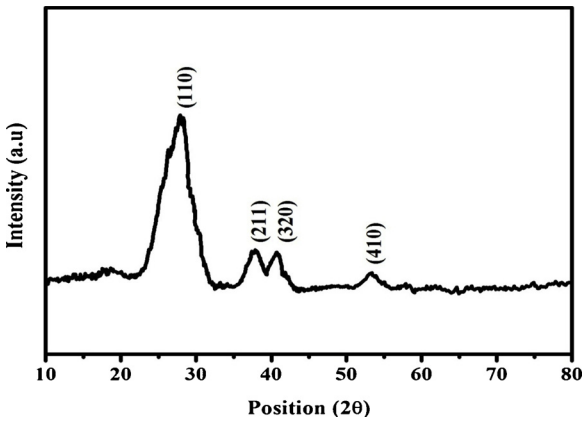

Fig. 1. XRD pattern of Al_2O_3 doped PVA capped ZnO nanoparticles.

by Debye-Scherrer equation.

$$D = (K \lambda / \beta \cos \theta) \quad (1)$$

where

D is the mean crystallite size,
K = 0.9 is Scherrer's constant,
λ is the wavelength of the occurrence pillar,
θ is the diffraction edge,
β is the full width half greatest power of the diffraction top.
From the XRD pattern, the determined estimation of normal crystallite size was 12 nm.

3.2. SEM analysis

Surface morphology and grain size of Al_2O_3 doped PVA capped ZnO nanoparticles were shown in Fig. 2. The prepared nanoparticles were annealed to remove the impurities because the nanoparticles are distributed uniformly with small sized grains consisting of nano dots like tips. This may be due to the agglomeration of particles [12]. At some regions the fusion of agglomerated walls is also observed. The SEM image has been taken at 200 nm resolution. The higher surface harshness is formed due to the capping of PVA polymer and dispersion is plotted at the inset of Fig. 2. The rest of agglomeration of particles are the combination of ZnO doped Al particles which is plotted in the inset of Fig. 2. Figure speaks to the run of the mill SEM micrograph of ZnO-Al nanopowder installed in PVA framework. It has been seen that ZnO-Al nanoparticles like structures lie inside the PVA grid. This micrograph showed that this small concentration of PVA doping in ZnO lattice causes growth of sized grains in some regions which result in porous surface [13]. The bigger ionic radii of aluminium ions distort crystal structure due to ionic radii mismatch which increases grains/particles growth activity of ZnO and formation of bigger particles.

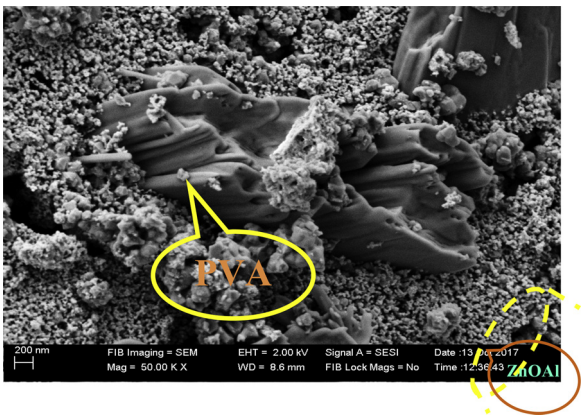

Fig. 2. SEM image of Al_2O_3 doped PVA capped ZnO nanoparticles.

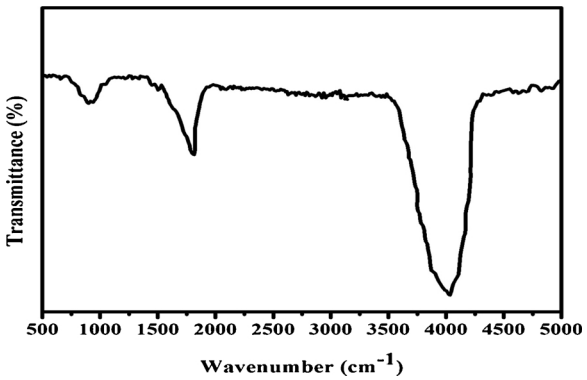

Fig. 3. FTIR spectrum of Al_2O_3 doped PVA capped ZnO nanoparticles.

3.3. FT-IR studies

The characterization peaks of surface useful gatherings of Al_2O_3 doped PVA capped ZnO nanoparticles in the wavenumber range $500-5000\,cm^{-1}$ at room temperature were shown in Fig. 3. The characteristic groups in the FTIR range were formed because of stretching vibrations of Al-O, C═O and C—H, gatherings. The absorption peaks formed at $870\,cm^{-1}$ were expected to C═O extending vibration. The peaks formed at $1700\,cm^{-1}$ were allocated to C—H extending vibration. Moreover, the characteristic peaks of Al-O gatherings were shown at $4800\,cm^{-1}$ viewed as the related aluminium bond among the particles [14]. Hence once again it was confirmed that aluminium oxide decomposes followed by the dissolution of Al^{+} ions within ZnO host lattice by occupying most probably Al^{2+} sites.

3.4. Optical properties

The UV-VIS absorbance spectra in the locale 200–800 nm for Al_2O_3 doped PVA capped ZnO nanoparticles were appeared in Fig. 4. It is obvious from the figure that the assimilation spectrum of the particles is diminished with expanding wavelength. From the figure it is observed that the ingestion expanded with expanding doping convergence of ZnO in PVA matrix [15], as per Beer-lamberts law; the assimilation is corresponding to the quantity of engrossing atoms [16]. Arrangement of new peaks for the sample in the wake of doping and furthermore widening of those peaks with expanding ZnO demonstrate a significant collaboration among PVA and ZnO [17]. This figure shows that the transmittance power increments with the expanding of the wavelength and as the convergence of doped material nano ZnO builds, the transmittance diminishes. The explanation behind this nature is that the increments of grouping of ZnO lead to expanding the limited state of thickness which lessens the transmittance values. The transmission range increments and it is roughly steady at lower absorbance value. It is seen that the composite nanoparticles after doping of aluminium nanoparticles have new peaks were shown in the short wavelengths.

Diffuse reflectance spectrum of prepared nanopowders is shown in Fig. 5. The spectra of all samples display close band edge retention at 351 nm (3.26 eV). Fig. 4 shows the UV–noticeable room temperature optical ingestion spectra of the PVA-ZnO-Al_2O_3 composites. The common place close to band edge ingestion of mass ZnO (3.26 eV) is plainly observed for the sample. It may be seen that the ingestion peaks of the composite containing the bigger size is not standard fit as a fiddle likely because of the arrangement of totals. On account of the particles having size of 200 nm the state of the assimilation peaks are smaller.

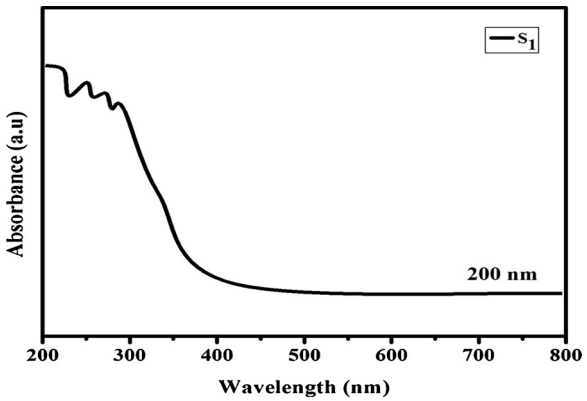

Fig. 4. Optical absorption spectrum of Al_2O_3 doped PVA capped ZnO nanoparticles.

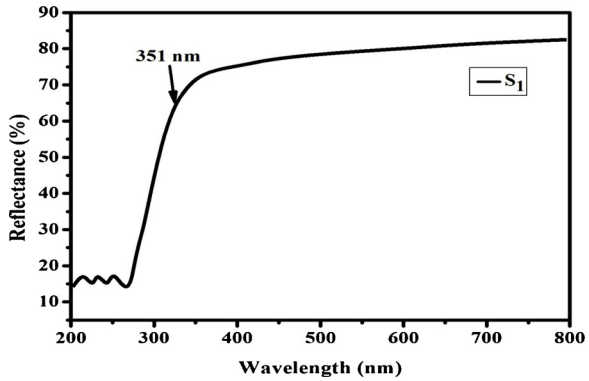

Fig. 5. Reflectance vs wavelength of Al_2O_3 doped PVA capped ZnO nanoparticles.

3.5. DC electrical conductivity studies

The DC electrical conductivity of Al_2O_3 doped PVA capped ZnO nanoparticles were shown in Fig. 6. DC electrical conductivity estimations have been done in the temperature range 200–373 K. The electrical resistivity is calculated by the following equation

$$\rho = \frac{\pi t}{\ln 2}\left(\frac{V}{I}\right) \tag{2}$$

where ρ is the resistivity (Ω-cm), t is the sample thickness (cm), V is the applied voltage and I is the source current (A).

The above plot shows an expansion in conductivity with respect to temperature. This might be because of the hopping mechanism between planning sides, nearby structure unwinding and segmental movement of the polymer. This plot seem to be Arrhenius conduct, with two areas (I & II) with initiation vitality gives above and beneath the dissolving locale 2.9–3.2 K of the polymer. In locale I, the conductivity increments gradually while in area II, it increments at higher rate. The last might be because of the adjustment in stage from a semi- crystalline to an indistinct state at the dissolving point. Further the shapeless area dynamically increments in district II because of which polymer chain gains quicker inward modes for which bond pivot produce segmental movement. This favours bouncing of particles with in the middle of the chains and thus the conductivity turns out to be high [18]. Comparable reports have likewise been accounted for electrolytes dependent on PVA.

The temperature reliance of the DC resistivity can be shown by the outstanding Arrhenius condition. Micheletti and Mark evaluated the intergranular boundary stature (φ_b) from the accompanying condition:

$$\mu = \mu_0 \exp(-\varphi_b/KT) \tag{3}$$

where each one of the terms have their typical implications. The estimation of (φ_b) acquired from plot Fig. 6, log (ρ) versus $1/T$ is 0.61 eV. Charge bearer versatility μ is resolved from the relation given by

$$\mu = \sigma/ne, \text{ (3)} \tag{4}$$

Where n is electron thickness and σ is the conductivity. It infers the semiconducting idea of the example since conductivity increments with increment in working temperature because of increasing of transport of ions. From the plot the calculated conductivity was found to be at 3.24×10^{-3} S/cm. The expansion conductivity with increment of temperature demonstrates total undefined stage and is like similar in daintily doped PVA film. It was recommended that a variable range jumping conduction model can be applied for

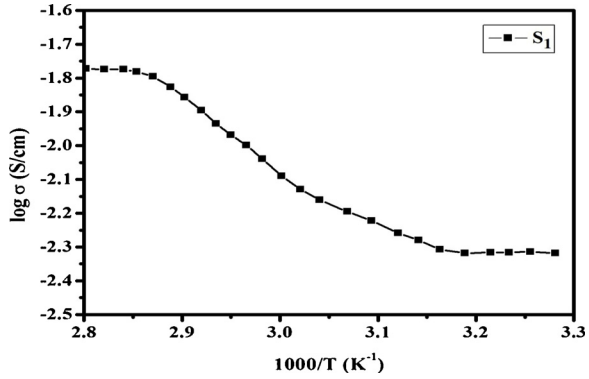

Fig. 6. DC conductivity of Al_2O_3 doped PVA capped ZnO nanoparticles.

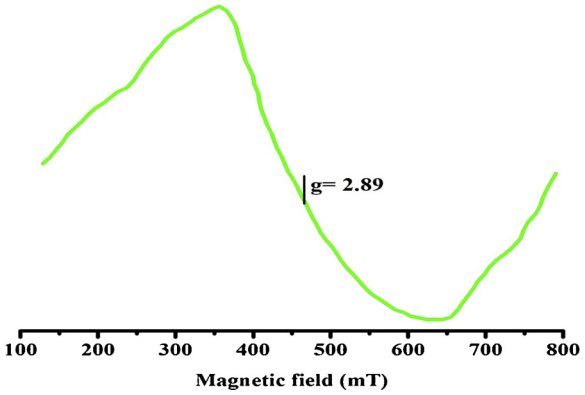

Fig. 7. EPR spectrum of Al_2O_3 doped PVA capped ZnO nanoparticles.

such situation where the conductivity is estimated.

3.6. EPR studies

EPR spectrum of Al_2O_3 doped PVA capped ZnO nanoparticles were measured on JEOL JES-FA200 having 100 kHz field regulation at room temperature was shown in Fig. 7. The reverberation sign was determined at g = 2.89 for 100 K temperature. The variation in the magnetic field was observed due to the insertion of Al^+ ions in the ZnO crystal lattice. The insertion of Al^+ ions in a host polymer induced the magnetic behaviour in the ZnO nanoparticles and also exhibit ferromagnetic nature at room temperature [19]. The Al_2O_3 doping may change the perfect ZnO structure to make it possible for forming defects and holes which could be regarded as additional charge carriers. It was clear that Al^+ (d6) particles have octahedral coordination and orbital singlet $^3A_{2g}$ has the most reduced vitality level, which split in to 3 F ground state as an outcome of crystal field. Turn Hamiltonian is utilized to speak to the EPR range of Al^+ particle for an isotropic g factor. An isotropic line is acquired which relates to the |0–1' | ± 1' attractive dipole changes. The turn - Hamiltonian can be represented as,

$$H = g\beta BS + SAI + SDS \quad (5)$$

where g is the isotropic factor,
β is the Bohr magnetron,
B is the external magnetic field,
S is the vector operator of the electron spin momentum,
A is the hyperfine interaction parameter,
I is the vector operator of nuclear spin momentum,
and D is the zero field splitting parameter.

From the above relations the accompanying parameters can be determined. The isotropic factor 'g' esteem is 2.89. The Δ worth is 9532 cm^{-1} in the wavelength of λ = 353 cm^{-1}. The communication with the electric field segment of the proper recurrence of electromagnetic radiation can start a change between the two states and results in the assimilation of photons. The fundamental rule in the EPR method is the ingestion of concoction substance in the vitality levels, which may reach out over a wide wavelength run in an outer attractive field. By EPR and UV-noticeable investigations the ionic parameter, α^2 can be assessed by,

$$g = 2.0023 - (\alpha^2 8\lambda/\Delta) \quad (6)$$

The ionic parameter lies in the middle of 0.2 and 1.5 which means the readied nanoparticles contain ionic and covalent holding. The acquired ionic parameter estimation of α^2 is 0.84. This unequivocally recommends that there exists a covalent holding between doped Al^+ particles and its ligands presence in the host lattice [20].

3.7. I–V characteristics

I–V characteristics of the prepared nanoparticles were shown in Fig. 8. The basic principle includes in I–V qualities is the charge move of electrons upgrade through the doped sample. Consequently the ionic conduction happens in the sample. Al^+ doped particles get quickly circulated over the stick gaps in the sample. At the point when the temperature of the sample should be brought up in the conduction phenomenon, at that point the charge transport is conceivable through the nanoparticles in the host material [21]. From the obtained plot, it clearly shows that the prepared nanoparticles possess the semi-conduction behaviour. Fig. 8 plainly demonstrates the voltage required for current and is obtained above the + ve side indicates the bright light. It is obvious that the voltage necessary for current is obtained below the + ve side indicates the dark light [22]. It is also obviously clear that the Al_2O_3 doped PVA capped ZnO nanoparticles, is a perfect material which is utilized for semiconducting applications. The dull current in the turnaround inclination is exceptionally close to zero and it could be considered a perfect case for diode qualities.

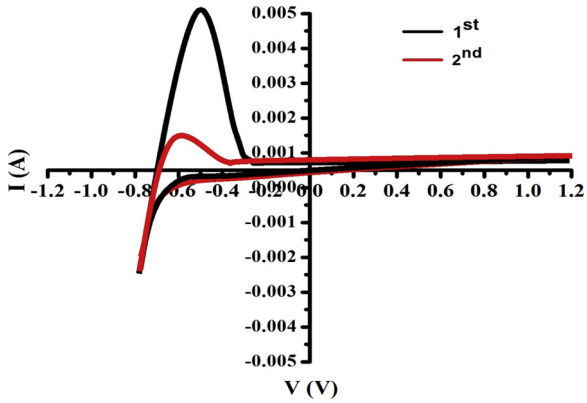

Fig. 8. Current- voltage characteristics of Al_2O_3 doped PVA capped ZnO nanoparticles.

3.8. Photoluminescence studies

The photoluminescence spectrum of Al_2O_3 doped PVA capped ZnO was shown in Fig. 9. Blue emission states are attributed to surface defects. These are hidden in the crystalline surface, whereas the bond formation and their respective boundaries are additionally perceived. Band twisting will bring about formation of a consumption district at the grain limits and it will influence the ionization condition of the deformities inside the exhaustion locale. Since the annealed sample comprises of fine particles with an enormous surface territory and bunches of grain limits, the green outflow likely to begin from contributor acceptor changes, where benefactor and additionally acceptor imperfections are situated at surfaces or grain limits [23,24]. From the figure, it is seen that, annealed sample has showed two excitation peaks at 416 and 619 nm. Everything happens because of excitation wavelength of 353 nm at room temperature. The acquired groups demonstrate the shading organized in the unmistakable district and furthermore the locale demonstrates that the main band is seen in violet area and the subsequent band in blue locale [25]. In this way the readied nanoparticles are valuable in the showcase gadget applications.

CIE color chromaticity is framed by the interesting combination of three coordinates which are green, blue and red with proper proportions. The light emission radiated by Xe source has monochromatic wavelength which is incident on the sample. The yield of the sample blower recognizes the approaching radiation. The subsequent radiation is sifted by an outflow monochromator which results in to a sign of a photomultiplier identifier [26]. CIE 1931 chromaticity directions are observed to be at x = 0.2053 and y = 0.1453. The related CIE outline is appeared in Fig. 10. The CIE chromaticity, organized locale for the readied nanoparticles is found in blue region.

4. Conclusions

Al_2O_3 doped PVA dopped ZnO nanoparticles were obtained by co-precipitation method. From the XRD pattern, the diffraction peaks observed close to 2θ = 21.2°, 38.2°, 42.1°, and 53.6° were attributed to the (1 1 0), (2 1 1), (3 2 0), and (4 1 0) planes. The

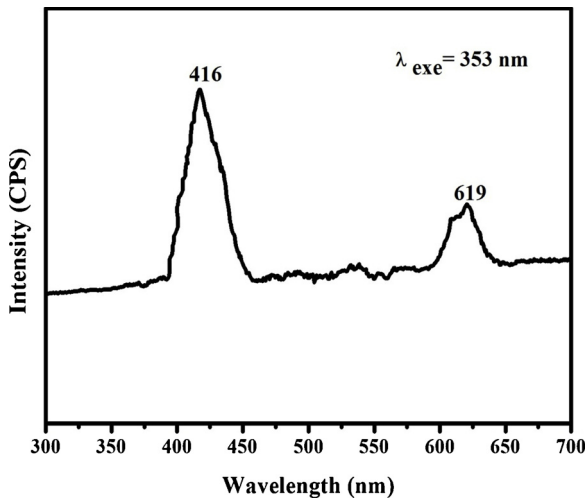

Fig. 9. Photoluminescence spectrum of Al_2O_3 doped PVA capped ZnO nanoparticles.

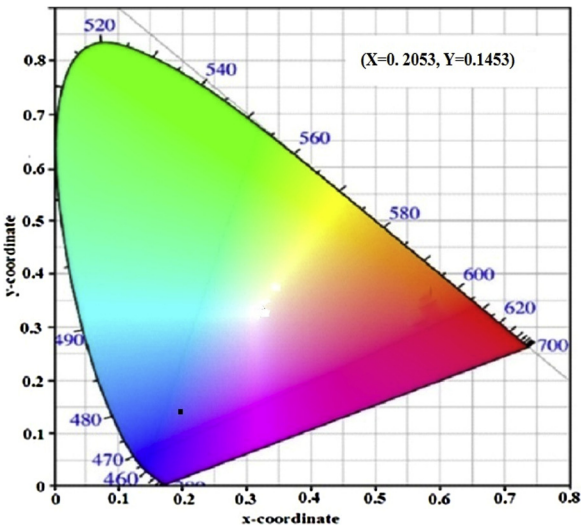

Fig. 10. Chromaticity diagram of Al_2O_3 doped PVA capped ZnO nanoparticles.

normal crystallite size was 12 nm. SEM image showed that the nanoparticles are distributed uniformly with small sized grains consisting of nano dots like tips due to the agglomeration of particles. The characteristic groups in the FTIR range were formed due to stretching vibrations of Al-O, C═O and C−H, gatherings. The absorption peaks formed at 870 cm^{-1} were expected to C═O extending vibration. The optical spectrum of all examples displays close band edge retention at 351 nm (3.26 eV). From the DC plot the calculated conductivity was found to be at 3.24×10^{-3} S/cm. The expansion in conductivity with increment of temperature demonstrates total undefined stage and is like similar in daintily doped PVA film. The voltage required for current was obtained above the + ve side indicated as bright light and the voltage below the + ve side indicated as dark light. Photoluminescence studies revealed that the annealed sample have showed two excitation peaks at 416 and 619 nm. CIE chromaticity of the readied nanoparticles was found in blue region. These studies revealed that the prepared nanoparticles can be utilized in many applications like luminescence, optoelectronic and display devices.

Role of the funding sources

There are no funding sources for this article work.

Declaration of Competing Interest

The authors declare that there is no conflict of interest regarding the publication of this paper.

References

[1] A. Van Dijken, E.A. Meulenkamp, D. Vanmaekelbergh, A. Meijerink, J. Lumin. 454 (2000) 87–89.
[2] I. Shalish, H. Temkin, V. Narayananmurti, Phys. Rev. B 69 (2004) 245401.
[3] M. Ghosh, A.K. Raychaudhuri, Appl. Phys. Lett. 93 (2008) 123113.
[4] S. Deka, P.A. Joy, Solid State Commun. 142 (2007) 190–194.
[5] A. Debernardi, M. Fanciulli, Physica B 401–402 (2007) 451–453.
[6] A.J. Chen, X.M. Wu, Z.D. Sha, L.J. Zhug, Y.D. Meng, J. Phys. D 39 (2006) 4762.
[7] Y.Q. Wang, S.L. Yuan, P. Liu, X.X. Lan, Z.M. Tian, J.H. He, S.Y. Yin, J. Magn. Magn. Mater. 320 (2008) 1423–1426.
[8] S. Bachiv, C. Sandouly, J. Kossanyi, J.C. Ranford-Haret, J. Phys. Chem. Solids 57 (1996) 1869–1879.
[9] M. Naeem, S.K. Hasanain, M. Kobayashi, Y. Ishida, A. Fujimori, S. Buzby, S.I. Shah, Nanotech 17 (2006) 2675–2680.
[10] M. Naeem, S.K. Hasanain, A. Mumtaz, J. Phys. Condens. Mater 20 (2008) 025210.
[11] A.K. Srivastava, M. Deepa, N. Bahadur, M.S. Goyat, Mater. Chem. Phys. 114 (2009) 194–198.
[12] N. Bouropoulos, G.C. Psarras, N. Moustakas, A. Chrissanthopoulos, S. Baskoutas, Phys Stat Sol 205 (2008) 2033–2037.
[13] J. Lee, E.M. Bourim, W. Lee, J. Park, M. Jo, S. Jung, J. Shin, H. Hwang, Appl. Phys. Lett. 97 (2010) 172105.
[14] R. Viswanatha, S. Sapra, S.S. Gupta, B.B. Satpati, P.V. Satyam, B.N. Dev, D.D. Sarma, J. Phys. Chem. B 108 (2004) 6303–6310.
[15] A.S. Roy, S. Gupta, S. Sidhu, A. Praveen, C. Ramamurthy, Compos. Part B Eng. 47 (2013) 314–319.
[16] A. Wasan, T. Mohammed, K. Tagreed, J. Baghdad Sci. 8 (2011) 543–550.
[17] M. Hamed, H. Sabah, A. Sarkawt, Asian Trans. Sci. Tech. 1 (2012) 16–20.
[18] A. Kurt, Turkish J. Chem. 34 (2010) 67–79.
[19] J. Antony, S. Pendyala, D.E. McCready, M.H. Engelhard, D. Meyer, A. Sharma, Y. Qiang, IEEE Trans. Magn. 42 (2006) 2697–2699.
[20] Y.Y. Tay, S. Li, C.Q. Sun, P. Chen, Appl. Phys. Lett. 88 (2006) 173118.
[21] K.J. Albert, N.G. Lewis, C.L. Sahauer, G.A. Sotzing, S.E. Stizel, T.P. Vaid, D.R. Walt, Chem. Rev. 100 (2000) 2595–2626.
[22] B. Ashkenov, N. Mbenkum, C. Bundesmann, V. Riede, M. Lorenz, D. Spemann, M. Kaidashev, A. Kasic, M. Schubert, M. Grundmann, G. Wagner, H. Neumann, V. Darakchieva, H. Arwin, B. Monemar, J. Appl. Phys. 93 (2003) 126–133.
[23] G. Xiong, U. Pal, J.D. Serrano, J. Appl. Phys. 101 (2007) 024317.

[24] F. Decremps, J.P. Porres, A.M. Saitta, J.C. Chervin, A. Polian, Phys. Rev. B 65 (2002) 092101.
[25] V.A. Fonoberov, A.A. Balandin, Phys. Rev. B 70 (2004) 233205.
[26] J. Yang, X. Liu, L. Yang, Y. Wang, Y. Zhang, L. Lang, M. Gao, B. Feng, J. Alloys Compd. 477 (2009) 632–635.

Preparation and structural characterization of P_2O_5-CaO-Na_2O: CuO glasses

SATYANARAYANA TALAM[a,*], RAMBABU BUSI[a], NAGARJUNA GUNNAM[b], P. SYAM PRASAD[c], VENKATESWARA RAO PENUGONDA[d]
[a]*Department of EIE, Lakireddy Bali Reddy College of Engg. (A), Mylavaram-521230, Krishna, A.P., India*
[b]*Department of Chemistry, S.R.R. & C.V.R. Govt. Degree College, Vijayawada – 520004, India*
[c]*Department of Physics, National Institute of Technology (NIT), Warangal-506 004, Telangana State, India*
[d]*Department of Physics, The University of the West Indies, Mona Campus, Kingston 7, Jamaica*

Glasses of particular composition (65-x) P_2O_5-23CaO-12Na_2O: x CuO ($0.5 \le x \le 2.0$) mol% was synthesized. Further, the samples were characterized by X-Ray Diffraction (XRD), Scanning Electron Microscopy (SEM), Differential Thermal Analyses (DTA), Fourier Transform Infrared, optical Absorption and luminescence spectroscopy techniques.The XRD patterns recorded at room temperature have confirmed the non-crystalline nature to all glass samples which was also supported by SEM pictures. Shifting of glass transition temperature (T_g) towards lower temperature with the CuO addition is observed from the DTA scans.This observation is an indication of more disorder of glass network. Basic phosphate bands and possible cross linkages with CuO addition have been observed in FTIR spectra of all samples. Optical absorption spectra exhibted two bands in the regions about 335 and 795 nm. Luminescence spectra has exhibited two emission peaks corresponding to the transition of $^3D_1 \rightarrow {}^1S_0$ single Cu^+ centers and Cu^+-Cu^+ pairs respectively. From all the results, the sample with high content of CuO found to exhibit more degree of disorder. The reasons for more disorder have been discussed in detail by means of spectroscopic properties.

(Received April 21, 2018; accepted August 20, 2019)

*Keywords:*Phosphate glasses, XRD, DTA, Optical absorption, Copper ions

1. Introduction

Phosphate based glasses have been extensively investigated because of their superior properties [1-3]. High refractive index and low dispersion properties enable phosphate glasses to act as suitable hosts for different lasing ions than that of conventional borate and silicate glasses [4]. It also has been demonstrated that metal containing phosphate glasses can be considered as promising materials for a variety of photonic applications [4-6]. In addition, phosphate glasses may be considered as bioactive materials since they exhibit high dissolution with controlled rate in aqueous solutions [7]. Introducing transition metals into phosphate glass network would result in improving chemical durability and stability against devitrification and moisture [4-6]. Basically, phosphate network consisting of phosphate tetrahedra with different numbers of bridging oxygens, including cross-linked networks (Q^3), polymer-like chains (Q^2+Q^1) or small pyro(Q^1) and orthophosphate groups (Q^0) [7].

Semiconducting copper ion, one of the interesting transition metal ions in various glasses. Usually, copper exists in two stable states viz., Cu^+ which does not produce colouring and Cu^{2+} ions create colour centres [8]. Lot of attention has been given to the investigations on copper ions in different glass systems to provide structure-physical properties relation. It is found that copper ions have strong impact on spectral and electric features of various glass systems. The addition of CuO and Na_2O to phosphate glass network would modify the phosphate network resulting in change of physical properties as these properties depending on metal oxide dopant concentration and coordination environments. A large number of studies on copper ions in different glass systems are available; still there is a scope to investigate the structural changes resulting from addition of CuO in phosphate glasses. Hence, a considerable interest is attached on structure-properties relation of copper doped phosphate glasses. In this scenario, to explore the structural modifications in phosphate glass network with CuO, a particular glass system P_2O_5-CaO-Na_2O: CuO has been chosen and investigated.

2. Experimental

The nominal glass composition of the present study is selected as (65-x) P_2O_5-23CaO-12Na_2O: x CuO ($0.5 \le x \le 2.0$) and the samples are labelled with the following:

PC_5: 64.5 P_2O_5-23CaO-12Na_2O: 0.5 CuO
PC_{10}: 64.0 P_2O_5-23CaO-12Na_2O: 1.0 CuO
PC_{15}: 63.5 P_2O_5-23CaO-12Na_2O: 1.5 CuO
PC_{20}: 63.0 P_2O_5-23CaO-12Na_2O: 2.0 CuO

P_2O_5, a strong glass former was introduced in the glass composition in a form of $NH_4H_2PO_4$ while CaO and Na_2O were added in their natural form of anhydrous carbonates. The hygroscopic nature of P_2O_5 is controlled by adding suitable metal oxides. It is also expected that de-

polymerization of the phosphate network for the formation of P-OH bonds. CuO chemical powder was directly taken as per mol%. The chemical composition of the studied glass is chosen such that contents of Na_2O and CaO remain constant while the contents of P_2O_5 and CuO vary from 64.5 to 63 mol% and 0.5 to 2.0 mol% respectively. The present glasses were prepared using the melt quenching method. For preparing the glasses, powders of constituents corresponding to mol% were weighed using an electronic balance and the contents thoroughly mixed homogeneously in an agate pestle-mortar. The mixture was then poured into an aluminium crucible and placed in Termolab 1800 - Shimaden FP21 Controlled high temperaturefurnace set at the 1000 ºC for approximately one hour. Halfway during the melting period, the mixture would be stirred to allow for proper mixing of compounds. After one hour completed, the mixture was then poured into graphite moulds and placed in an annealing furnace set at the 300 ºC for approximately six hours. The glass samples were grounded and optical polished to the dimensions of 1.2 cm x 1.2 cm x 0.2 cm. The amorphous nature of the prepared glass samples was confirmed by the X-ray diffractometer (XRD, Rigaku D/Max ULTIMA III) and HITACHI S-3400N Scanning Electron Microscope. The glass transition temperature and temperatures of crystallization were determined by using the Netzsch Simultaneous DSC/TG Thermal Analyser STA409C. The densities of the samples were calculated using the Archimedes principle. Infrared absorption spectra were noted on a JASCO-FT/IR–5300 spectrophotometer up to a resolution of 0.1 cm^{-1} in the spectral range 400–4000cm^{-1} using potassium bromide pellets (300 mg) containing pulverized sample (1.5 mg). These pellets were pressed in a vacuum die at ~680MPa.Optical absorption spectra of the glasses were recorded at room temperature in the wavelength range 250-1000 nm with a resolution of 0.1nm using UV-3092 spectrophotometer. The photoluminescence spectra of glass samples were carried out using F-2500 FL Spectrophotometer, Hitachi.

3. Results and discussion

At first, calculation of physical parameters was done as they provide very important information about structural changes in the glasses with rise in CuO content. The density values of all samples were measured by Archimedes principle. Addition of CuO in place of P_2O_5 results little increase in density that might be due to slightly larger molecular weight and density of copper oxide than calcium oxide, sodium oxide. Degree of structural packaging, change in coordination& position of phosphate ions were assumed as few reasons for density changes. It is also observed that the values of average molecular weight found to decrease with the content of copper oxide while ion concentration found to increase. It could be due to replacing by CuO with P_2O_5 of high molecular weight [9].

Using the measured density and average molecular weight M of glasses, other essential physical parameters viz., copper ion concentration N_i, mean copper ion separation r_i and polaron radius r_p have been evaluated and presented in Table 1. Another interesting observation is that the decreasing trend of interionic distancer_i and polaron radius $r_p$with CuO content which supports the loosely packed glass network resulting more structural degree of disorder.

Fig. 1 presents the X-ray diffraction patterns of P_2O_5-CaO-Na_2O: CuO glasses recoreded at room temperature. These patterns did not show any sharp peaks except wide ranging halo that confirms non-crystalline nature to the samples. The broad halo observed was the characterisitc peak of glass samples. This result also supports the abscence of signs of crystalization tendency that might be occured sometimes during quenching process.

Table 1. Physical parametersof P_2O_5-CaO-Na_2O: CuO glasses

Sample	Avg. Mol. Wt. (g/mol)	Density (g/cm^3)	Conc. of 'Cu' ions N_i ($10^{21}/cm^3$)	Interionic distance of 'Cu' ions $r_{i\,(A°)}$	Polaron radius $r_{p\,(A°)}$
PC_5	203.8	2.616	3.85	6.38	2.57
PC_{10}	202.7	2.635	7.80	5.04	2.03
PC_{15}	201.8	2.658	11.84	4.38	1.77
PC_{20}	200.5	2.679	15.98	3.97	1.59

Another interesting study is recording of scanning electron microscopic pictures which reveal the morphological details of glass samples. Fig. 2 displays the SEM images of PC_{10} and PC_{20} recorded at room temperature with magnification of 20 μm. These pictures clearly indicating the absence of micro-crystals those usually might occurred due to quenching process. Thus it confirms non-crystalline nature and also supports the XRD patterns.

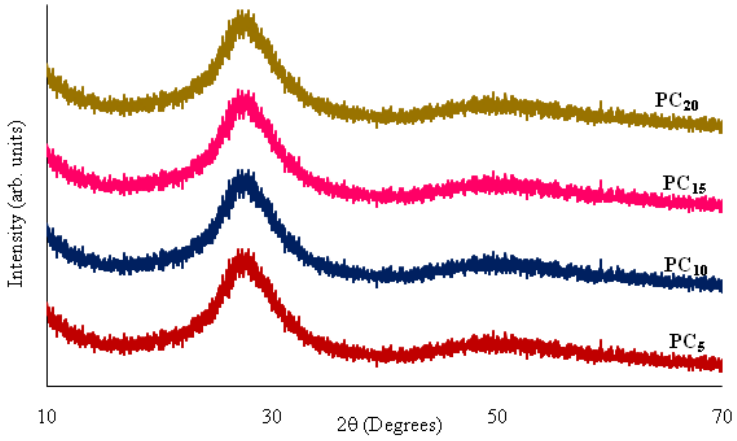

Fig. 1. XRD patterns of P_2O_5-CaO-Na_2O: CuO glasses.

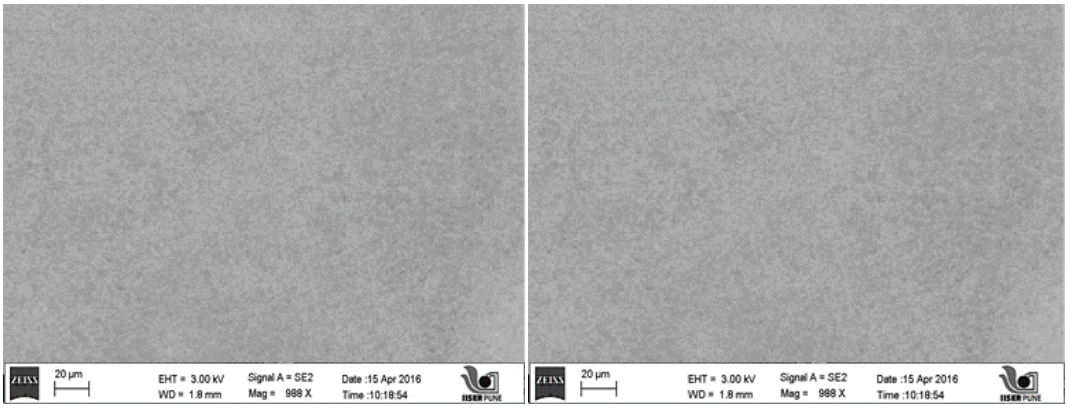

Fig. 2. Scanning Electron Microscopic pictures of P_2O_5-CaO-Na_2O: CuO glasses.

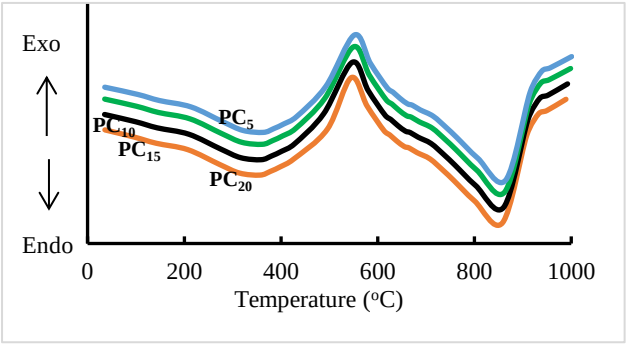

Fig. 3. DTA traces of P_5O_5-CaO-Na_2O: CuO glasses

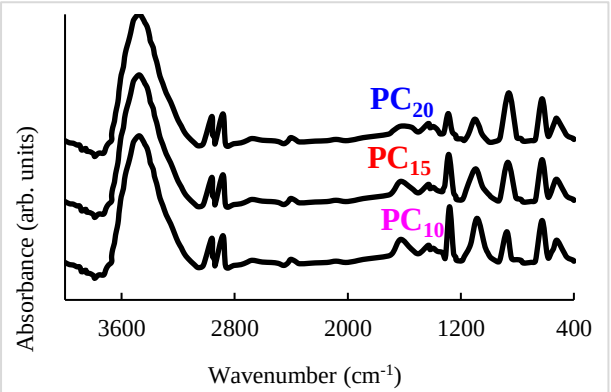

Fig. 4. FT-IR absorption spectra of P_2O_5- CaO- Na_2O: CuO glasses.

Differential thermal analysis (DTA) traces of P_2O_5-CaO-Na_2O: CuO glasses are presented in Fig. 3. The traces indicating broad range endothermic and exothermic peaks that confirms homogeneity of glass samples. It is observed that the addition of copper oxide resulted decrease in glass transition and melting temperatures. DTA trace of PC_{20} glass exhibits glass transition at about 375ºC which was small among other samples. From the traces, it was very clear that the glass transition Tg and melting temperature shift towards lower temperature region with copper oxide addition. Divalent copper ions act as modifiers and make the phosphate glass network weak by inducing many non-bridging oxygens leading to more structural network disorder. This could be the reason for above thermal changes [9].

The prepared glass samples are mixtures of glass network former (P_2O_5), intermediate oxides and modifiers (CaO& Na_2O). Phosphorous pentaoxide is one of the strong glass network formers and possesses PO_4 tetrahedron network structure. With bridging oxygens, PO_4 tetrahedrons forming chains through covalent bonding. Modifier calcium oxide enters the phosphate glass network by breaking P–O–P bonds that causing bonding defects leading to network disorder. Na_2O is considered to be incipient glass network formers which can form glass with the help of modifier oxides like CaO [10, 11].

Table 2. Summary of data on optical absorption spectra of P_2O_5-CaO-Na_2O: CuOglasses

Sample	Cut-off wavelength (nm)	$^2B_{1g} \rightarrow {}^2B_{2g}$(nm)	Optical band gap E_o (eV)
PC_5	325	752	2.88
PC_{10}	329	757	2.82
PC_{15}	336	759	2.76
PC_{20}	339	764	2.70

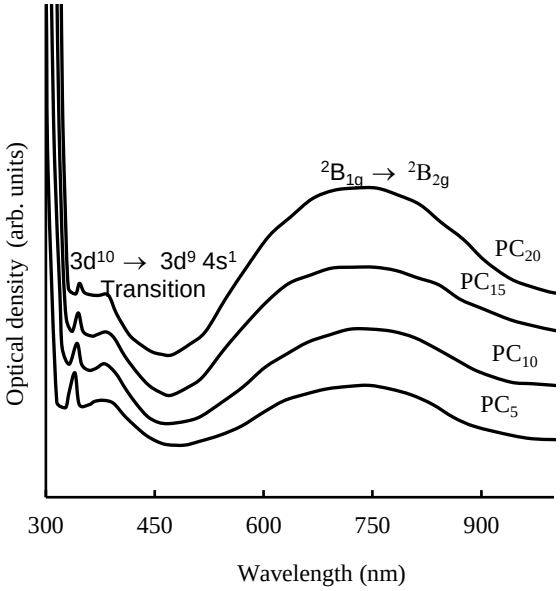

Fig. 5. Optical absorption spectra of P_2O_5-CaO-Na_2O: CuO glasses.

To investigate the structural changes in P_2O_5-CaO-Na_2O: CuO glasses,FTIR absorbance spectra is recorded and shown in Fig. 4. The positions of spectral bands for samples PC_5 and PC_{10} almost ensemble the same due to low concentration of CuO. Hence, the Fig.4 has shown only three IR traces corresponding to samples PC_{10}, PC_{15} and PC_{20}. Various characteristic absorption bands corresponding to P-O-P stretching, $\mathbf{PO_4^{3-}}$group, P-O-P asymmetric bending and pyrophosphate groups ($P_2O_7^{4-}$) in the wavenumber regions 1265-1286, 1057-1085 and 887-893 cm^{-1} have been observed in the spectra of all samples [2, 12-15]. Another interesting observation is that the small band located in the region 1600-1640 cm^{-1} could be due to the deformation mode of water molecule. Stretching mode vibrations of hydroxyl groups were also observed in the region 3140 to 3740 cm^{-1}. One more interesting vibrational band located in the region 440–610 cm^{-1} was identified and assigned to Na^+ and Ca^{2+} modifier cations [16]. With rise in the content of CuO, $\mathbf{PO_2^-}$ vibrational bands observed to grow and bending mode of $\mathbf{PO_4^{3-}}$ tetrahedron groups found to decrease. Reduction in wavenumber of vibrational bands corresponding to O–P–O vibrations and $\mathbf{PO_4^{3-}}$ tetrahedral groups clearly supports the more structural degree of disorder around phosphate groups. From these observations, the glass sample with high amount of CuO found to exhibit high degree of disorder due to more loosely cross-linked phosphate glass network with cations and it also supports DTA results.

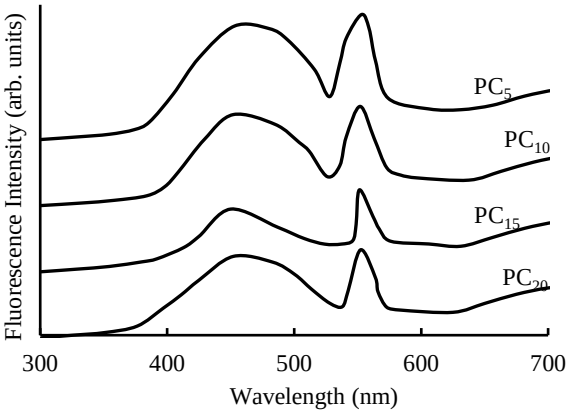

Fig. 6. Luminescence spectra of P_2O_5-CaO-Na_2O: CuO

Room temperature UV-visible absorption spectra of CuO doped P_2O_5-CaO-Na_2O glasses is presented as Fig.5. One strong absorption band and another small kink located at about 335 and 375nm assigned to $3d^{10} \rightarrow 3d^9\ 4s^1$ transitions observed in the spectrum of every glass sample [17, 18]. The CuO content rise in sample has shown that intensity and half-width of these bands found to decrease which caused by the larger existence of monovalent copper ions. One more broad absorption band centered at 794nm assigned to the transition $^2B_{1g} \rightarrow {}^2B_{2g}$ of divalent copper ions in octahedral coordination. [17, 19, 20]. Increase in CuO content has resulted in changing of absorption edge from higher wavenumber to lower wavenumber side. Interesting observation is that increase of intensity and half-width of broad absorption band with CuO rise at the expense of primary two bands. It is strongly felt that there exists conversion of Cu^+ ions to Cu^{2+} ions into octahedral environment. There was decrease in optical band gap with rise of CuO content.

Divalent octahedrally coordinated copper ions act as modifiers leading to growth of non-bridging oxygens (NBOs) that resulting prominent rise in donor centres by localized electrons. This rise moves the absorption edge to higher wavelength side by causing decrease in optical band gap (Table 2).

Fig. 6 shows the luminescence spectra of P_2O_5-CaO-Na_2O: CuO glasses excited with their corresponding absorption edges recorded in the wavelength region 300 to 900 nm at room temperature.

The spectra exhibited two emission peaks; one broad band at about 484 nm and another sharp peak at 595 nm. Both the bands are assigned to $^3D_1 \rightarrow {}^1S_0$ single Cu^+ centres and Cu^+-Cu^+ pairs transitions respectively [20]. Interesting detail is that the intensity and half width of these emission peaks found to diminish with CuO. This could be due to the fact that the conversion of Cu^+ ions into octahedrally coordinated Cu^{2+} ions. From the fluorescence results, it is clear that the sample PC_5 exhibit high emission intensity due to the presence of more Cu^+ ions [8]. With increase in the content of CuO, there is a change in the glass structure and was observed by FTIR , which also supports the conversion of Cu^+ to Cu^{2+}.

4. Conclusion

Glasses of particular composition P_2O_5-CaO-Na_2O: CuO were synthesized by melt quenching. Later, characterization of samples by XRD, SEM, DTA, optical absorption, FTIR and photoluminescence spectra. Absence of sharp peaks in XRD confirming amorphous nature, but characteristic glassy broad halo was observed. SEM pictures indicating signs of absence of micro-crystals which also supports XRD results. DTA traces have clearly indicated that glass transition and melting temperatures move close to lower temperature with CuO reveals decrease in rigidity of glass network that supports FTIR result. Infrared spectra have shown various distinctive phosphate vibrational bands and possible cross linkages. The sample PC_{20} found to exhibit more structural degree of disorder. Optical absorption spectra indicated the characteristic copper absorption transitions and decrease in band gap due to the larger concentrations of donor centres. Luminescence spectra has exhibited two emission peaks; one broad band at about 484 nm and another sharp peak at 595 nm corresponding to the transition of $^3D_1 \rightarrow {}^1S_0$ single Cu^+ centres and Cu^+-Cu^+ pairs respectively.

Acknowledgements

One of the authors Dr. T. Satyanarayana would like to acknowledge Science and Engineering Research Board (SERB)-DST, Govt. of India for the financial assistance (Ref. No.: SB/FTP/PS-044/2014).

References

[1] D. Bellucci, A. Sola, I. Cacciotti, C. Bartoli, M. Gazzarri, A. Bianco, F. Chiellini, V. Cannillo, Mater. Sci. Eng.C**42,**312 (2014).
[2] T. Satyanarayana, T. Kalpana, N. Veeraiah, J. Lumin. **130**, 498 (2010).
[3] D. E. Day, Z. Wu, C. S. Ray, P. Hrma, J. Non-Cryst. Solids **241**, 1 (1998).
[4] S. Shailajha, K. Geetha, P. Vasantharani, Mater Sci. **39**, 1001 (2016).
[5] M. Chemnitz, J. Wei, Ch. Jain, P. B. Rodrigues, T. Wieduwilt, J. Kobelke, L. Wondraczek, A. M. Schmidt, Optics Letters **41**(15), 3519 (2016**)**.
[6] I. Konidakis, S. Pissadakis, Materials**7**(8), 5735 (2014).
[7] D. A. Magdas, R. Stefan, D. Toloman, N. S. Vedeanu, J. Mol**.** Structure**1056–1057**, 314 (2014).
[8] A. Samir, M.A. Hassan, A. Abokhadra, L. I. Soliman, M. Elokr, Opt. Quant. Electron. **51**, 123 (2019).
[9] T. Satyanarayana, M. A. Valente, G. Nagarjuna, N. Veeraiah, J. Phys. and Chem. of Solids **74**, 229 (2013).
[10] T. Satyanarayana, Tilak Mukherjee, G. Nagarjuna, J. Optoelectron. Adv. M. **18**(9-10), 827 (2016).
[11] S. V. G. V. A. Prasad, M. Srinivasa Reddy,

V. Ravi Kumar, N. Veeraiah, J. Lumin.**127**, 637 (2007).
[12] D. Palles, I. Konidakis, C. P. E. Varsamis, E. I. Kamitsos, RSC Adv. **6**(20), 16697 (2016).
[13] P. Stoch, W. Szczerba, W. Bodnar, M. Ciecinska, A. Stoch, E. Burkel, Phys. Chem. Chem. Phys. **16**, 19917 (2014).
[14] M. A. Marzouk, H. A. ElBatal, A. M. Abdel Ghany, F. M. EzzEldin, J. Mol. Struct. **997**, 94 (2011).
[15] R. K. Brow, J. Non-Cryst. Solids **263-264**, 1 (2000).
[16] M. A. Ouis, A. M. Abdelghany, H. A. ElBatal, Processing and Applications of Ceram. **6**(3), 141 (2012).
[17] L. Srinivasa Rao, M. Srinivasa Reddy, D. Krishna Rao, N. Veeraiah, Solid State Sci. **11**, 78 (2009).
[18] H. A. El-Batal, Z. S. El-Mandouh, H. A. Zayed, S. Y. Marzouk, G. M. El-Komy, A. Hosny, Indian J. of Pure & Appl. Phys. **50**, 398 (2012).
[19] T. Satyanarayana, K. Srinivasa Rao, N. T. V. Naga Lakshmi, G. Nagarjuna, Solid State Phenomena **207**, 55 (2014).
[20] B. Padlyak, W. Ryba-Romanowski, R. Lisiecki, I. M. Teslyuk, J. Non-Crystalline Solids **356**, 2033 (2010).

*Corresponding author:drtsatyam@gmail.com

Send Orders for Reprints to reprints@benthamscience.net

Letters in Organic Chemistry, 2020, *17*, 000-000

RESEARCH ARTICLE

Design, Synthesis and Anticancer Evaluation of Acetamides Comprising 1,2,3-triazole, 1,3,4-thiadiazole and Isothiazolo[4,3-*b*]pyridine Rings

Shaik Shahinshavali[1,2], Nuthalapati Poojith[2], Venkat Rao Guttikonda[3], Reddymasu Sreenivasulu[4], and Mandava Venkata Basaveswara Rao[1,*]

[1]*Department of Chemistry, Krishna University, Machilipatnam, Andhra Pradesh, 521001 India;* [2]*Sri Ramachandra Institute of Higher Education and Research, Ramachandra Nagar, Porur, Chennai, 600116, Tamilnadu, India;* [3]*Department of Chemistry, SRR and CVR Government Degree College (Autonomous), Vijayawada, Andhra Pradesh, 520004 India;* [4]*Department of Chemistry, University College of Engineering (Autonomous), Jawaharlal Nehru Technological University, Kakinada, Andhra Pradesh, 533003 India*

ARTICLE HISTORY

Received: June 29, 2019
Revised: January 07, 2020
Accepted: January 30, 2020

DOI:
10.2174/1570178617666200225102939

Abstract: We have synthesized a library of new 1,2,3-triazole incorporated 1,3,4-thiadiazole-isothiazolo[4,3-*b*]pyridine derivatives **12a-j** and have screened these products for their anticancer activities against four human cancer cell lines such as MCF-7 (breast cancer), A549 (lung cancer), DU-145 (prostate cancer), and MDA MB-231 (breast cancer) using MTT assay with etoposide as a positive control. Among them, compound **12e** has shown excellent activities against MCF-7, A549, DU-145, and MDA-MB-231 with IC_{50} values of 0.53±0.055 µM, 0.18±0.077 µM, 0.10±0.082 µM, and 0.92±0.041 µM, respectively.

Keywords: 1,2,3-triazole, 1,3,4-thiadiazole, anticancer activity, azetepa, Carboxyamido triazole (CAI), isothiazolo[4,3-*b*]pyridine.

1. INTRODUCTION

Cancer is the second leading cause of death in both developing as well as undeveloped countries [1]. It is a very dangerous disease with rapid growth and uncontrolled spread of abnormal cells. Cancer can be due to several factors such as environment, diet, tobacco, radiations, *etc*. [2, 3]. Cancer cell lines can be destroyed by three different ways such as surgery, radiation therapy and chemotherapy. Among them, chemotherapy is a potent treatment for the inhibition of cancer cells. Most of the nitrogen-containing heterocyclic moieties act as cytotoxic agents in cancer chemotherapy [4-25].

1,3,4-thiadiazole constitutes a significant class of five-membered heterocyclic compounds and are extensively used in medicinal chemistry, organic synthesis, and material chemistry [26, 27]. The structure of –N=C=S in 1,3,4-thiadiazole derivatives can work as the active centre, chelate certain metal ions *in vivo,* and show good tissue permeability [28]. Recently, several 1,3,4-thiadiazole derivatives have been reported with different types of biological properties such as anticancer [29], antileishmanial [30], antihistamine [31], antibacterial [32], antioxidant [33], antiviral [34], anti-psychotic [35], anti-inflammatory [36], antihypertensive [37], analgesic [38], antimicrobial [39], antihepatitis B [40] and antidiabetic activities [41]. Some of the drugs such as azetepa (**1**, Fig. **1**), has 1,3,4-thiadiazole unit as a part of the structure and showed antineoplastic activity [42].

On the other hand, 1,2,3-triazoles are among the most privileged *N*-heterocyclic pharmacophores and are also able to form hydrogen bonds with suitable targets [43, 44]. There is a common method for the synthesis of triazoles *via* copper-catalyzed azide-alkyne cycloaddition, a "click-chemistry" reaction firstly introduced by Sharpless [45, 46]. The 1,2,3-triazole containing compounds have been reported to demonstrate a broad spectrum of biological activities including anticancer [47], antineoplastic [48], antitubercular [49], antibacterial [50], antiHIV [51], antifungal [52], antimalarial [53], antidiabetic [54], anti-inflammatory [55], glycosidase inhibitors [56], and antiplatelet properties [57]. The carboxyamidotriazole (CAI, **2**) is an anticancer agent containing 1,2,3-triazole ring as a part of the structure [58-60] (Fig. **1**).

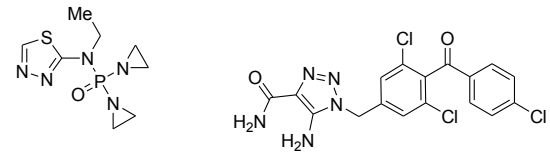

Azepeta (1) **CAI (2)**

Fig. (1). Structures of azepeta (1) and CAI (20).

*Address correspondence to this author at the Department of Chemistry, Krishna University, Machilipatnam, Andhra Pradesh, 521001 India;
E-mail: professormandava@gmail.com

1570-1786/20 $65.00+.00

Based on the above-mentioned reports on noteworthy biological significances of 1,3,4-thiadiazole and 1,2,3-triazole derivatives, it appeared that these frameworks could be the key moieties responsible for a wide range of biological properties. Indeed, we were particularly interested in knowing the anticancer properties of combined moieties (*i.e.* 1,3,4-thiadiazole and 1,2,3-triazole) in a single molecular entity. Accordingly, we have designed and synthesized a series of new acetamides **12a-j** including 1,2,3-triazole, 1,3,4-thiadiazole, and isothiazolo[4,3-b]pyridine rings. Furthermore, all the synthesized compounds (12) have been screened for their anticancer activity against human cancer cell lines.

2. RESULTS AND DISCUSSION

2.1. Chemistry

The synthetic route for the preparation of a series of new 2-(4-aryl-1*H*-1,2,3-triazol-1-yl)-*N*-[6-[[5-(3,4,5-trimethoxyphenyl)-1,3,4-thiadiazol-2-yl]amino]isothia zolo[4,3-*b*]pyridin-3-yl]acetamides **12a-j** is shown in Scheme (**1**). Compounds **3-7, 9, 11** are known, while **8, 10,** and **12** have not been previously reported in the literature. The starting compound **3 [61]** was submitted to reduction with iron in acetic acid (AcOH) at room temperature (rt) over 3 h time period to afford the amino derivative **4** [61, 62]. This amino derivative **4** was refluxed with Lawesson's reagent [2,4-bis(4-methoxyphenyl)-1,3,2,4-dithiadiphosphetane 2,4-disulfide] in ethanol (EtOH) for 24 h to afford pure carbothio amide **5** [62]. This thioamide derivative **5** underwent cyclization by reaction with 30% H_2O_2 in methanol (MeOH) at rt over 12 h time period then afforded pure 6-bromoisothiazolo[4,3-*b*]pyridin-3-amine (**6**) [62]. Product 6 was refluxed with 5-(3,4,5-trimethoxy phenyl)-1,3,4-thiadiazol-2-amine (**7**) [63] in the presence of triethyl amine (Et_3N) in 1-butanol for 4 h time period then afforded isothiazolo pyridinamine derivative **8**. It underwent coupling with 2-azidoacetic acid (**9**) in the presence of EDCI [N^3-(ethylcarbonimidoyl)-N^1,N^1-dimethyl-1,3-propanediamine hydrochloride (1:1)], and HOBt (1-hydroxy-1*H*-benzotriazole) in anhydrous CH_2Cl_2 (DCM) at rt over 7 h time period then afforded pure azido derivative **10**. Finally, product 10 underwent clik-chemistry reaction with differently substituted ethynylbenzenes **11a-j** in the presence of CuI in anhydrous tetrahydrofuran (THF) for 16 h to give target compounds **12a-j**.

2.2. Biological Evaluation: *In vitro* Cytotoxicity

All these derivatives **12a-j** were examined for their anticancer activity against four human cancer cell lines [MCF-7 (breast cancer), A549 (lung cancer), DU-145 (prostate cancer) and MDA-MB-231 (breast cancer)] by the use of MTT [2-(4,5-dimethyl-2-thiazolyl)-3,5-diphenyl-2*H*-tetrazolium bromide (1:1)] assay and etoposide as positive reference drug. The obtained results are incorporated in Table **1** and most of the synthesized derivatives **12** exhibited better anticancer activity than the positive control. Derivatives **12** showed IC_{50} (half maximal inhibitory concentration) values

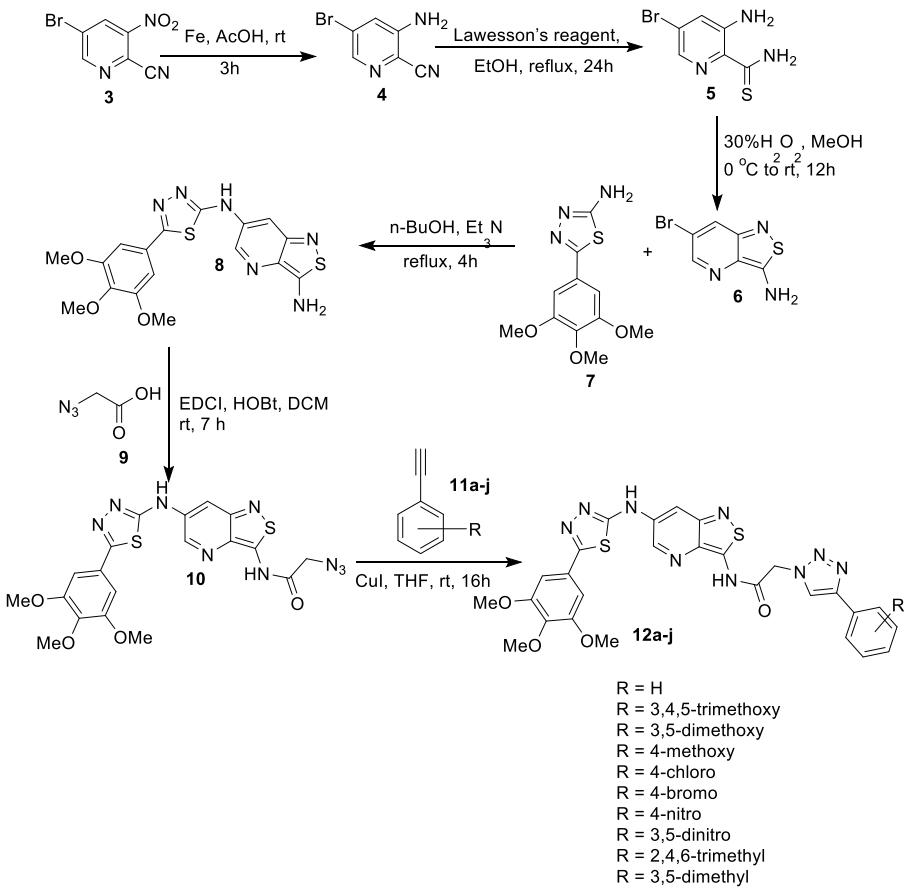

Scheme (1). Synthesis of 2-(4-aryl-1*H*-1,2,3-triazol-1-yl)-*N*-[6-[[5-(3,4,5-trimethoxyphenyl)-1,3,4-thiadiazol-2-yl]amino]isothiazolo[4,3-*b*]pyridin-3-yl]acetamides **12a-j**.

Table 1. ***In vitro*** **cytotoxicity of synthesized compounds 12a-j with IC_{50} in µM.**

Compound	MCF-7[a]	A549	DU-145	MDA-MB-231
12a	3.76±1.85	2.18±1.09	4.77±2.44	ND[b]
12b	0.67±0.093	0.22±0.034	0.11±0.071	1.09±0.83
12c	1.87±0.56	1.23±0.47	2.03±1.20	1.94±0.39
12d	2.98±1.77	2.12±1.32	4.76±2.60	3.16±1.94
12e	0.53±0.055	0.18±0.077	0.10±0.082	0.92±0.041
12f	2.44±2.03	7.43±2.30	3.08±1.88	ND
12g	1.32±0.12	1.49±0.48	2.10±1.56	2.77±1.70
12h	5.14±3.45	ND	ND	2.56±3.20
12i	8.12±4.56	10.2±4.10	6.29±3.86	2.64±1.99
12j	ND	12.4±4.65	14.7±6.21	3.72±2.66
Etoposide	2.11 ± 0.024	3.08 ± 0.135	1.97 ± 0.45	1.91 ± 0.84

[a]MCF-7: human breast cancer cell lines; A549: human lung cancer cell lines; DU-145: human prostate cancer cell lines; MDA-MB-231: human breast cancer cell lines.

[b]ND = Not determined.

in the range of 0.10±0.082 to 14.7±6.21 µM, and positive control in the range of 1.91±0.84 to 3.08±0.135 µM. Among all the synthesized **12**, four derivatives **12b,c,e**,**g** exhibited more potent activity. Structure-activity relationship results indicated that compound **12b** with 3,4,5-trimethoxy electron-donating substitution on phenyl ring showed better anti-cancer activity on four cell lines (MCF-7 0.67±0.093 µM, A549 0.22±0.034 µM, DU-145 0.11±0.071 µM and MDA-MB-231 1.09±0.83 µM) than the positive control, while compound **12c**, having 3,5-dimethoxy substitution, exhibited lower activity (MCF-7 1.87±0.56 µM, A549 1.23±0.47 µM, DU-145 2.03±1.20 µM and MDA-MB-231 1.94±0.39 µM) than **12b.** Compound **12d** with 4-methoxy substitution demonstrated much less activity (MCF-7 2.98±1.77 µM, A549 2.12±1.32 µM, DU-145 4.76±2.60 µM and MDA-MB-231 3.16±1.94 µM) than that of compounds **12b**,**c**. From the above results, we deduced that the decrease of electron-donating methoxy substituents should decrease the activity. Replacement of 4-methoxy with 4-chloro substituent yielded compound **12e** which showed the most promising activity (MCF-7 0.53±0.055 µM, A549 0.18±0.077 µM, DU-145 0.10±0.082 µM and MDA-MB-231 0.92±0.041 µM) compared to all the other compounds **12**, whereas compound **12g**, having 4-nitro substitution, displayed lesser activity (MCF-7 1.32±0.12 µM, A549 1.49±0.48 µM, DU-145 2.10±1.56 µM and MDA-MB-231 2.77±1.70 µM) in comparison with **12e.** The other compounds **12f**,**h**, showing electron-withdrawing substitution, exhibited moderate activity (MCF-7 = 2.44±2.03µM, A549 = 7.43±2.30µM, DU-145 = 3.08±1.88µM) and (MCF-7 = 5.14±3.45 µM, MDA-MB-231 = 2.56±3.20 µM) respectively in comparison with both compounds **12e,12g**. The compounds **12i**,**j**, with 2,4,6-trimethyl and 3,5-dimethyl substitution, showed very poor activity.

3. EXPERIMENTAL SECTION

All chemicals and reagents were obtained from Aldrich (Sigma–Aldrich, St. Louis, MO, USA), Lancaster (Alfa Aesar, Johnson Matthey Company, Ward Hill, MA, USA), and were used without further purification. Reactions were monitored by TLC, performed on silica gel 60 F_{254} glass plates, and visualization on TLC was achieved by UV light or iodine indicator. ^{1}H spectra were recorded on Brucker advance – 1 300 MHz and Brucker advance HD 400 MHz NMR spectrometer and ^{13}C NMR spectra were recorded on Brucker advance HD 400 MHz NMR spectrometer. Chemical shifts (δ) were reported in ppm downfield from internal TMS standard. ESI spectra were recorded on Micromass Quattro LC spectrometer using ESI+ software with capillary voltage 3.98 kV and MS (FAB) and MS (ESI) mode positive ion trap detector. Melting points were determined with an electrothermal melting point apparatus, and are uncorrected.

3.1. 3-Amino-5-bromo-2-pyridinecarbonitrile (4) [61,62]

5-Bromo-3-nitro-2-pyridinecarbonitrile (**3**) [61, 62] (13 g, 57.017 mmol) in one portion was added to a stirred solution of iron powder (6.4 g, 114.603 mmol) in AcOH (50 mL) at rt. The resulting reaction mixture was allowed to stir over 3 h time period. After completion of the reaction, ethyl acetate (65 mL) was added and the reaction mixture was filtered through a paper filter. The filtered cake was washed thoroughly with ethyl acetate (30 mL) and the filtrate was evaporated under reduced pressure. The crude product was purified by flash silica gel column chromatography with DCM to afford pure compound **4** (7.4 g, 37.370 mmol, 66% yield). ^{1}H NMR (300 MHz, DMSO-d_6): δ 6.57 (bs, 2H), 7.27-7.36 (m, 1H), 7.66-7.70 (m, 1H); MS (FAB): 197 $[M]^+$.

3.2. 3-Amino-5-bromo-2-pyridinecarbothioamide (5)

Lawesson's reagent (28.6 g, 70.710 mmol) was added to a solution of 3-amino-5-bromo pyridine-2-carbonitrile (**4)** (7 g, 35.350 mmol) in absolute EtOH (50 mL) [62]. This reaction mixture was allowed to stir at reflux temperature over 24 h time period. After completion of the reaction confirmed

by TLC, the solvent was evaporated under reduced pressure. The residue was redissolved in water (100 mL) and extracted three times with DCM (3 X 20 = 60 mL). The combined organic layers were evaporated under reduced pressure. The crude product was purified by flash silica gel column chromatography with heptane/acetone 6:4 to afford pure compound **5** (7 g, 30.159 mmol, 85% yield). ^{1}H NMR (300 MHz, DMSO-d_6) δ 6.96 (bs, 2H), 7.28 (d, 1H, *J* = 1.95 Hz), 7.89 (d, 1H, *J* = 1.95 Hz), 9.39 (bs, 2H); ^{13}C NMR (100 MHz, DMSO-d6) *δ* 129.3, 139.6, 141.7, 144.6, 147.3, 179.6; MS (FAB): 233 $[M+2H]^+$.

3.3. 6-Bromoisothiazolo[4,3-b]pyridin-3-amine (6)

30% aqueous H_2O_2 solution (2 mL, 19.6 mmol) was added dropwise to a solution of 3-amino-5-bromopyridine-2-carbothioamide (**5**) (6 g, 25.851 mmol) in MeOH (30 mL) at 0°C. The reaction mixture was stirred at rt overnight. After consumption of the starting material, the reaction mass was cooled to 0 °C. The precipitate was filtered off and washed with cold MeOH (4 mL) to afford pure compound **6** (3.1 g, 13.473 mmol, 52% yield). ^{1}H NMR (300 MHz, DMSO-d_6): δ 8.04 (d, 1H, *J* = 2.0 Hz), 8.08 (bs, 2H), 8.30 (d, 1H, *J* = 2.0 Hz); ^{13}C NMR (100 MHz, DMSO-d6): δ 109.6, 120.8, 138.9, 146.1, 155.8, 159.0; MS (FAB): 231$[M+2H]^+$.

3.4. *N*^{6}-[5-(3,4,5-Trimethoxyphenyl)-1,3,4-thiadiazol-2-yl)isothiazolo[4,3-b]pyridine-3,6-diamine (8)

The compound 6-bromoisothiazolo[4,3-*b*]pyridin-3-amine (**6**) (10 g, 43.461 mmol) was heated with 5-(3,4,5-trimethoxyphenyl)-1,3,4-thiadiazol-2-amine (**7**) [63] (11.6 g, 43.397 mmol) in anhydrous 1-butanol (50 mL). To this, Et_3N (12.1 mL, 86.753 mmol) was added dropwise to the reaction mixture under stirring conditions and refluxed for 4 h. After completion of the reaction, water (70 mL) was added and the crude product was extracted using ethyl acetate (3 X 10 = 30 mL). The compound was purified by silica gel column chromatography using ethyl acetate/hexane 4:6 to afford **8** (12.6 g, 30.254 mmol, 70% yield). Mp;163-164 ^{o}C. ^{1}H NMR (300 MHz, DMSO-d_6): δ 3.87 (s, 6H), 3.90 (s, 3H), 7.34 (s, 2H), 7.91 (d, 1H, *J* = 2.1 Hz), 8.07 (bs, 2H), 8.23 (s, 1H), 8.27 (d, 1H, *J* = 2.1 Hz); ^{13}C NMR (100 MHz, DMSO-d_6): δ 56.8, 60.3, 106.7, 115.3, 121.6, 134.7, 144.7, 149.3, 149.9, 150.1, 151.1, 154.7, 156.7, 163.2; MS (ESI): 417 $[M+H]^+$. Anal. Calcd for $C_{17}H_{16}N_6O_3S_2$: C, 49.03; H, 3.87; N, 20.18; found: C, 49.18; H, 4.01; N, 20.07%.

3.5. 2-Azido-*N*-[6-[[5-(3,4,5-trimethoxyphenyl)-1,3,4-thiadiazol-2-yl]amino]isothiazolo[4,3-*b*]pyridin-3-yl) acetamide (10)

Compound **8** (12 g, 28.813 mmol), EDCI (10.5 g, 54.773 mmol), HOBt (38 mg, 0.281 mmol) were dissolved in 50 mL anhydrous DCM and stirred at 0 ^{o}C for 1 h. 2-Azidoacetic acid (**9**) (2.2 mL, 29.388 mmol) was then added into the mixture and stirred at rt for 7 h (Reaction time of 7 h is reported in Scheme **1**). After completion of the reaction, the mixture was washed with saturated sodium bicarbonate solution. The organic layer was evaporated under reduced pressure to afford the pure compound **10** (11.6 g, 23.222 mmol, 81% yield). Mp;181-183 ^{o}C ^{1}H NMR (300 MHz, DMSO-d_6): δ 3.87 (s, 6H), 3.91 (s, 3H), 4.68 (s, 2H), 7.34 (s, 2H), 7.90 (d, 1H, *J* = 2.2 Hz), 8.28 (d, 1H, *J* = 2.2 Hz), 10.54 (s, 1H), 12.85 (bs, 1H); ^{13}C NMR (100 MHz DMSO-d_6): δ 47.8, 56.7, 60.1, 105.9, 115.3, 133.8, 144.3, 147.6, 148.7, 150.1, 152.3, 156.7, 157.8, 163.1, 168.2; MS (ESI): 500 $[M+H]^+$. Anal. Calcd for $C_{19}H_{17}N_9O_4S_2$: C, 45.68; H, 3.43; N, 25.24; found: C, 45.54; H, 3.58; N, 25.05%.

3.6. *N*-[6-[[5-(3,4,5-Trimethoxyphenyl)-1,3,4-thiadiazol-2-yl]amino]isothiazolo[4,3-*b*]pyridin-3-yl]-2-(4-phenyl-1*H*-1,2,3-triazol-1-yl)acetamide (12a)

The azide **10** (300 mg, 0.601 mmol) and 1-ethynylbenzene (**11a**) (0.067 mL, 0.601 mmol) were dissolved in 15 mL of anhydrous THF and CuI (0.6 mg, 0.5 mol%, 0.003 mmol) was added. The mixture was stirred vigorously at rt for 16 h. After completion of the reaction, THF was evaporated in vacuum and the crude product was handled with ethyl acetate (3 × 30 mL = 90 mL). The organic phase was washed with water (3 × 30 mL = 90 mL) and dried over with Na_2SO_4. After removal of the solvent in vacuum the crude product was purified by silica gel column chromatography with ethyl acetate/hexane 4:6 to obtain pure compound **12a** (143.4 mg, 0.238 mmol, 40% yield). Mp: 201-203^{o}C; ^{1}H NMR (400 MHz, DMSO-d_6): δ 3.88 (s, 6H), 3.91 (s, 3H), 4.81 (s, 2H), 7.33 (s, 2H), 7.45-7.57 (m, 3H), 7.66 (d, 2H, *J* = 7.8 Hz), 7.91 (d, 1H, *J* = 2.3 Hz), 7.96 (s, 1H), 8.34 (d, 1H, *J* = 2.3 Hz), 10.53 (s, 1H), 13.44 (bs, 1H); ^{13}C NMR (100 MHz, DMSO-d_6): δ 45.4, 57.6, 61.8, 106.3, 114.8, 116.3, 126.8, 128.4, 129.3, 131.2, 134.7, 143.2, 144.5, 148.5, 149.3, 150.5, 154.6, 155.7, 156.8, 157.8, 162.6, 169.8; MS (ESI): 602 $[M+H]^+$. Anal. Calcd for $C_{27}H_{23}N_9O_4S_2$: C, 53.90; H, 3.85; N, 20.95; found: C, 54.04; H, 3.98; N, 20.99%.

3.7. *N*-[6-[[5-(3,4,5-Trimethoxyphenyl)-1,3,4-thiadiazol-2-yl]amino]isothiazolo[4,3-*b*]pyridin -3-yl]-2-[4-(3,4,5-trimethoxyphenyl)-1*H*-1,2,3-triazol-1-yl]acetamide (12b)

Compound **12b** was prepared by the method described for **12a**, employing **10** (300 mg, 0.601 mmol) which was dissolved in 15 mL of THF, followed by the addition of 5-ethynyl-1,2,3-trimethoxybenzene (**11b**) (115 mg, 0.598 mmol) and CuI (0.6 mg, 0.5 mol%, 0.003 mmol). The crude product was purified by silica gel column chromatography with ethyl acetate/hexane 6:4 to afford pure compound **12b** (139.6 mg, 0.202 mmol, 34% yield). Mp: 256-258^{o}C; ^{1}H NMR (400 MHz, DMSO-d_6): δ 3.85 (s, 6H), 3.88 (s, 6H), 3.91 (s, 3H), 3.95 (s, 3H), 4.78 (s, 2H), 7.33 (s, 2H), 7.40 (s, 2H), 7.90 (d, 1H, *J* = 2.1 Hz), 7.95 (s, 1H), 8.33 (d, 1H, *J* = 2.1 Hz), 10.54 (s, 1H), 13.45 (bs, 1H); ^{13}C NMR (100 MHz, DMSO-d_6): δ 45.5, 56.7, 57.8, 61.4, 62.6, 105.7, 110.5, 114.3, 116.8, 127.3, 134.2, 143.4, 144.6, 145.6, 148.3, 149.4, 150.2, 154.6, 155.3, 156.7, 157.3, 157.8, 162.7, 170.2; MS (ESI): 692 $[M+H]^+$. Anal. Calcd for $C_{30}H_{29}N_9O_7S_2$: C, 52.09; H, 4.23; N, 18.22; found: C, 52.24; H, 4.11; N, 18.39%.

3.8. *N*-[6-[[5-(3,4,5-Trimethoxyphenyl)-1,3,4-thiadiazol-2-yl]amino]isothiazolo[4,3-*b*]pyridin-3-yl]-2-[4-(3,5-dimethoxyphenyl)-1*H*-1,2,3-triazol-1-yl]acetamide (12c)

Compound **12c** was prepared by the method described for **12a**, employing **10** (300 mg, 0.601 mmol) which was

dissolved in 15 mL of THF, followed by the addition of 1-ethynyl-3,5-dimethoxybenzene (**11c**) (97 mg, 0.598 mmol) and CuI (0.6 mg, 0.5 mol%, 0.003 mmol). The crude product was purified by silica gel column chromatography with ethyl acetate / hexane 6:4 to afford pure compound **12c** (131.7 mg, 0.199 mmol, 33% yield). Mp: 230-232°C; ^{1}H NMR (400 MHz, DMSO-d_6): δ 3.79 (s, 6H), 3.88 (s, 6H), 3.91 (s, 3H), 4.80 (s, 2H), 7.09 (s, 1H), 7.34 (s, 2H), 7.39 (s, 2H), 7.91 (d, 1H, *J* = 2.0 Hz), 7.96 (s, 1H), 8.35 (d, 1H, *J* = 2.0 Hz), 10.54 (s, 1H), 13.44 (bs, 1H); ^{13}C NMR (100 MHz, DMSO-d_6): δ 45.6, 57.4, 58.3, 61.8, 99.4, 106.4, 110.6, 114.5, 116.3, 132.4, 134.5, 143.7, 145.6, 148.3, 149.2, 150.4, 154.6, 155.4, 156.7, 157.8, 162.4, 164.6, 169.7; MS (ESI): 662 $[M+H]^+$. Anal. Calcd for $C_{29}H_{27}N_9O_6S_2$: C, 52.64; H, 4.11; N, 19.05; found: C, 52.49; H, 4.01; N, 18.02%.

3.9. *N*-[6-[[5-(3,4,5-Trimethoxyphenyl)-1,3,4-thiadiazol-2-yl]amino]isothiazolo[4,3-*b*]pyridin-3-yl]-2-[4-(4-methoxyphenyl)-1*H*-1,2,3-triazol-1-yl]acetamide (12d)

Compound **12d** was prepared by the method described for **12a**, employing **10** (300 mg, 0.601 mmol) which was dissolved in 15 mL of THF, followed by the addition of 1-ethynyl-4-methoxybenzene (**11d)** (0.077 mL, 0.587 mmol) and CuI (0.6 mg, 0.5 mol%, 0.003 mmol). The crude product was purified by silica gel column chromatography with ethyl acetate / hexane 6:4 to afford pure compound **12d** (112.8 mg, 0.179 mmol, 30% yield). Mp: 199-201°C; ^{1}H NMR (400 MHz, DMSO-d_6): δ 3.76 (s, 3H), 3.89 (s, 6H), 3.92 (s, 3H), 4.83 (s, 2H), 7.18 (d, 2H, *J* = 7.6 Hz), 7.34 (s, 2H), 7.44 (d, 2H, *J* = 7.6 Hz), 7.91 (d, 1H, *J* = 2.2 Hz), 7.95 (s, 1H), 8.34 (d, 1H, *J* = 2.2 Hz), 10.43 (s, 1H), 13.45 (bs, 1H); ^{13}C NMR (100 MHz, DMSO-d_6): δ 45.6, 57.5, 58.2, 61.8, 106.5, 114.5, 115.8, 116.4, 124.3, 127.6, 134.5, 141.4, 143.6, 148.7, 149.3, 150.5, 154.3, 156.7, 157.2, 157.8, 160.4, 162.5, 169.8; MS (ESI): 632 $[M+H]^+$. Anal. Calcd for $C_{28}H_{25}N_9O_5S_2$: C, 53.24; H, 3.99; N, 19.96; found: C, 53.09; H, 4.14; N, 20.13%.

3.10. 2-[4-(4-Chlorophenyl)-1*H*-1,2,3-triazol-1-yl]-*N*-[6-[[5-(3,4,5-trimethoxyphenyl)-1,3,4-thiadiazol-2-yl]amino]isothiazolo[4,3-*b*]pyridin-3-yl]acetamide (12e)

Compound **12e** was prepared by the method described for **12a**, employing **10** (300 mg, 0.601 mmol) which was dissolved in 15 mL of THF, followed by the addition of 1-chloro-4-ethynylbenzene (**11e)** (82 mg, 0.600 mmol) and CuI (0.6 mg, 0.5 mol%, 0.003 mmol) and the crude product was purified by silica gel column chromatography with ethyl acetate / hexane 4:6 to afford pure compound **12e** (191.6 mg, 0.301 mmol, 50% yield). Mp: 266-268°C; ^{1}H NMR (400 MHz, DMSO-d_6): δ 3.88 (s, 6H), 3.92 (s, 3H), 4.90 (s, 2H), 7.34 (s, 2H), 7.52 (d, 2H, *J* = 7.9 Hz), 7.67 (d, 2H, *J* = 7.9 Hz), 7.90 (d, 1H, *J* = 2.3 Hz), 7.98 (s, 1H), 8.35 (d, 1H, *J* = 2.3 Hz), 10.44 (s, 1H), 13.48 (bs, 1H); ^{13}C NMR (100 MHz, DMSO-d_6): δ 45.7, 57.8, 61.9, 106.5, 114.7, 116.8, 128.6, 130.3, 130.8, 133.4, 134.9, 143.5, 144.2, 148.7, 149.7, 150.3, 154.4, 156.7, 157.1, 157.6, 162.7, 170.4; MS (ESI): 636 $[M+H]^+$. Anal. Calcd for $C_{27}H_{22}ClN_9O_4S_2$: C, 50.98; H, 3.49; N, 19.82; found: C, 51.12; H, 3.61; N, 19.66%.

3.11. 2-[4-(4-Bromophenyl)-1*H*-1,2,3-triazol-1-yl]-*N*-[6-[[5-(3,4,5-trimethoxyphenyl)-1,3,4-thiadiazol-2-yl]amino]isothiazolo[4,3-*b*]pyridin-3-yl]acetamide (12f)

Compound **12f** was prepared by the method described for **12a**, employing **10** (300 mg, 0.601 mmol) which was dissolved in 15 mL of THF, followed by the addition of 1-bromo-4-ethynylbenzene (**11f**) (108 mg, 0.597 mmol) and CuI (0.6 mg, 0.5 mol%, 0.003 mmol). The crude product was purified by silica gel column chromatography with ethyl acetate / hexane 5:5 to afford pure compound **12f** (159.4 mg, 0.234 mmol, 39% yield). Mp: 259-261°C; ^{1}H NMR (400 MHz, DMSO-d_6): δ 3.89 (s, 6H), 3.92 (s, 3H), 4.93 (s, 2H), 7.33 (s, 2H), 7.57 (d, 2H, *J* = 8.0 Hz), 7.69 (d, 2H, *J* = 8.0 Hz), 7.92 (d, 1H, *J* = 2.4 Hz), 7.99 (s, 1H), 8.36 (d, 1H, *J* = 2.4 Hz), 10.44 (s, 1H), 13.50 (bs, 1H); ^{13}C NMR (100 MHz, DMSO-d_6): δ 45.8, 57.8, 61.6, 106.7, 114.5, 116.7, 122.4, 128.5, 130.5, 132.6, 134.8, 143.5, 144.7, 148.2, 149.6, 150.2, 154.6, 156.7, 157.3, 157.9, 162.7, 170.2; MS (ESI): 680 $[M+H]^+$. (The exact mass of **12f** is 679.04. Is this line M+3?) Anal. Calcd for $C_{27}H_{22}BrN_9O_4S_2$: C, 47.65; H, 3.26; N, 18.52; found: C, 47.51; H, 3.42; N, 18.67%.

3.12. *N*-[6-[[5-(3,4,5-Trimethoxyphenyl)-1,3,4-thiadiazol-2-yl]amino]isothiazolo[4,3-*b*]pyridin-3-yl]-2-[4-(4-nitrophenyl)-1*H*-1,2,3-triazol-1-yl]acetamide (12g)

Compound **12g** was prepared by the method described for **12a**, employing **10** (300 mg, 0.601 mmol) which was dissolved in 15 mL of THF, followed by the addition of 1-ethynyl-4-nitrobenzene (**11g**) (88 mg, 0.598 mmol) and CuI (0.6 mg, 0.5 mol%, 0.003 mmol). The crude product was purified by silica gel column chromatography with ethyl acetate / hexane 4:6 to afford pure compound **12g** (178.2 mg, 0.276 mmol, 46% yield). Mp: 280-282°C; ^{1}H NMR (400 MHz, DMSO-d_6): δ 3.89 (s, 6H), 3.92 (s, 3H), 4.97 (s, 2H), 7.34 (s, 2H), 7.72 (d, 2H, *J* = 8.1 Hz), 7.92 (d, 1H, *J* = 2.3 Hz), 8.01 (s, 1H), 8.28-8.40 (m, 3H), 10.44 (s, 1H), 13.53 (bs, 1H); ^{13}C NMR (100 MHz, DMSO-d_6): δ 46.3, 57.8, 61.8, 106.5, 114.8, 116.8, 125.3, 130.8, 134.6, 135.8, 143.4, 144.7, 147.3, 148.6, 149.2, 150.3, 154.6, 156.7, 157.4, 157.8, 162.8, 170.4; MS (ESI): 647 $[M+H]^+$. Anal. Calcd for $C_{27}H_{22}N_{10}O_6S_2$: C, 50.15; H, 3.43; N, 21.66; found: C, 50.32; H, 3.61; N, 21.83%.

3.13. *N*-[6-[[5-(3,4,5-Trimethoxyphenyl)-1,3,4-thiadiazol-2-yl]amino]isothiazolo[4,3-*b*]pyridin-3-yl]-2-[4-(3,5-dinitrophenyl)-1*H*-1,2,3-triazol-1-yl]acetamide (12h)

Compound **12h** was prepared by the method described for **12a**, employing **10** (300 mg, 0.601 mmol) which was dissolved in 15 mL of THF, followed by the addition of 1-ethynyl-3,5-dinitrobenzene (**11h**) (115 mg, 0.599 mmol) and CuI (0.6 mg, 0.5 mol%, 0.003 mmol). The crude product was purified by silica gel column chromatography with ethyl acetate / hexane 5:5 to afford pure compound **12h** (210.5 mg, 0.304 mmol, 51% yield). Mp: 290-292°C; ^{1}H NMR (400 MHz, DMSO-d_6): δ 3.88 (s, 6H), 3.92 (s, 3H), 4.98 (s, 2H), 7.33 (s, 2H), 7.92 (d, 1H, *J* = 2.3 Hz), 8.04 (s, 1H), 8.34 (d, 1H, *J* = 2.3 Hz), 8.47 (s, 2H), 8.86 (s, 1H), 10.44 (s, 1H), 13.56 (bs, 1H); ^{13}C NMR (100 MHz, DMSO-d_6): δ 46.8, 57.8, 61.7, 106.5, 114.8, 115.8, 118.4, 133.4, 134.2, 134.6, 143.6, 147.3, 147.8, 148.3, 149.6, 150.3, 154.6, 156.3, 157.5,

157.9, 162.7, 170.6; MS (ESI): 692 $[M+H]^+$. Anal. Calcd for $C_{27}H_{21}N_{11}O_8S_2$: C, 46.89; H, 3.06; N, 22.28; found: C, 46.72; H, 3.19; N, 22.44%.

3.14. *N*-[6-[[5-(3,4,5-Trimethoxyphenyl)-1,3,4-thiadiazol-2-yl]amino]isothiazolo[4,3-*b*]pyridin-3-yl]-2-[4-(2,4,6-trimethylphenyl)-1*H*-1,2,3-triazol-1-yl)acetamide (12i)

Compound **12i** was prepared by the method described for **12a**, employing **10** (300 mg, 0.601 mmol) which was dissolved in 15 mL of THF, followed by the addition of 2-ethynyl-1,3,5-trimethylbenzene (**11i**) (0.09 mL, 0.573 mmol) and CuI (0.6 mg, 0.5 mol%, 0.003 mmol). The crude product was purified by silica gel column chromatography with ethyl acetate / hexane 4:6 to afford pure compound **12i** (166.8 mg, 0.259 mmol, 45% yield). Mp: 210-212°C; ^{1}H NMR (400 MHz, DMSO-d_6): δ 2.46 (s, 3H), 2.64 (s, 6H), 3.89 (s, 6H), 3.91 (s, 3H), 4.78 (s, 2H), 6.98 (s, 2H), 7.33 (s, 2H), 7.91 (d, 1H, J = 2.2 Hz), 7.95 (s, 1H), 8.33 (d, 1H, J = 2.2 Hz), 10.42 (s, 1H), 12.67 (bs, 1H); ^{13}C NMR (100 MHz, DMSO-d_6): δ 24.8, 27.6, 45.6, 57.7, 61.6, 106.5, 114.7, 116.8, 129.4, 130.5, 134.2, 136.7, 138.2, 143.2, 144.6, 148.4, 149.7, 150.4, 154.6, 156.8, 157.3, 157.8, 162.7, 169.6; MS (ESI): 644 $[M+H]^+$. Anal. Calcd for $C_{30}H_{29}N_9O_4S_2$: C, 55.97; H, 4.54; N, 19.58; found: 56.11; H, 4.42; N, 19.41%.

3.15. *N*-[6-[[5-(3,4,5-Trimethoxyphenyl)-1,3,4-thiadiazol-2-yl]amino]isothiazolo[4,3-*b*]pyridin-3-yl]-2-[4-(3,5-dimethylphenyl)-1*H*-1,2,3-triazol-1-yl]acetamide (12j)

Compound **12j** was prepared by the method described for **12a**, employing **10** (300 mg, 0.601 mmol) which was dissolved in 15 mL of THF, followed by the addition of 1-ethynyl-3,5-dimethylbenzene (**11j**) (0.08 mL, 0.571 mmol) and CuI (0.6 mg, 0.5 mol%, 0.003 mmol). The crude product was purified by silica gel column chromatography with ethyl acetate/hexane 4:6 to afford pure compound **12j** (152.7 mg, 0.242 mmol, 42% yield). Mp: 205-207°C; ^{1}H NMR (400 MHz, DMSO-d_6): δ 2.55 (s, 6H), 3.89 (s, 6H), 3.92 (s, 3H), 4.77 (s, 2H), 7.09 (s, 1H), 7.24 (s, 2H), 7.34 (s, 2H), 7.91 (d, 1H, J = 2.1 Hz), 7.96 (s, 1H), 8.32 (d, 1H, J = 2.1 Hz), 10.43 (s, 1H), 12.68 (bs, 1H); ^{13}C NMR (100 MHz, DMSO-d_6): δ 26.5, 45.7, 57.6, 61.8, 106.4, 114.8, 116.4, 129.6, 131.5, 134.2, 135.8, 140.4, 143.8, 146.3, 148.4, 149.6, 150.4, 154.6, 156.7, 157.4, 157.8, 162.7, 169.8; MS (ESI): 630 $[M+H]^+$. Anal. Calcd for $C_{29}H_{27}N_9O_4S_2$: C, 55.31; H, 4.32; N, 20.02; found: C, 55.14; H, 4.46; N, 20.17%.

3.16. MTT Assay

Each datum is represented as mean ±SD (standard deviation) value from three different experiments performed in triplicates. Individual wells of a 96-well tissue culture microtiter plate were inoculated with 100 µL of complete medium containing 10^4 cells. The plates were incubated at 37°C in a humidified 5% CO_2 incubator for 18 h prior to the experiment. After medium removal, 100 µL of fresh medium containing the test compounds and etoposide at different concentrations such as 0.5, 1, and 2 µM was added to each well and incubated at 37°C for 24 h. Then the medium was discarded and replaced with 10 µL MTT dye. Plates were incubated at 37°C for 2 h. The resulting formazan (diazene carboxaldehyde hydrazone) crystals were solubilized in 100 µL extraction buffer. The optical density was read at 570 nm with a microplate reader (Thermo Scientific Varioskan LUX Multimode instrument). The percentage of DMSO in the medium never exceeded 0.25%.

CONCLUSION

In summary, we have reported a series of new acetamides **12a-j** incorporating 1,2,3-triazole, 1,3,4-thiadiazole, and isothiazolo[4,3-*b*]pyridine rings. Their chemical structures were confirmed by elemental analyses, ^{1}H NMR, ^{13}C NMR, and mass spectral data. Furthermore, these derivatives **12** were tested for their anticancer activity towards four human cancer cell lines [MCF-7 (breast cancer), A549 (lung cancer), DU-145 (prostate cancer) and MDA-MB-231 (breast cancer)] by the use of MTT assay. Etoposide was used as a positive control and all the synthesized derivatives **12** displayed good to moderate activity. Among them, compounds **12b,c,e,g** showed more potent activity. Compound **12e** showed excellent anticancer activity on all cell lines.

CONSENT FOR PUBLICATION

Not applicable.

AVAILABILITY OF DATA AND MATERIALS

The authors confirm that the data supporting the findings of this research are available within the article and its supplementary materials.

FUNDING

None.

CONFLICT OF INTEREST

The authors declare no conflict of interest, financial or otherwise.

ACKNOWLEDGEMENTS

Declared none.

SUPPLEMENTARY MATERIAL

Supplementary material is available on the publisher's website along with the published article.

REFERENCES

[1] Eckhardt, S. *Curr. Med. Chem. Anticancer Agents,* **2002**, *2*(3), 419-439. http://dx.doi.org/10.2174/1568011024606389 PMID: 12678741

[2] Anand, P.; Kunnumakkara, A.B.; Sundaram, C.; Harikumar, K.B.; Tharakan, S.T.; Lai, O.S.; Sung, B.; Aggarwal, B.B. *Pharm. Res.,* **2008**, *25*(9), 2097-2116. http://dx.doi.org/10.1007/s11095-008-9661-9 PMID: 18626751

[3] Vogelstein, B.; Kinzler, K.W. *The Genetic Basis of Human Cancer*; McGraw-Hill Education / Medical, **2005**.

[4] Hatti, I.; Sreenivasulu, R.; Jadav, S.S.; Ahsan, M.J.; Raju, R.R. *Monatsh. Chem.,* **2015**, *146*, 1699-1705. http://dx.doi.org/10.1007/s00706-015-1448-1

[5] Hatti, I.; Sreenivasulu, R.; Jadav, S.S.; Jayaprakash, V.; Kumar, C.G.; Raju, R.R. *Med. Chem. Res.,* **2015**, *24*, 3305-3313. http://dx.doi.org/10.1007/s00044-015-1375-z

[6] Ahsan, M.J.; Choudhary, K.; Jadav, S.S.; Yasmin, S.; Ansari, M.Y.; Sreenivasulu, R. *Med. Chem. Res.,* **2015**, *24*, 4166-4180. http://dx.doi.org/10.1007/s00044-015-1457-y

[7] Reddy, N.B.; Burra, V.R.; Ravindranath, L.K.; Sreenivasulu, R.; Kumar, V.N. *Monatsh. Chem.,* **2016**, *147*, 593-598. http://dx.doi.org/10.1007/s00706-016-1685-y

[8] Reddy, N.B.; Burra, V.R.; Ravindranath, L.K.; Kumar, V.N.; Sreenivasulu, R.; Sadanandam, P. *Monatsh. Chem.,* **2016**, *147*, 599-604. http://dx.doi.org/10.1007/s00706-016-1684-z

[9] Sreenivasulu, R.; Sujitha, P.; Jadav, S.S.; Ahsan, M.J.; Kumar, C.G.; Raju, R.R. *Monatsh. Chem.,* **2017**, *148*, 305-314. http://dx.doi.org/10.1007/s00706-016-1750-6

[10] Madhavi, S.; Sreenivasulu, R.; Raju, R.R. *Monatsh. Chem.,* **2017**, *148*, 933-938. http://dx.doi.org/10.1007/s00706-016-1790-y

[11] Agarwal, M.; Singh, V.; Sharma, S.K.; Sharma, P.; Ansari, M.Y.; Jadav, S.S.; Yasmin, S.; Sreenivasulu, R.; Hassan, M.Z.; Saini, V.; Ahsan, M.J. *Med. Chem. Res.,* **2016**, *25*, 2289-2303. http://dx.doi.org/10.1007/s00044-016-1672-1

[12] Madhavi, S.; Sreenivasulu, R.; Yazala, J.P.; Raju, R.R. *Saudi Pharm. J.,* **2017**, *25*(2), 275-279. http://dx.doi.org/10.1016/j.jsps.2016.06.005 PMID: 28344479

[13] Madhavi, S.; Sreenivasulu, R.; Ansari, Md. *Lett. Org. Chem.,* **2016**, *13*, 682-692. http://dx.doi.org/10.2174/1570178613666161021105317

[14] Sreenivasulu, R.; Durgesh, R.; Jadav, S.S.; Sujitha, P.; Kumar, C.G.; Raju, R.R. *Chem. Pap.,* **2018**, *72*, 1369-1378. http://dx.doi.org/10.1007/s11696-017-0372-8

[15] Subramanyam, M.; Sreenivasulu, R. *Lett. Drug Des. Discov.,* **2018**, *15*, 1299-1307. http://dx.doi.org/10.2174/1570180815666180219165119

[16] Rudavath, D.; Sreenivasulu, R.; Pinapati, S.R.; Raju, R.R. *J. Indian Chem. Soc.,* **2018**, *95*, 433-438.

[17] Suma, V.R.; Sreenivasulu, R.; Subramanyam, M.; Rao, K.R.M. *Russ. J. Gen. Chem.,* **2019**, *89*, 499-504. http://dx.doi.org/10.1134/S1070363219030228

[18] Shahinshavali, S.; Sreenivasulu, R.; Guttikonda, V.R.; Kolli, D.; Rao, M.V.B. *Russ. J. Gen. Chem.,* **2019**, *89*, 324-329. http://dx.doi.org/10.1134/S1070363219020257

[19] Spandana, Z.; Sreenivasulu, R.; Rao, M.V.B. *Lett. Org. Chem.,* **2019**, *16*, 662-667. http://dx.doi.org/10.2174/1570178616666181211094526

[20] Spandana, Z.; Sreenivasulu, R.; Rekha, T.M.; Rao, M.V.B. *Lett. Drug Des. Discov.,* **2019**, *16*, 656-662. http://dx.doi.org/10.2174/1570180816666181031125946

[21] Devi, E.R.; Sreenivasulu, R.; Rao, K.P.; Nadh, R.V.; Sireesha, M. *Lett. Org. Chem.,* **2020**, *17*, 54-60. http://dx.doi.org/10.2174/1570178616666190528095548

[22] Reddy, K.T.; Sreenivasulu, R.; Raju, R.R. *J. Indian Chem. Soc.,* **2019**, *96*, 1085-1090.

[23] Murthy, I.S.; Sreenivasulu, R.; Alluraiah, G.; Raju, R.R. *Russ. J. Gen. Chem.,* **2019**, *89*, 1718-1723. http://dx.doi.org/10.1134/S1070363219080279

[24] Rao, B.V.D.; Sreenivasulu, R.; Rao, M.V.B. *Russ. J. Gen. Chem.,* **2019**, *89*, 2115-2120. http://dx.doi.org/10.1134/S1070363219100207

[25] Yakantham, T.; Sreenivasluu, R.; Raju, R.R. *Russ. J. Gen. Chem.,* **2019**, *89*, 1485-1490. http://dx.doi.org/10.1134/S1070363219070181

[26] Sayed, A.R. *Tetrahedron,* **2012**, *68*, 2784-2789. http://dx.doi.org/10.1016/j.tet.2012.02.011

[27] Shahcheragh, S.M.; Habibi, A.; Khosravi, S. *Tetrahedron Lett.,* **2017**, *58*, 855-859. http://dx.doi.org/10.1016/j.tetlet.2017.01.057

[28] Luo, Z.; Chen, B.; He, S.; Shi, Y.; Liu, Y.; Li, C. *Bioorg. Med. Chem. Lett.,* **2012**, *22*(9), 3191-3193. http://dx.doi.org/10.1016/j.bmcl.2012.03.043 PMID: 22483583

[29] Aliabadi, A.; Eghbalian, E.; Kiani, A. *Iran. J. Basic Med. Sci.,* **2013**, *16*(11), 1133-1138. PMID: 24494064

[30] Poorrajab, F.; Ardestani, S.K.; Emami, S.; Behrouzi-Fardmoghadam, M.; Shafiee, A.; Foroumadi, A. *Eur. J. Med. Chem.,* **2009**, *44*, 1758-1762. http://dx.doi.org/10.1016/j.ejmech.2008.03.039 PMID: 18485538

[31] Gupta, J.K.; Yadav, R.K.; Dudhe, R.; Sharma, P.K. *Int. J. Pharm. Tech. Res.,* **2010**, *2*, 1493-1507.

[32] Li, P.; Shi, L.; Gao, M-N.; Yang, X.; Xue, W.; Jin, L-H.; Hu, D-Y.; Song, B-A. *Bioorg. Med. Chem. Lett.,* **2015**, *25*(3), 481-484. http://dx.doi.org/10.1016/j.bmcl.2014.12.038 PMID: 25563889

[33] Gür, M.; Muglu, H.; Çavus, M.S.; Güder, A.; Sayiner, H.S.; Kandemirli, F. *J. Mol. Struct.,* **2017**, *1134*, 40-50. http://dx.doi.org/10.1016/j.molstruc.2016.12.041

[34] Chen, Z.; Xu, W.; Liu, K.; Yang, S.; Fan, H. *Molecules,* **2010**, *15*, 9046-9056. http://dx.doi.org/10.3390/molecules15129046 PMID: 21150824

[35] Kaur, H.; Kumar, S.; Vishwakarma, P.; Sharma, M.; Saxena, K.K.; Kumar, A. *Eur. J. Med. Chem.,* **2010**, *45*(7), 2777-2783. http://dx.doi.org/10.1016/j.ejmech.2010.02.060 PMID: 20392546

[36] Hafez, H.N.; Hegab, M.I.; Ahmed-Farag, I.S.; El-Gazzar, A.B.A. *Bioorg. Med. Chem.,* **2008**, *18*, 4538-4543. http://dx.doi.org/10.1016/j.bmcl.2008.07.042

[37] Turner, S.; Myers, M.; Gadie, B.; Nelson, A.J.; Pape, R.; Saville, J.F.; Doxey, J.C.; Berridge, T.L. *J. Med. Chem.,* **1988**, *31*, 902-906. http://dx.doi.org/10.1021/jm00400a003 PMID: 3361578

[38] Ragab, F.A.; Heiba, H.I.; El-Gazzar, M.G.; Abou-Seri, S.M.; El-Sabbagh, W.A.; El-Hazek, R.M. *J. Photochem. Photobiol. B,* **2017**, *166*, 285-300. http://dx.doi.org/10.1016/j.jphotobiol.2016.12.007 PMID: 28013183

[39] El-Gohary, N.S.; Shaaban, M.I. *Eur. J. Med. Chem.,* **2013**, *63*, 185-195. http://dx.doi.org/10.1016/j.ejmech.2013.02.010 PMID: 23474904

[40] Balaji, K.; Bhatt, P.; Mallika, D.; Jha, A. *Int. J. Pharm. Pharm. Sci.,* **2015**, *7*, 145-149.

[41] Pattan, S.R.; Kekare, P.; Dighe, N.S.; Nirmal, S.A.; Musmade, D.S.; Parjane, S.K.; Daithankar, A.V. *J. Chem. Pharm. Res.,* **2009**, *1*, 191-198.

[42] Choy, D.S.; Arandia, J.; Rosenbaum, I. *Int. J. Cancer,* **1967**, *2*(2), 189-193. http://dx.doi.org/10.1002/ijc.2910020213 PMID: 6039768

[43] Dalvie, D.K.; Kalgutkar, A.S.; Khojasteh-Bakht, S.C.; Obach, R.S.; O'Donnell, J.P. *Chem. Res. Toxicol.,* **2002**, *15*(3), 269-299. http://dx.doi.org/10.1021/tx015574b PMID: 11896674

[44] Horne, W.S.; Yadav, M.K.; Stout, C.D.; Ghadiri, M.R. *J. Am. Chem. Soc.,* **2004**, *126*(47), 15366-15367. http://dx.doi.org/10.1021/ja0450408 PMID: 15563148

[45] Kolb, H.C.; Finn, M.G.; Sharpless, K.B. *Angew. Chem. Int. Ed.,* **2001**, *40*, 2004-2021. http://dx.doi.org/10.1002/1521-3773(20010601)40:11<2004::AID-ANIE2004>3.0.CO;2-5

[46] Kolb, H.C.; Sharpless, K.B. *Drug Discov. Today,* **2003**, *8*(24), 1128-1137. http://dx.doi.org/10.1016/S1359-6446(03)02933-7 PMID: 14678739

[47] Cho, S.; Oh, S.; Um, Y.; Jung, J-H.; Ham, J.; Shin, W-S.; Lee, S. *Bioorg. Med. Chem. Lett.,* **2009**, *19*(2), 382-385. http://dx.doi.org/10.1016/j.bmcl.2008.11.067 PMID: 19081249

[48] Al-Masoudi, N.A.; Al-Soud, Y.A. *Tetrahedron Lett.,* **2002**, *43*, 4021-4022. http://dx.doi.org/10.1016/S0040-4039(02)00733-5

[49] Kumar, K.K.; Seenivasan, S.P.; Kumar, V.; Das, T.M. *Carbohydr. Res.,* **2011**, *346*, 2084-2090. http://dx.doi.org/10.1016/j.carres.2011.06.028 PMID: 21767828

[50] Lal, K.; Kaushik, C.P.; Kumar, A. *Med. Chem. Res.,* **2015**, *24*, 3258-3271. http://dx.doi.org/10.1007/s00044-015-1378-9

[51] da Silva, F.C.; de Souza, M.C.B.V.; Frugulhetti, I.I.P.; Castro, H.C.; Souza, S.L.O.; de Souza, T.M.L.; Rodrigues, D.Q.; Souza, A.M.T.; Abreu, P.A.; Passamani, F.; Rodrigues, C.R.; Ferreira, V.F. *Eur. J. Med. Chem.,* **2009**, *44*, 373-383. http://dx.doi.org/10.1016/j.ejmech.2008.02.047 PMID: 18486994

[52] Costa, M.S.; Boechat, N.; Rangel, E.A.; da Silva, Fde.C.; de Souza, A.M.T.; Rodrigues, C.R.; Castro, H.C.; Junior, I.N.; Lourenço, M.C.S.; Wardell, S.M.S.V.; Ferreira, V.F. *Bioorg. Med. Chem.,* **2006**, *14*(24), 8644-8653. http://dx.doi.org/10.1016/j.bmc.2006.08.019 PMID: 16949290

[53] Kumar, K.; Pradines, B.; Madamet, M.; Amalvict, R.; Kumar, V. *Eur. J. Med. Chem.,* **2014**, *86*, 113-121. http://dx.doi.org/10.1016/j.ejmech.2014.08.053 PMID: 25147153

[54] Bokor, E.; Docsa, T.; Gergely, P.; Somsák, L. *Bioorg. Med. Chem.,* **2010**, *18*(3), 1171-1180. http://dx.doi.org/10.1016/j.bmc.2009.12.043 PMID: 20080412

[55] Biagi, G.; Dell'Omodarme, G.; Ferretti, M.; Giorgi, I.; Livi, O.; Scartoni, V.; Tiscione, E. *Farmaco,* **1990**, *45*(11), 1181-1192. PMID: 2128450

[56] Ferreira, S.B.; Sodero, A.C.R.; Cardoso, M.F.C.; Lima, E.S.; Kaiser, C.R.; Silva, F.P., Jr; Ferreira, V.F. *J. Med. Chem.,* **2010**, *53*(6), 2364-2375. http://dx.doi.org/10.1021/jm901265h PMID: 20170190

[57] Cunha, A.C.; Figueiredo, J.M.; Tributino, J.L.M.; Miranda, A.L.P.; Castro, H.C.; Zingali, R.B.; Fraga, C.A.M.; de Souza, M.C.B.V.; Ferreira, V.F.; Barreiro, E.J. *Bioorg. Med. Chem.,* **2003**, *11*, 2051-2059. http://dx.doi.org/10.1016/S0968-0896(03)00055-5 PMID: 12670656

[58] Felder, C.C.; Ma, A.L.; Liotta, L.A.; Kohn, E.C. *J. Pharmacol. Exp. Ther.,* **1991**, *257*(3), 967-971. PMID: 1646332

[59] Kohn, E.C.; Sandeen, M.A.; Liotta, L.A. *Cancer Res.,* **1992**, *52*(11), 3208-3212. PMID: 1591730

[60] Wasilenko, W.J.; Palad, A.J.; Somers, K.D.; Blackmore, P.F.; Kohn, E.C.; Rhim, J.S.; Wright, G.L., Jr; Schellhammer, P.F. *Int. J. Cancer,* **1996**, *68*(2), 259-264. http://dx.doi.org/10.1002/(SICI)1097-0215(19961009)68:2<259::AID-IJC20>3.0.CO;2-4 PMID: 8900438

[61] Berrie, A.H.; Newbold, G.T.; Spring, F.S. *J. Chem. Soc.,* **1952**, 2042-2046. http://dx.doi.org/10.1039/jr9520002042

[62] Kovackova, S.; Chang, L.; Bekerman, E.; Neveu, G.; Barouch-Bentov, R.; Chaikuad, A.; Heroven, C.; Šála, M.; De Jonghe, S.; Knapp, S.; Einav, S.; Herdewijn, P. *J. Med. Chem.,* **2015**, *58*(8), 3393-3410. http://dx.doi.org/10.1021/jm501759m PMID: 25822739

[63] Rao, V.R.; Srinivasan, V.R. *Indian J. Chem.,* **1970**, *8*, 509-513.

Growth hormone induces Notch1 signaling in podocytes and contributes to proteinuria in diabetic nephropathy

Received for publication, April 19, 2019, and in revised form, August 28, 2019 Published, Papers in Press, September 11, 2019, DOI 10.1074/jbc.RA119.008966

Rajkishor Nishad[‡], **Dhanunjay Mukhi**[‡], **Syed V. Tahaseen**[§], **Sathish Kumar Mungamuri**[¶], **and Anil K. Pasupulati**[‡1]

From the [‡]*Department of Biochemistry, School of Life Sciences, University of Hyderabad, Hyderabad, India 500046, the* [§]*Department of Biochemistry, SRR & CVR Degree College, Vijayawada, India 520010, and the* [¶]*Division of Food Safety, National Institute of Nutrition, Hyderabad, India 500007*

Edited by Jeffrey E. Pessin

Growth hormone (GH) plays a significant role in normal renal function and overactive GH signaling has been implicated in proteinuria in diabetes and acromegaly. Previous results have shown that the glomerular podocytes, which play an essential role in renal filtration, express the GH receptor, suggesting the direct action of GH on these cells. However, the exact mechanism and the downstream pathways by which excess GH leads to diabetic nephropathy is not established. In the present article, using immortalized human podocytes *in vitro* and a mouse model *in vivo*, we show that excess GH activates Notch1 signaling in a γ-secretase–dependent manner. Pharmacological inhibition of Notch1 by γ-secretase inhibitor DAPT (*N*-[*N*-(3,5-Difluorophenacetyl)-L-alanyl]-*S*-phenyl glycine *t*-butylester) abrogates GH-induced epithelial to mesenchymal transition (EMT) and is associated with a reduction in podocyte loss. More importantly, our results show that DAPT treatment blocks cytokine release and prevents glomerular fibrosis, all of which are induced by excess GH. Furthermore, DAPT prevented glomerular basement membrane thickening and proteinuria induced by excess GH. Finally, using kidney biopsy sections from people with diabetic nephropathy, we show that Notch signaling is indeed up-regulated in such settings. All these results confirm that excess GH induces Notch1 signaling in podocytes, which contributes to proteinuria through EMT as well as renal fibrosis. Our studies highlight the potential application of γ-secretase inhibitors as a therapeutic target in people with diabetic nephropathy.

Renal interstitial fibrosis is the hallmark of progressive chronic kidney disease, which correlates well with renal failure (1). Renal fibrosis is characterized by myofibroblast proliferation and activation, epithelial cell dysfunction, leukocyte migration, excessive production, and deposition of extracellular matrix (2). In response to kidney damage, there will be infiltration of mature myofibroblasts from various sources including interstitial fibroblasts, pericytes, endothelial cells, and circulating fibrocytes (2). Previous studies have shown that multiple pathways such as the transforming growth factor-β (TGF-β)[2]/Smad2/3 and Notch signaling are involved in epithelial cell dysfunction and fibroblast activation, which leads to the progression of kidney fibrosis (2).

In the early glomerular development, particularly at the S-shaped body formation, podocyte fate determination is regulated by the highly conserved Notch signaling, which transduces short-range signals between neighboring cells (3–6). The Notch pathway comprises 4 transmembrane Notch receptors (Notch 1–4) and 5 Notch ligands (Delta-like 1, 3, and 4, and Jagged 1 and 2). After ligand binding, Notch receptors undergo a series of cleavages catalyzed by the ADAM proteases and γ-secretase complex, which results in the release of the Notch intracellular domain (NICD, Fig. S1); this process can be inhibited by the γ-secretase inhibitor and dibenzoazepine (7). The resulting NICD translocates into the nucleus (8), wherein it forms a ternary complex by associating with the DNA-binding protein, retinol-binding protein-jk and the coactivator, Mastermind-like protein 1 and activates expression of target genes (9–12).

Vooijs *et al.* (13) have reported that Notch1 is highly active in the developing kidney; however, in the mature kidney detection of active Notch1 is very little. Inhibition of Notch signaling during early development of the mouse kidney results in a severe deficiency of glomerular podocytes, indicating the importance of Notch signaling during kidney development (3). On the other hand, persistent activation of Notch signaling in the mature kidney leads to podocyte damage and subsequent kidney failure (14). Further studies had also shown that ectopic Notch activation in terminally differentiated podocytes is correlated with both diffuse mesangial sclerosis and focal segmental glomerulosclerosis, which are associated with *de novo* Pax2 expression and p53-induced podocyte apoptosis, respectively (14, 15). It was also observed that the genetic deletion of the

This work was supported by Science and Engineering Research Board Grant EMR/2015/2076 (to A. K. P.), Research Fellowships from the University Grants Commission, India (to R. N. and D. M.), and a Ramanujan Fellowship from Department of Science and Technology - Science and Engineering Research Board Grant (to S. K. M.). The authors declare that they have no conflicts of interest with the contents of this article.

This article contains Figs. S1–S5.

The microarray data reported in this paper have been submitted to the Gene Expression Omnibus (GEO) database under GEO accession no. GSE21327.

[1] To whom correspondence should be addressed. Tel.: 91-40-23134519; E-mail: pasupulati.anilkumar@gmail.com.

[2] The abbreviations used are: TGF-β, transforming growth factor β; NICD, Notch intracellular domain; GH, growth hormone; GBM, glomerular basement; EMT, epithelial to mesenchymal transition; qRT, quantitative RT; DAPT, *N*-[*N*-(3,5-difluorophenacetyl)-L-alanyl]-*S*-phenylglycine *t*-butyl ester; UACR, urinary albumin-creatinine ratio; GFR, glomerular filtration rate; DN, diabetic nephropathy; PAS, periodic acid-Schiff; TEM, transmission electron microscope; DAPI, 4′,6-diamidino-2-phenylindole; α-SMA, α-smooth muscle actin.

Notch pathway in tubular epithelial cells ameliorates renal fibrosis in the unilateral ureteral obstruction murine model and folic acid-induced renal fibrosis (16). These data reveal that Notch signaling plays an essential role in the fibrotic pathogenesis. However, the precise underlying cellular mechanisms are not fully understood.

Although many studies show that the role of Notch1 signaling in glomerular diseases (17–19), the correlation between activated Notch1 signaling and diabetic proteinuria remains to be elucidated. Elevated levels of circulating growth hormone (GH) are associated with the development of nephropathy in "type 1 diabetes" and "acromegaly" (20, 21). Conditions of elevated GH are typified by hyperfiltration, glomerulosclerosis, and albuminuria. On the other hand, both decreased GH secretion and action can protect from glomerular complications (22). Previously, we have established the role of GH on glomerular cells, particularly on podocytes (23, 24). Our present study demonstrates that excess GH activates Notch signaling in human podocytes as well as in the murine kidneys. Blocking the activated Notch signaling through pharmacological inhibition of γ-secretase function reverted the excess GH-induced kidney fibrosis, interstitial infiltration of plasma-lymphocytic cells and proteinuria, hindered the glomerular basement membrane (GBM) thickening with severe foot process effacement in mice as well as epithelial to mesenchymal transition (EMT) and fibrotic marker expression of podocytes. Our present study demonstrates that an elevated level of circulatory GH after embryonic development may compromise the podocyte function by activation of Notch signaling and could represent a new pharmacological target.

Results

GH induces Notch1 activation in immortalized human podocytes

To identify the biochemical pathways downstream of GH signaling that are hyperactivated in podocytes in response to excess GH, we previously performed microarray analysis (GEO accession number GSE21327) on immortalized human podocytes treated with GH and identified transcriptional activation of EMT regulator "ZEB2" (24). By reanalyzing the same microarray data, we now identified that in response to GH treatment, Notch1 signaling is up-regulated in human podocytes (Fig. S2). To reconfirm the up-regulation of Notch signaling pathway by GH in podocytes, we also analyzed the expression of Notch1 and its targets Hes1 and Jag1 in nondiabetic mouse kidney ($n = 18$) *versus* diabetic nephropathy mouse kidney ($n = 21$) in the Hodgin diabetes mouse glomerulus data set available at Nephroseq (https://nephroseq.org),[3] which shows that diabetic nephropathy kidneys overexpress Notch1 and its target genes, *Hes1* and *Jag1* (Fig. 1*A*). Next, to validate the data obtained in our microarray analysis as well as that from Nephroseq, we measured the mRNA levels of both Notch1 and its target genes by quantitative RT (qRT)-PCR, and as expected, the levels of Notch1 (full-length) and its targets were up-regulated with GH treatment in the human podocytes (Fig. 1*B*). GH had induced the expression of activated Notch1 (NICD1) and its target proteins in both concentration (Fig. 1*C*) and time-dependent (Fig. 1*D*) manners. γ-Secretase is an intramembrane protease that cleaves many membrane proteins including Notch1, which generates the NICD1 (25). Accordingly, we also observed a time-dependent increase in γ-secretase activity with GH treatment in human podocytes (Fig. 1*E*). All these data suggests that Notch1 signaling is up-regulated in response to GH treatment in human podocytes.

γ-Secretase activity is required for GH-mediated Notch activation

To confirm the role of γ-secretase in GH-induced Notch1 activation, we next treated the human podocytes with GH in the absence or presence of well-established γ-secretase inhibitor, DAPT (*N*-[*N*-(3,5-difluorophenacetyl)-L-alanyl]-*S*-phenylglycine *t*-butyl ester). As expected, DAPT treatment to the GH-exposed human podocytes has decreased the γ-secretase activity in a time-dependent manner (Fig. 2*A*). GH was not able to induce the expression of Notch1 or its target genes (*Hes1* and *Hey1*) in the presence of DAPT in human podocytes as measured by qRT-PCR (Fig. 2*B*), Western blotting (Fig. 2*C*), and immunofluorescence (Fig. 2*D*). Furthermore, we continued our quest of understanding the effect of GH on Notch signaling *in vivo*. Similar to the observations *in vitro*, GH treatment led to the induction of NICD1, Jag1, and NICD targets: Hes1 and Hey1 in glomerular sections from mice as measured with immunostaining (Fig. 3, *A–D*) and Western blotting (Fig. 3, *E* and *F*). DAPT inhibited NICD1 accumulation and induction of its targets in glomerular sections (Fig. 3, *A*, *C*, and *D*), glomerular lysates (Fig. 3*E*), and primary podocytes (Fig. 3*F*) isolated from GH-treated mice. However, the expression of Jag1 was unaffected by DAPT treatment (Fig. 3, *B*, *E*, and *F*). It should be noted that the data from isolated podocytes corroborate with that from glomerular lysate (Fig. 3, *E* and *F*). Together, the data confirm that GH stimulates NICD1 expression in glomeruli and podocytes, and functional γ-secretase is required to activate GH-dependent Notch1 signaling.

Activated Notch signaling is required for GH-induced EMT in podocytes

Previously, we established that excess GH elicits EMT in podocytes (24). Thus, we analyzed the influence of Notch signaling in GH-induced EMT in podocytes. GH treatment induced the EMT markers (E-Cad, N-Cad, Snail, Slug, ZEB2, Vimentin, and α-SMA) in human podocytes and mouse glomerulus as shown at both mRNA (Fig. 4*A*) and protein levels (Fig. 4, *B* and *C*). DAPT treatment abrogated this effect of GH in human podocytes (Fig. 4, *A* and *B*) and mouse glomerulus (Fig. 4*C*).

Remodeling of actin filaments is necessary for EMT (26). To confirm the physiological function of EMT induced by GH, we next performed the phalloidin staining of the podocytes treated with GH, with or without DAPT treatment. The results presented in Fig. 4*D* suggests that there is complete disorganization of the actin filaments in the podocytes treated with GH, and can be rescued by co-treatment with DAPT (Fig. 4*D*). Quantification of F-actin stress fiber distribution revealed a sig-

[3] Please note that the JBC is not responsible for the long-term archiving and maintenance of this site or any other third party hosted site.

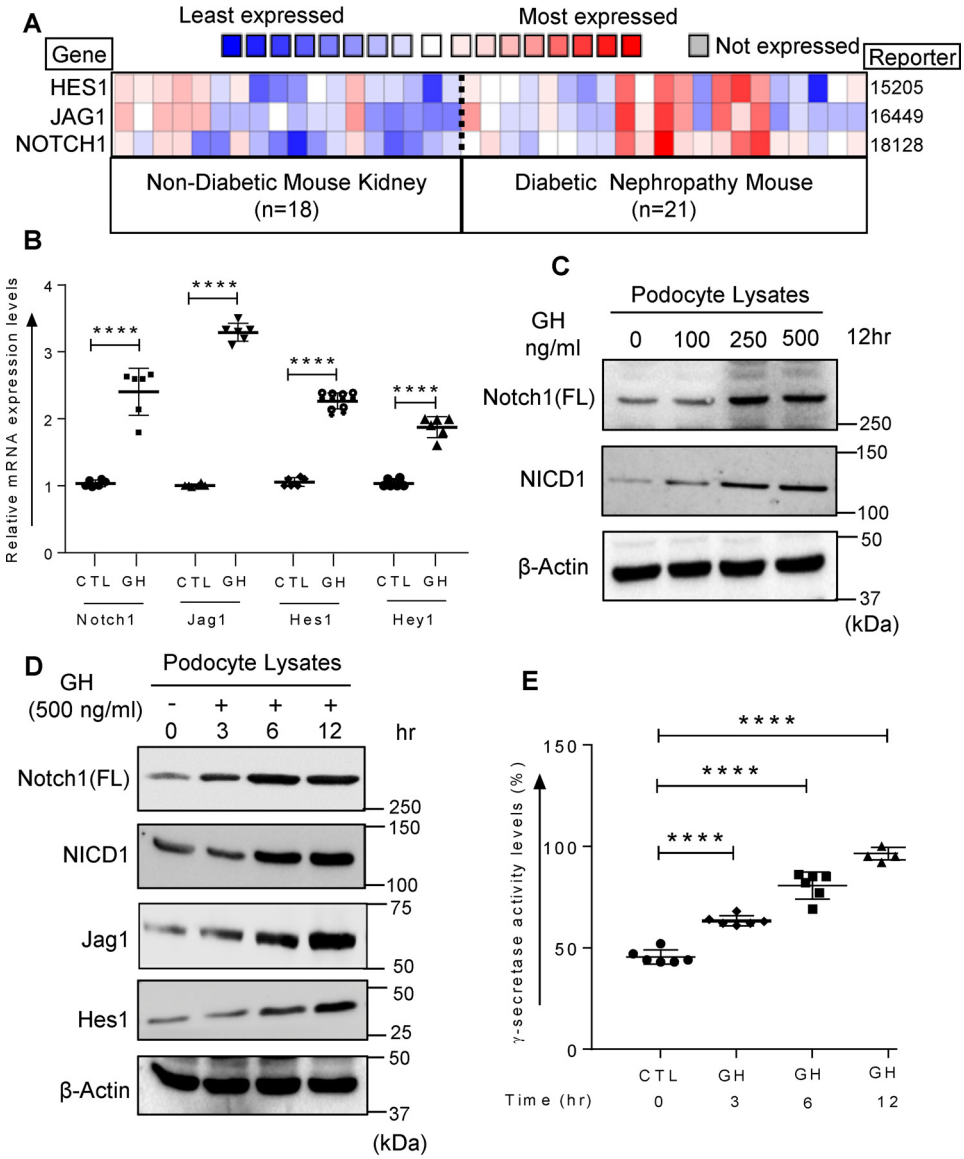

Figure 1. GH induces Notch1 activation in immortalized human podocytes. *A*, Nephroseq (University of Michigan O'Brien Renal Center, Michigan, Ann Arbor, MI) analysis comparing *HES1*, *JAG1*, and *NOTCH1* expression levels from nondiabetic mouse kidney ($n = 18$) *versus* diabetic nephropathy mouse kidney ($n = 21$) in Hodgin diabetes mouse glomerulus. Data indicate that expression of these genes increased >1.5-fold in the diabetic group. *B*, qRT-PCR analysis showing the expression of Notch pathway genes (*Notch1*, *Jag1*, *Hes1*, and *Hey1*) in human podocytes treated with GH (500 ng/ml) or without GH (*CTL*) for 30 min. mRNA levels were normalized to β-Actin levels and presented as fold-change on the *y* axis. ****, $p < 0.0001$. *C*, immunoblotting analysis showing the expression of Notch1 full-length (*FL*), active Notch1 (NICD1), and β-Actin in human podocytes treated with GH (100 to 500 ng/ml) for 12 h. *D*, immunoblotting analysis showing the expression of Notch1 (*FL*), NICD1, Jag1, Hes1, and β-Actin in human podocytes treated with GH (500 ng/ml) or the indicated time intervals (0 to 12 h). *E*, γ-secretase activity in human podocytes treated with or without GH (500 ng/ml) for 0–12 h. ****, $p < 0.0001$. Data represent the mean ± S.D. ($n = 6$) and statistical significance was analyzed by Student's *t* test.

nificant loss (60 ± 5%) of stress fibers in podocytes exposed to GH, whereas DAPT ameliorated GH-induced injury to the actin stress fibers (Fig. 4*E*).

Furthermore, to confirm the role of Notch1 signaling in GH-induced EMT in the podocytes, we also performed the cell migration assay. Although GH treatment alone to the podocytes completely covered the wound by 12 h, DAPT treatment abrogated this GH-induced phenotype (Fig. 4*F*). Quantification of wound coverage in response to CTL, GH, and GH + DAPT exposure, GH solely enhanced the migration of podocytes (90 ± 8%, Fig. 4*G*). All these results confirm that excess GH induces EMT in the podocytes and activated Notch signaling is essential for GH-induced EMT in podocytes.

Activated Notch signaling is required for GH-induced interstitial infiltration of plasma-lymphocytic cells and fibrosis in kidneys

Diabetes is characterized by mild, but significant glomerulosclerosis, and GH has been shown to contribute to the glomerulosclerosis (27). Next, we treated the mice with GH and prepared the paraffin-embedded kidney sections to look for interstitial infiltration of plasma-lymphocytic cells. As previously noted, our hematoxylin and eosin staining of the kidney sections showed interstitial infiltration of plasma-lymphocytic cells in mice treated with the GH (Fig. 5*A*). We also observed enhanced fibrosis in the mice kidneys treated with the GH, as analyzed by both periodic acid-Schiff (PAS) (Fig. 5*B*) and Mas-

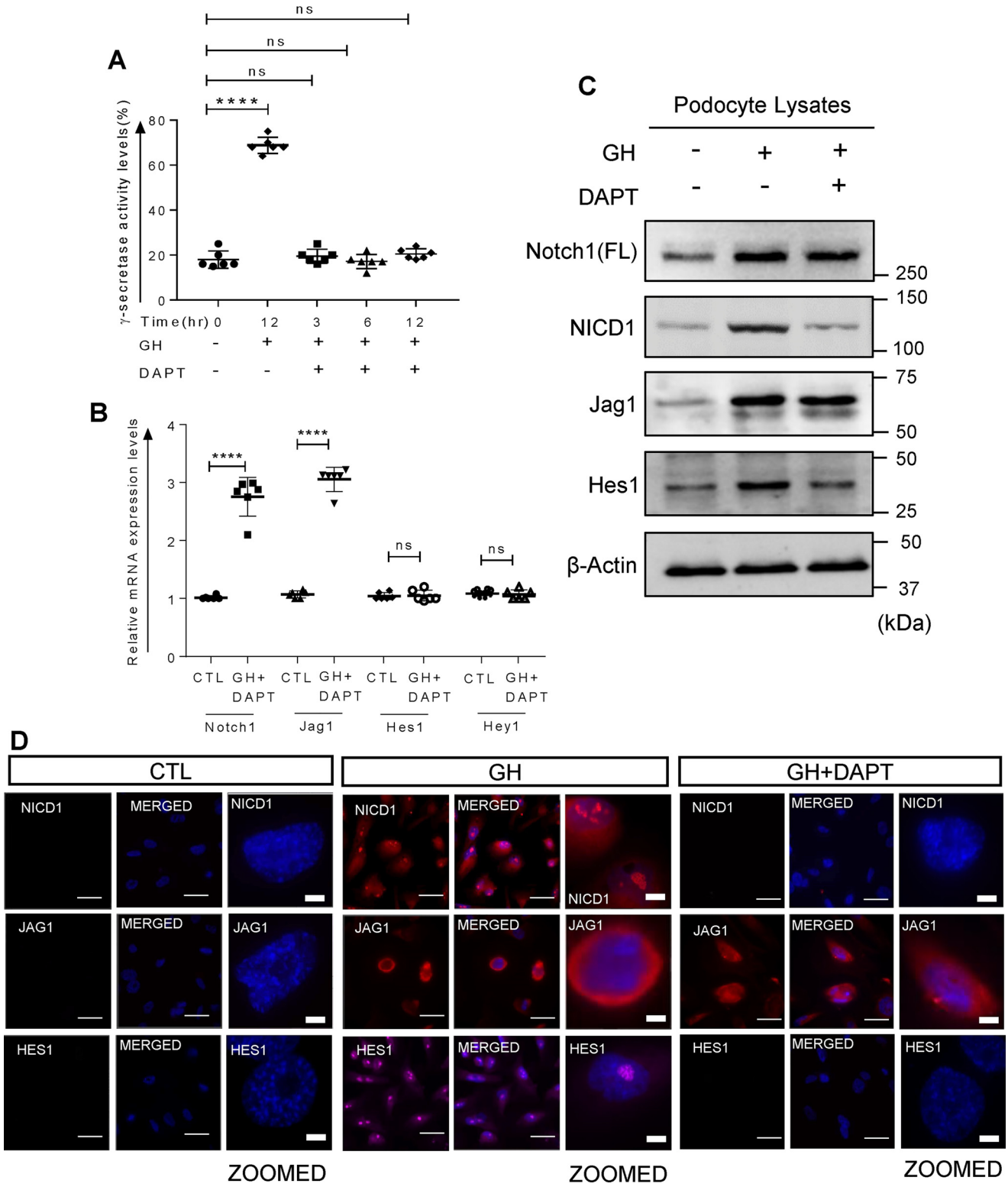

Figure 2. DAPT limits the hyperactive Notch signaling in human podocytes by inhibiting the γ-secretase activity. *A*, γ-secretase activity in human podocytes treated with GH or GH + DAPT for the indicated time intervals (3–12 h). ****, $p < 0.0001$, *ns*, not significant. *B*, qRT-PCR analysis showing the expression of *Notch1*, *Jag1*, *Hes1*, and *Hey1* in human podocytes treated with GH (500 ng/ml) + DAPT (5 μg/ml). β-Actin was used as an internal control. ****, $p < 0.0001$. *C*, immunoblotting analysis showing the expression of Notch1 (*FL*), NICD1, Jag1, and Hes1 in CTL, GH, and GH + DAPT-treated (12 h) human podocytes. *D*, immunofluorescence analysis for NICD1, Jag1, and Hes1 in CTL, GH, and GH + DAPT treated (12 h) human podocytes (×630). *Scale bar* = 20 μm. Data presented as mean ± S.D. ($n = 6$) and statistical significance was analyzed by Student's *t* test.

son's trichrome (Fig. S3*A*) stainings. Quantification of the Masson's trichrome-stained area revealed that GH enhanced glomerular fibrosis (50 ± 10%, Fig. S3*B*). These data also correlated with increased expression of cytokines (Fig. 5*C*) and fibrotic marker in GH-treated mice, as measured at both mRNA and protein (Fig. S3, *C* and *D*) levels.

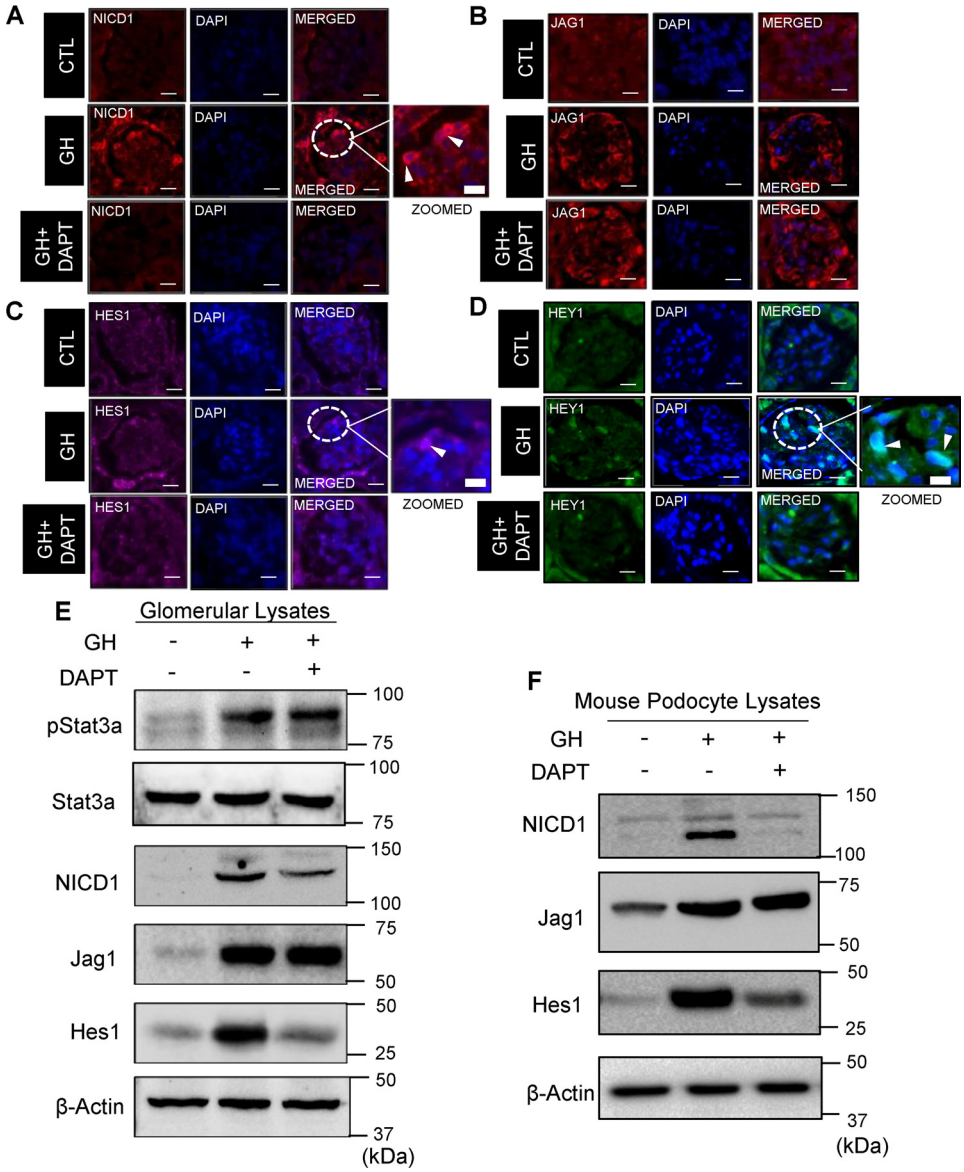

Figure 3. GH induces Notch signaling in glomerulus of mice kidney. *A–D*, representative images of immunostaining for NICD1 (*A*), Jag1 (*B*), Hes1 (*C*), and Hey1 (*D*) in glomeruli from CTL, GH, and GH + DAPT mice ($n = 6$). We employed DyLight 594-conjugated secondary antibody for NICD1 and Jag1; Cy5-conjugated secondary antibody for Hes1; and DyLight 488-conjugated secondary antibody for Hey1. These sections were counterstained with DAPI. *Scale bars* = 20 μm (×630). *E*, Western blot analysis showing the expression of pStat3a, total Stat3a, NICD1, Jag1, and Hes1 from CTL, GH, and GH + DAPT-treated mice glomerular lysates ($n = 6$). Expression of β-Actin was used as an internal control. *F*, Western blot analysis showing the expression of NICD1, Jag1, and Hes1 in primary mouse podocytes isolated from CTL, GH, and GH + DAPT- treated mice. Expression of β-Actin was used as an internal control. Data are presented as mean ± S.D. and statistical significance was calculated by using Student's *t* test.

Indeed, treatment of mice with DAPT had reversed the GH-induced nonresident cell infiltration into the kidneys (Fig. 5*A*) and was able to reverse the fibrosis as evidenced by periodic acid-Schiff (Fig. 5*B*) and Masson's trichrome (Fig. S3*A*) stainings. Mesangial expansion and glomerular damage score were found elevated with GH treatment (Fig. 5, *C* and *D*). DAPT treatment also inhibited the GH-induced cytokine and fibrotic gene induction (Fig. 5*E*); and reversed podocyte-specific marker genes expression as measured at both mRNA and protein levels (Fig. S3, *C* and *D*). To further evaluate whether the cytokines released from these podocytes are indeed functional, and DAPT blocked the function of these cytokines, we next performed classical chemotaxis assay using J774A.1 macrophages. As expected, the macrophages were able to fill the gap, when treated with conditioned medium collected from podocytes treated with the GH, whereas this function was completely blocked when similar conditioned medium from podocytes treated with GH + DAPT was used (Fig. S4*A*). The conditioned medium from the untreated podocytes was used as a control. Quantification of the wound coverage in response to CTL, GH, GH + DAPT, and C5a exposure, GH-treated spent medium solely enhanced the migration of J774A.1 macrophages (70 ± 10% increase, $p < 0.001$, Fig. S4*B*).

Kidney fibrosis leads to thickening of the GBM, which consequently results in podocyte foot process effacement (28). To confirm whether a similar phenomenon also happens in our GH-induced proteinuria mice model, we next performed transmission EM studies to analyze the structural changes in the

GBM as well as podocyte foot processes in mice kidney samples. Our results show that whereas GH treatment in the mice leads to GBM thickening and podocyte foot process effacement, similar treatment of GH along with DAPT completely abrogated this effect (Fig. 5, *F* and *G*). All these results confirm that excess GH activates Notch1 signaling, which in turn leads to infiltration of circulating cells in the kidneys and leading to its fibrosis.

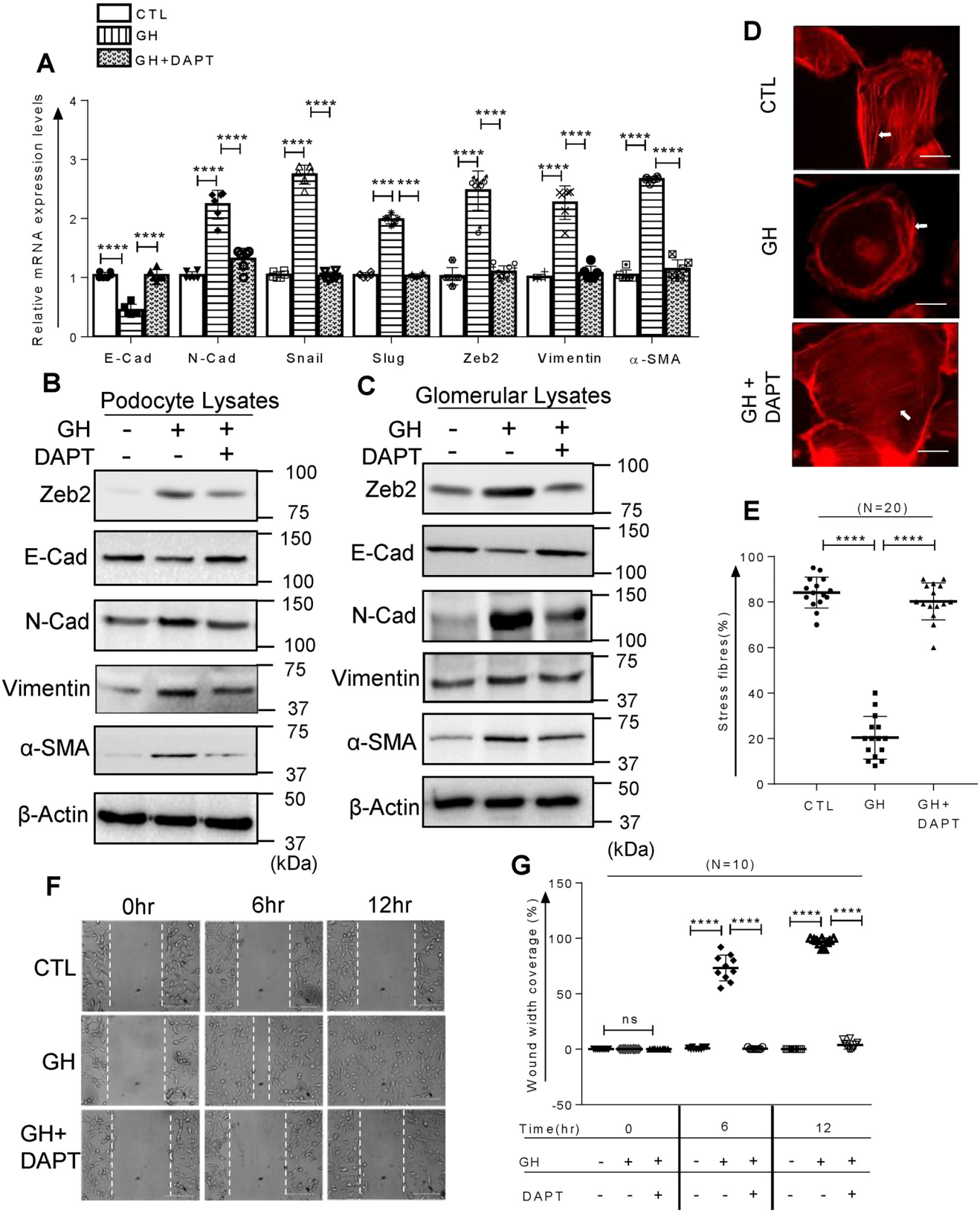

Blocking activated Notch1 signaling abrogates GH-induced proteinuria

Previously, we showed that GH treatment to rodents induces loss of podocyte number (23). GH-treated mice kidney sections were probed for WT1, which specifically express in podocytes. Our data reconfirm that GH treatment results in depletion of podocytes (Fig. 6, *A* and *B*). We also confirmed that GH treatment reduced the physiological functional ability of the kidneys in the mice as analyzed by an increase in urinary albumin-creatinine ratio (UACR) (Fig. 6*C*), and decrease in glomerular filtration rate (GFR) (Fig. 6*D*). We also assessed the extent of proteinuria in GH-treated mice by analyzing the urinary protein content on SDS-PAGE and staining with silver nitrate. GH treatment had increased the amount of protein in urine. Co-treatment of mice with DAPT has rescued the decrease in podocyte number induced by the GH (Fig. 6, *A* and *B*). We also observed that DAPT ameliorated GH-induced UACR (Fig. 6*C*) and GH-induced loss of GFR (Fig. 6*D*). Finally, DAPT also blocked the proteinuria induced by the GH in these mice (Fig. 6*E*). Albumin influx assay (*in vitro*) revealed that DAPT has prevented GH-induced albumin leakage across podocyte monolayer (Fig. 6*F*). Together the data suggest that excess GH impair the podocyte function and induces proteinuria through activated Notch1 signaling.

Notch signaling is hyperactivated in people with diabetic nephropathy

Finally, to confirm the results obtained so far that excess GH induces activated Notch1 signaling in humans, we evaluated the extent of NICD1 expression in people with diabetic nephropathy (DN). As expected, urine from these people showed higher albumin (Fig. S5*A*) and elevated serum creatinine (Fig. S5*B*) levels and decreased glomerular filtration rate (Fig. S5*C*). We observed that there is more urinary protein in these patients as observed by Coomassie Brilliant Blue staining of the urine samples (Fig. 7*A*). Immunohistochemical analysis of the kidney sections from people with diabetes showed increased NICD1, Jag1, and Hes1 expression compared with the healthy controls (Fig. 7*B*). Furthermore, we observed elevated expression of EMT markers α-SMA, N-Cad, and Vimentin in glomerulus in patients with diabetic nephropathy (Fig. 7, *C–F*). All these data confirm that people with diabetic nephropathy have elevated functional Notch signaling in their kidney glomeruli and enhanced expression of EMT markers.

Discussion

In the present article, we show that GH activates Notch1 signaling in podocytes and pharmacological inhibition of γ-secretase blocks the GH-induced EMT induction, infiltration of nonresident cells, fibrosis, GBM thickening, and podocyte foot-process effacement. Glomerular sclerosis and albuminuria are associated with failure of the normal kidney functions. GH induces the albuminuria, whereas the γ-secretase inhibitor treatment under similar conditions kept a constant check on these parameters and thus protects the mice kidneys from fibrosis. More importantly, GH treatment in mice leads to proteinuria, a common symptom associated with diabetic nephropathy, which was successfully abrogated with the γ-secretase inhibitor treatment.

Notch signaling is essential during nephrogenesis, *i.e.* during the embryonic development of glomerular podocytes and proximal tubules (29). On the contrary, Notch signaling is not required for podocyte formation, beyond the stage of the S-shaped body (29, 30). Although, Niranjan *et al.* (14) showed that NICD1 induces apoptosis in rat podocytes, whereas in the experiments performed by Waters *et al.* (15) show that the podocyte-specific expression of NICD1 promoted severe proteinuria and showed evidence of foot-process effacement and progressive glomerulosclerosis. The differences in these two reports can be attributed toward different mice strains used in their studies. Lasagni *et al.* (31) demonstrated that persistent activation of Notch signaling results in mitotic catastrophe and inhibition of the Notch pathway in renal progenitors is prerequisite for the differentiation toward podocyte lineage. Expression of Notch was undetectable in the glomeruli from healthy adult kidneys, whereas a strong up-regulation was observed in podocytes in patients affected by glomerular disorders. Inhibition of Notch signaling in mouse models of focal segmental glomerulosclerosis reduced podocyte loss and improved proteinuria (31). Mice with podocyte-specific deletion of Notch1 were shown to be protected from DN (32). Similarly, podocyte-specific deletion of retinol-binding protein-jk, which is an important downstream component of canonical Notch signaling, has lowered the severity of proteinuria and reduced the podocyte injury in DN rodent model (14). However, the mechanism by which NICD1 is induced during the DN conditions is not yet known. The data presented in our study confirms that excess GH, commonly observed during the DN (33), activates Notch signaling in the podocytes and inhibition of this signaling by γ-secretase inhibitor blocks GH-induced proteinuria and foot-process effacement in mice.

EMT, as well as renal fibrosis, are the shared pathological hallmarks of progressive chronic kidney disease, which comes with diverse etiologies. Hyperglycemia was demonstrated to provoke podocyte EMT through several molecular mechanisms, including activation of Notch signaling (34). Podocyte-specific Notch activation leads to dedifferentiation and its shedding (14, 15). In different models, either treatment with

Figure 4. Activated Notch signaling is required for GH-induced EMT in podocytes. *A*, qRT-PCR analysis showing the expression of EMT markers (E-Cad, N-Cad, Snail, Slug, Zeb2, Vimentin, and α-SMA) in human podocytes treated with GH in the presence or absence of DAPT. β-Actin was used as an internal control. ****, $p < 0.0001$. *B* and *C*, Western blot analysis showing the expression of Zeb2, E-Cad, N-Cad, Vimentin, and α-SMA in (*B*) human podocytes and (*C*) mice glomerular lysates (CTL, GH, and GH + DAPT treatments). *D*, phalloidin staining of podocytes showing F-actin arrangement and changes in stress fibers (indicated by *white arrow*). *E*, phalloidin-stained F-actin stress fibers in podocytes are quantified by ImageJ and data are presented as mean ± S.D. ($n = 20$). ****, $p < 0.0001$. *Scale bars* = 20 μm (×630). *F*, wound healing assay was performed to determine the extent of motility of podocytes from CTL, GH, and GH + DAPT groups and images were captured at the indicated times (0–12 h) using an Olympus inverted microscope (×100) and *scale bar* = 100 μm. *G*, the % area of wound covered by cells was quantified by ImageJ. ****, $p < 0.0001$. Data are presented as mean ± S.D. and statistical significance was analyzed by Student's *t* test. Results shown are representative of three independent experiments.

γ-secretase inhibitors or reducing Notch transcriptional binding protein levels showed a significant amelioration of glomerular injury and fibrosis, demonstrating the role of Notch signaling in podocyte EMT (35, 36). Several upstream master regulators like Wnt and TGF-β etc., are shown to increase the Notch activity (37–39).

Our data indicate that GH induces activated Notch1 signaling in podocytes, and since during DN, GH is up-regulated (20), and we observed increased NICD1 in people with DN, we presume that during DN, GH activates Notch signaling in podocytes. In mice treated with GH, we have shown enhanced glomerulosclerosis and more importantly, DAPT treatment had

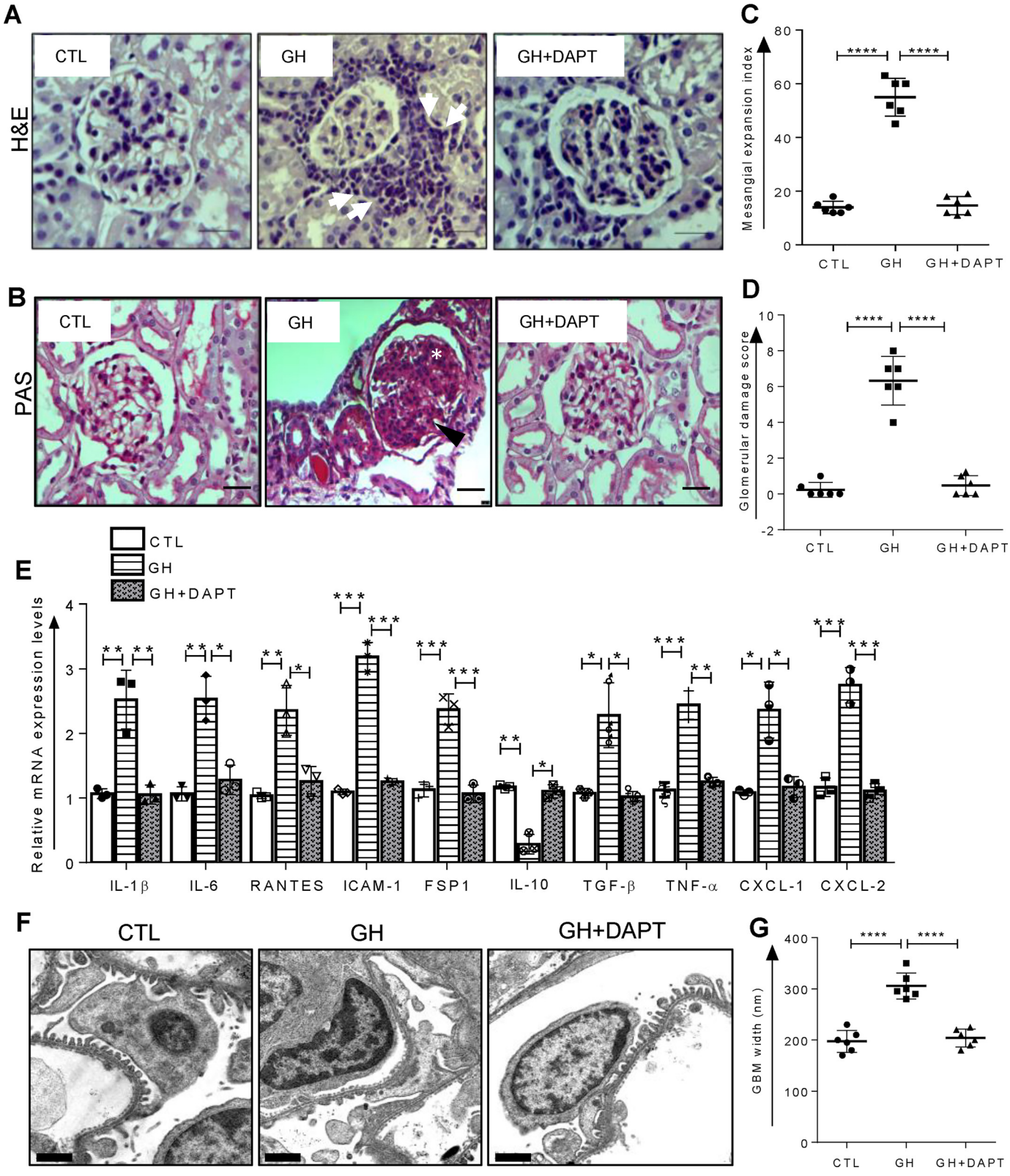

reduced the GH-induced glomerulosclerosis in these mice. Furthermore, our data indicate that activated Notch1 regulates the GH-induced EMT of the podocytes. We had shown previously that GH induces the expression of the EMT transcription factor, ZEB2, which transcriptionally down-regulates P- and E-cadherin expressions in the podocytes (24, 40). In the present article, we show that GH induces NICD1, and treatment of podocytes with γ-secretase inhibitor blocks GH-induced ZEB2 and thus EMT in podocytes.

TGF-β1 is a pro-sclerotic cytokine and it is accepted that TGF-β1 and its downstream SMAD signaling is involved in the development and progression of renal fibrosis in people with DN (41, 42). Studies from our laboratory report that GH regulates the bioavailability of TGF-β1 via regulating the expression of transforming growth factor-β-induced protein (TGFBIp) (23) and induces the expression of Smad-interacting protein, SIP1 (24). Recently, we identified that GH directly stimulates TGF-β expression in podocytes.[4] Whereas DAPT treatment successfully abrogated GH-induced Notch signaling, our data shows that DAPT was not able to reverse GH-induced Jag1 expression. TGF-β1 has been shown to independently regulate Jag1 and Hey1 expression in renal epithelial cells (43, 44). Furthermore, TGF-β–induced EMT can be inhibited by silencing either Hey1 or Jag1 as well as by chemical inactivation of Notch signaling (44). All these data suggest that there is a significant cross-talk between Notch and TGF-β signaling in fine-tuning the EMT phenomenon. How this cross-talk is specifically modulated during GH-depandant podocyte EMT and renal fibrosis needs further studies.

Preclinical studies have shown that DAPT could suppress the Notch signaling and also selective antibodies to preferentially target Notch receptors and ligands have proven successful (44). Based on our data that people with DN show stronger NICD1 staining in the podocytes, as well as blocking NICD1 function through γ-secretase inhibitor abrogates the proteinuria in mice, we believe that proteinuria and glomerulosclerosis in DN can be repressed using γ-secretase inhibitors. However, for the utilization of γ-secretase inhibitors, there are clinical concerns remaining over normal organ homeostasis and significant pathology in multiple organs. Because Notch signaling is not essential for the podocytes after embryonic development, we believe that tissue-specific administration of such inhibitors may offer protection against diabetic nephropathy.

[4] Mukhi D, Nishad R, Singh AK, Mungamuri SK and Pasupulati AK; unpublished data.

Experimental procedures

Reagents

The primary antibodies are as following: anti-activated Notch1 (ab8925), anti-WT-1(ab212951), anti-pSTAT3a (ab76315), anti-t-STAT3a (ab5073), anti-cleaved Notch1 (ab8925), anti-FSP1 (ab41532), and anti-HEY1 (ab154077) were purchased from Abcam (Cambridge, MA). Notch1 Full-length (FL) (number 3608), anti-E-Cadherin (number 3195), anti-N-Cadherin (number 13116), anti-αSMA (number 19245), anti-cleaved Notch1 (number 4147S), anti-ICAM-1 (number 4915), and anti-Actin (number 4970) were purchased from Cell Signaling Technology (Danvers, MA). The anti-HES1 (sc-166410) and anti-ZO-1 (sc-33725) were obtained from Santa Cruz Biotechnology (Dallas, TX). Anti-Vimentin (PAB040Hu01), anti-Col4 (PAA180Hu01), anti-Fibronectin (PAA037Hu01), and anti-JAG1 (PAB807Hu01) were purchased from Cloud-clone (Houston, TX). Anti-ZEB2 (PA5–20980) was purchased from Thermo Fisher Scientific. DAPT (D5942), SIGMAFAST DAB with Metal Enhancer Tablet Set (D0426), phalloidin fluorescein isothiocyanate labeled (P5282), and glutaraldehyde solution (G5882) were obtained from Sigma. Pink pre-stained marker protein (ABIN5662611, Nippon Genetics Europe), Precision Plus Protein Dual Color Standards (Bio-Rad, Hercules, CA), and ProLong™ Diamond Antifade Mountant (P36961) were purchased from Molecular Probes Life Technologies and DyLight 488 and DyLight 564, and Cy5-conjugated secondary antibody were obtained from Vector Laboratories (Burlingame, CA). Primers used in this study procured from Integrated DNA Technologies (Coralville, IA). cDNA reverse transcription kit and SYBR Green Master Mix reagents were obtained from Bio-Rad. All other reagents used were of analytical grade and obtained from Sigma.

Animals and tissues

All the experimental procedures for the animals were pre-approved by the Institutional Animal Ethics Committee of the University of Hyderabad, India. 8-Week-old Swiss Webster male mice weighing nearly 30 ± 5 g were used in this study. The mice were randomly assigned to three groups (6 mice per group): 1) control group (CTL), 2) GH-treated group, and 3) GH + DAPT-treated group. Experimental mice received a single i.p. dose of hGH (1.5 mg/kg/day), whereas control mice have received an equal volume of saline for 4 weeks. The inhibitor groups were received DAPT (10 mg/kg of body weight) per day prior to the GH treatment. After 4 weeks of the experimental period, the mice were placed in individual metabolic cages for collecting 24-h urine to estimate albumin and creatinine. An

Figure 5. Activated Notch signaling is required for GH-induced immune cell infiltration and fibrosis in kidneys. *A*, representative images of H&E staining in glomerular sections from CTL, GH, and GH + DAPT-treated mice. Interstitial infiltration of plasma-lymphocytic cells can be noticed in the GH-treated group (*white arrows*). *Scale bars* indicate 20 μm (×630). *B*, representative images of PAS staining in glomeruli from CTL, GH, and GH + DAPT-treated mice ($n = 6$). *Scale bars* = 20 μm (×630). *C*, mesangial expansion index from PAS-stained images was quantified using ImageJ. Each *dot* represents the average value of 20 glomeruli from a single animal of each group ($n = 6$). ***, $p < 0.004$. *D*, glomerular damage score was derived from PAS-stained images by summing the mesangial expansion (*asterisks*), glomerular capillary blockage, and adhesin of glomerular tuft to Bowman's capsule (*black arrowhead*). Each *dot* represents the average value of 20 glomeruli from a single animal from each group ($n = 6$). ***, $p < 0.004$. *E*, expression of cytokines and chemokines in human podocytes (CTL, GH, and GH + DAPT) was analyzed qRT-PCR. Expression of β-Actin was used as an internal control. *, $p < 0.05$; **, $p < 0.01$; and ***, $p < 0.004$. *F*, TEM images of glomeruli from CTL, GH, and GH + DAPT mice ($n = 6$). Thickening of GBM and effacement of podocyte foot processes was noticed predominantly in GH-treated mice. *Scale bars* indicate 0.5 μm. *G*, thickness of GBM was quantified as described under "Experimental procedures." Data are presented as mean ± S.D. and statistical significance were analyzed by Student's *t* test.

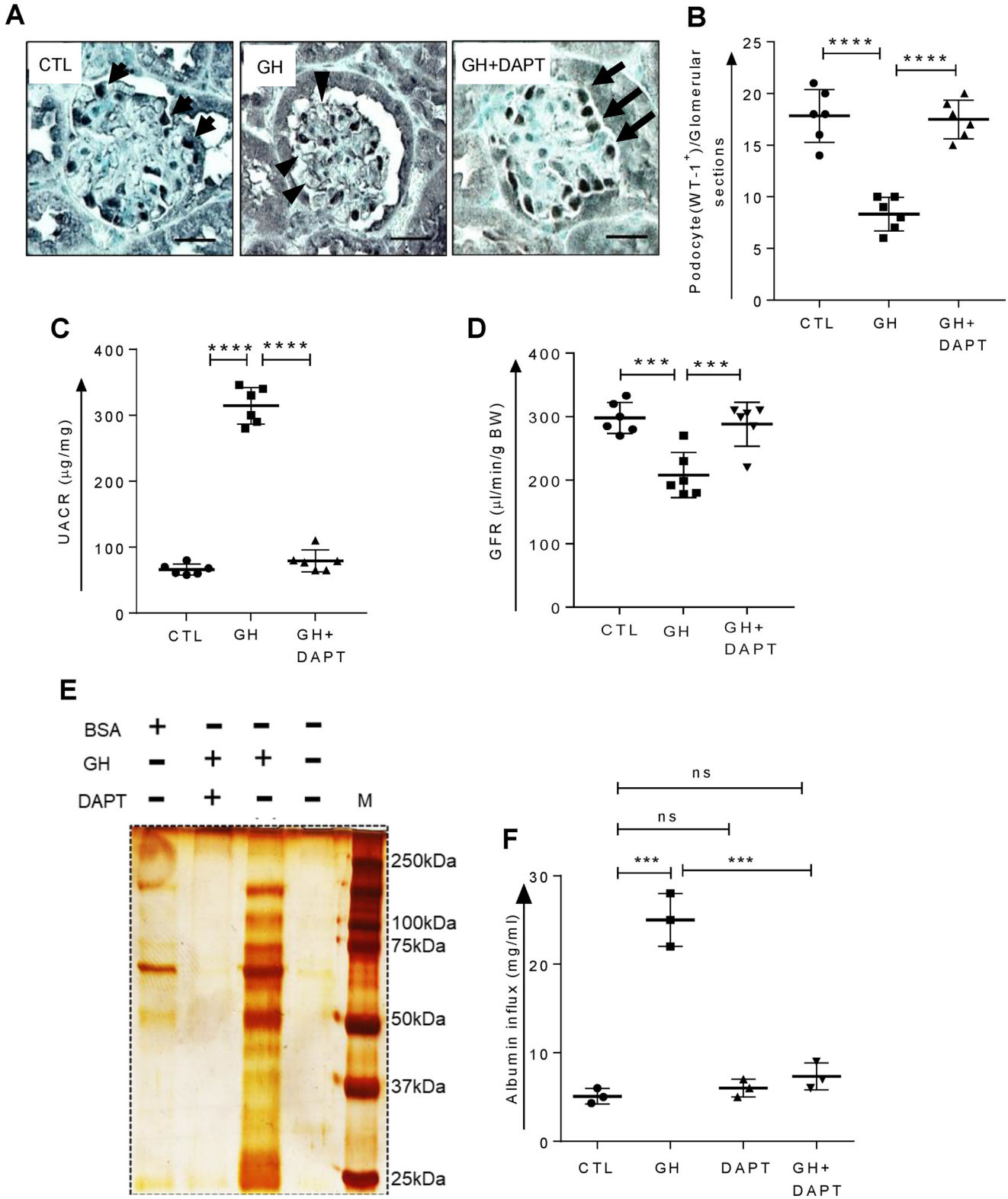

Figure 6. Blockade of Notch signaling protect mice from GH-induced proteinuria. *A*, representative images of immunohistochemical staining for WT1 (podocyte) in glomerulus from CTL, GH, and GH + DAPT-treated mice. *Scale bars* indicate 20 μm. *Arrow* indicates the podocyte and the arrow head indicates loss of podocyte. *B*, average number of $WT1^+$ cells from each mouse from CTL, GH, and GH + DAPT groups. ($n = 6$) **, $p < 0.01$ and ***, $p < 0.004$. We analyzed 20 glomeruli in each mouse for WT^+ cells. *C*, UACR was estimated in CTL, GH, and GH + DAPT-treated mice ($n = 6$). ***, $p < 0.004$; ***, $p < 0.004$. *D*, GFR in CTL, GH, and GH + DAPT-treated mice ($n = 6$). ***, $p < 0.004$. *E*, urinary samples from CTL, GH, and GH + DAPT group mice were subjected to SDS-PAGE and silver stained as described under "Experimental procedures." BSA was used as a standard. *F*, quantification of albumin influx across human podocyte monolayer after 4 h followed by treatment with GH, DAPT, and GH + DAPT for 12 h. ***, $p < 0.004$; *ns*, not significant. Data are presented as mean ± S.D. ($n = 3$) and statistical significance were analyzed by Student's *t* test.

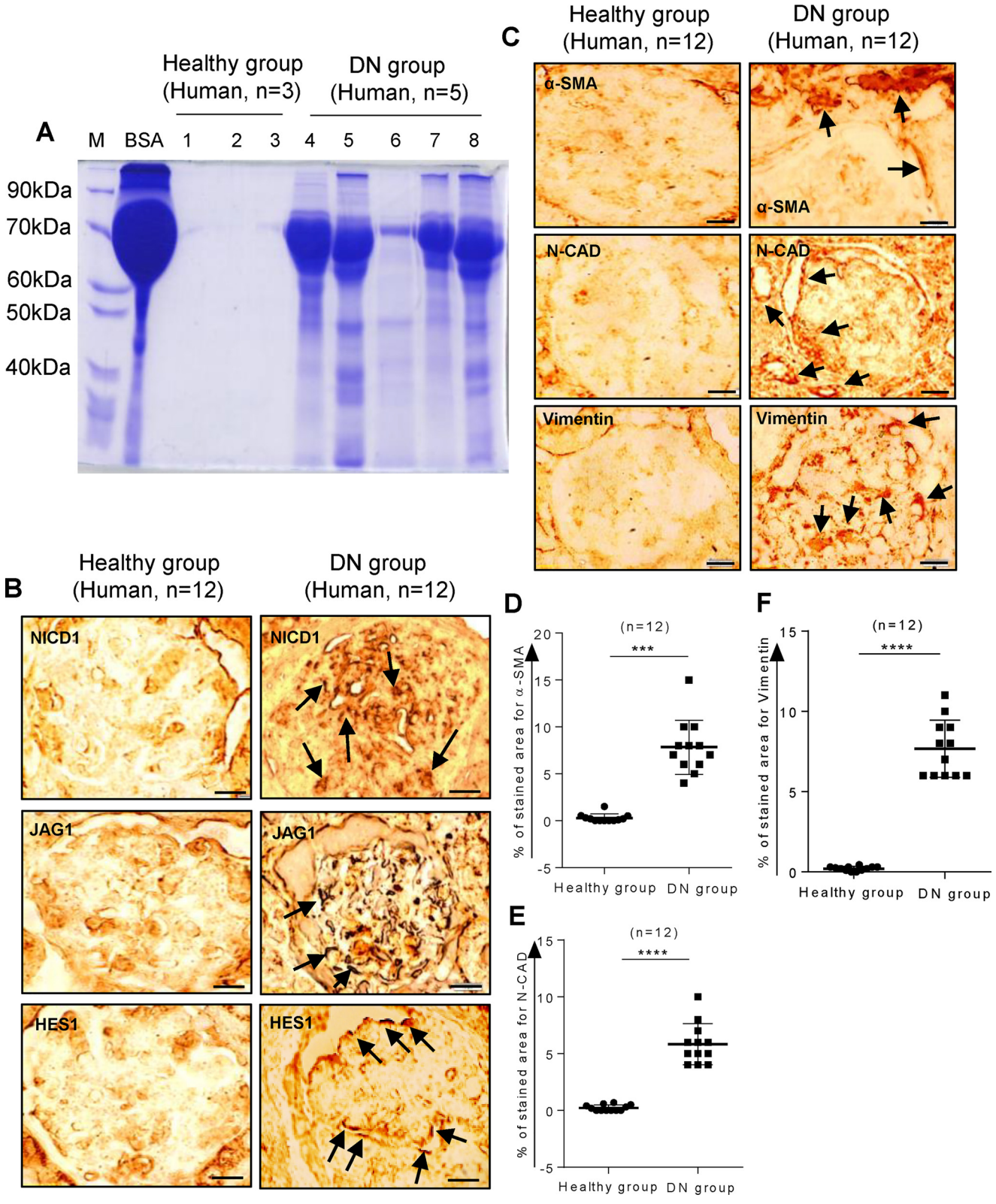

Figure 7. Elevated Notch pathway and EMT in podocytes and proteinuria in people with DN. *A*, urine samples from people with DN ($n = 5$) and healthy volunteers ($n = 3$) were resolved on SDS-PAGE and stained with Coomassie Blue. *B*, representative images of immunohistochemical staining for NICD1, Jag1, and Hes1 in glomerular sections from people with or without DN. *Scale bars* indicate 20 μm (×630). *C*, representative images of immunohistochemical staining for α-SMA, N-Cad, and Vimentin in glomerular sections from people with or without DN. *Scale bars* indicate 20 μm (×630). Quantification of expression of α-SMA (*D*), N-Cad (*E*), and Vimentin (*F*) in 20 glomeruli from each individual with DN compared with people without DN using ImageJ. Data are presented as mean ± S.D. ***, $p < 0.004$ and ****, $p < 0.0001$.

aliquot of urine from mice was subjected to SDS-PAGE gel and silver staining was performed to visualize proteins in the urine (40). We have also estimated GFR in these mice, as described previously (40). We performed immunohistochemistry and Western blotting for analyzing the expression of several markers. For Western blotting, kidneys were collected, and glomeruli were isolated. Protein and RNA were prepared from the glomerular lysate. For histological analysis, kidney cortex was fixed with 4% paraformaldehyde before embedding in paraffin. Paraffin-embedded tissues were sliced longitudinally into 3-μm thick sections, subjected to staining with hematoxylin and eosin, PAS, and Masson's trichrome stainings. Transmission electron microscopic (TEM) images were obtained for glomerular sections from experimental mice groups as described earlier (45).

Human kidney specimens

Kidney specimens were collected without patient identifiers from archived kidney biopsies at Guntur Medical College and Government General Hospital, Andhra Pradesh, India. We selected cases with biopsy-proven diabetic nephropathy and significant proteinuria. The study was approved by the Institutional Review Board of Guntur Medical College and Government General Hospital, Guntur, Andhra Pradesh, India (application number GMC/IEC/120/2018). Our studies abide by the Declaration of Helsinki principles.

Morphological studies

All histological quantifications were evaluated in a blinded manner by two independent investigators. Using kidney sections from these mice ($n = 6$ each group), 20 consecutive glomeruli per mouse were examined for evaluation of glomerular mesangial expansion and an average value of 120 glomeruli from each group presented as a dot plot. The index of the mesangial expansion was defined as the ratio of the mesangial area/glomerular tuft area. The mesangial area was determined by the assessment of the PAS-positive and nucleus-free area in the mesangium using ImageJ (NIH). Ultrastructure of glomerulus was recorded using TEM. For measurement of GBM thickness, we have randomly selected 6 glomeruli per animal ($n = 6$ each group). In each glomerulus, we have selected 6 spots and assessed the thickness of GBM using ImageJ. In the dot plot, each dot represents the average thickness of GBM from a single animal.

Estimation of glomerular filtration rate

GFR in mice was performed at 8 weeks of age using a FIT GFR Test Kit for Inulin according to the manufacturer's instructions (BioPal, Worcester, MA). Briefly, 5 mg/kg of inulin was injected intraperitoneally, followed by serial saphenous bleeds at 30, 60, and 90 min. Next, serum isolation was done and quantified on a inulin ELISA kit. Serum inulin clearance estimation was performed by the nonlinear regression method using a one-phase exponential decay formula ($y = Be - bx$), and GFR was calculated (GFR $= ((I)/(B/b))/KW$, where I is the amount of inulin delivered by the bolus injection, B is y intercept, b is the decay constant, x is time, and KW is kilo weight of the animal). Urinary albumin (number COD11573) and creatinine (number COD11502) levels were estimated using available assay kits (Biosystems, Barcelona, Spain).

Podocyte culture and experimentation

Conditionally immortalized HPC were cultured as described earlier (24). Differentiated podocytes were maintained for 12–16 h in serum-free medium before treating with hGH (Pfizer, NY), pegvisomant (Pfizer), and DAPT (Sigma). Unless otherwise mentioned all the experimental conditions for podocyte cells were given for 12 h. The cell lysate was prepared for RNA isolation or immunoblotting. For immunofluorescence, cells were cultured on coverslips, followed by treatment as mentioned above, subsequent fixation with paraformaldehyde (4%), and blocking with PBS containing normal BSA (5%) before incubation with primary antibodies. The next day, the samples were incubated with Alexa Fluor-conjugated secondary antibodies, and DAPI for 1 h. Images were acquired using a confocal microscope (Zeiss). Albumin influx assay across podocyte monolayer was performed as described earlier (23). Primary podocytes were isolated from mice kidney as described earlier (46).

Immunoblotting

Glomerular lysate from kidney or human podocytes was prepared with lysis buffer (150 mM NaCl, 1% Nonidet P-40, 0.1% SDS, 2 μg/ml of aprotinin, 1 mM PMSF) for 30 min at 4 °C. The homogenate was centrifuged at 12,000 $\times$ g for 25 min at 4 °C and supernatant was collected. An equal amount of protein from different groups was electrophoresed through 10 to 15% SDS-PAGE gel and Western blotting was performed with corresponding primary and secondary antibodies. Blots were developed using the ECL Western blotting substrate (number 1705060, Bio-Rad) and chemiluminescence device (Bio-Rad Versa Doc 5000 MFP).

RNA extraction and qRT-PCR

The total transcripts were extracted by using TRIzol reagent (Invitrogen) and isolated using RNA isolation kit (Qiagen). Next, 1 μg of total RNA was reverse transcribed using the cDNA synthesis kit (Thermo Fisher Scientific). qPCR analysis was performed by the QuantStudio 3 system (Applied Biosystem) with SYBR Green (KAPPABIOSYSTEM, USA) Master Mix using three-step standard cycling conditions with sequence-specific primers. To ensure a single PCR product was amplified, we examined the melting curve for each primer. mRNA expression of each gene was normalized using the expression of β-actin.

Enzyme-linked immunosorbent assay

γ-Secretase activity was quantified by fluorescent microscopy using a γ-secretase activity kit according to the manufacturer's instructions (ImmunoTag, G-Biosciences, St. Louis, MO). Briefly, the γ-secretase activity was determined by quantification of human APH1A (Gamma-Secretase subunit APH-1A) with biotin-conjugated anti-APH1A antibody as a detection antibody. The cleavage-dependent release was measured at 450 nm by using a fluorescent microplate reader (Multiskan GO Microplate Spectrophotometer, Thermo Scientific).

Chemotaxis assay

J774A.1 macrophages were cultured as a monolayer and were scratched using the sterile 10-μl tip and washed with PBS to remove cell debris. Conditioned media from podocytes treated with GH, GH + DAPT, or naive to any treatment was added to J774A.1 macrophage. C5a was used as a positive control with a concentration of 10 ng/ml (47). After the scratch, the images of the wounded area were captured at different time intervals to monitor J774A.1 macrophage migration into the wounded area. The migratory abilities were quantified by measuring the distance between cells in the scratch zone.

F-actin staining

Phalloidin staining for F-actin was performed to visualize the distribution of stress fibers in differentiated podocytes as described previously (48). Briefly, the cells were fixed in 4% paraformaldehyde at room temperature for 15 min after washing, and then permeabilized for 15 min with 0.3% Triton X-100 in PBS followed by 5% BSA blocking. Cells were incubated with rhodamine-phalloidin (Invitrogen Corp.) for 15 min at room temperature to stain F-actin. The slides were examined using confocal laser scanning microscopy. Fifty cells per group were counted to calculate the ratio of cells retaining distinct F-actin fibers. The slides were examined by Leica Microsystems trinocular or Zeiss confocal microscopy.

Wound healing assay

The phenomenon of EMT in podocyte cells was assessed using a wound healing migration assay. A confluent monolayer of podocytes in 6-well plates was wounded with a 10-μl pipette tip following two perpendicular diameters, giving rise to two acellular clear areas per well. After washing with PBS, podocyte cells were treated with GH and GH + DAPT and incubated for 0–12 h and images were captured at different time intervals. The extent of migration of cells to cover wounded area was determined by ImageJ.

Statistical analysis

The data are presented as mean ± S.D. of at least 6 independent experiments unless otherwise mentioned. Prism software (GraphPad Software Inc.) was used to analyze the data. Statistical differences between the groups made using Student's *t* test. Statistical significance was determined as $p < 0.05$.

Author contributions—R. N., D. M., S. V. T., and S. K. M. data curation; R. N., D. M., and S. V. T. methodology; R. N., S. K. M., and A. K. P. writing-original draft; R. N., S. K. M., and A. K. P. writing-review and editing; D. M., S. V. T., S. K. M., and A. K. P. formal analysis; S. K. M. and A. K. P. conceptualization; S. K. M. and A. K. P. supervision; A. K. P. funding acquisition; A. K. P. validation; A. K. P. investigation; A. K. P. visualization; A. K. P. project administration.

Acknowledgment—We acknowledge Prof. Ram K. Menon (University of Michigan, Ann Arbor) for sharing microarray data.

References

1. Nath, K. A. (1992) Tubulointerstitial changes as a major determinant in the progression of renal damage. *Am. J. Kidney Dis.* **20,** 1–17 CrossRef
2. Liu, Y. (2011) Cellular and molecular mechanisms of renal fibrosis. *Nat. Rev. Nephrology* **7,** 684–696 CrossRef Medline
3. Cheng, H. T., Miner, J. H., Lin, M., Tansey, M. G., Roth, K., and Kopan, R. (2003) Gamma-secretase activity is dispensable for mesenchyme-to-epithelium transition but required for podocyte and proximal tubule formation in developing mouse kidney. *Development* **130,** 5031–5042 CrossRef Medline
4. Cheng, H. T., Kim, M., Valerius, M. T., Surendran, K., Schuster-Gossler, K., Gossler, A., McMahon, A. P., and Kopan, R. (2007) Notch2, but not Notch1, is required for proximal fate acquisition in the mammalian nephron. *Development* **134,** 801–811 CrossRef Medline
5. Liu, Z., Chen, S., Boyle, S., Zhu, Y., Zhang, A., Piwnica-Worms, D. R., Ilagan, M. X., and Kopan, R. (2013) The extracellular domain of Notch2 increases its cell-surface abundance and ligand responsiveness during kidney development. *Dev. Cell* **25,** 585–598 CrossRef Medline
6. Chung, E., Deacon, P., and Park, J. S. (2017) Notch is required for the formation of all nephron segments and primes nephron progenitors for differentiation. *Development* **144,** 4530–4539 CrossRef Medline
7. Milano, J., McKay, J., Dagenais, C., Foster-Brown, L., Pognan, F., Gadient, R., Jacobs, R. T., Zacco, A., Greenberg, B., and Ciaccio, P. J. (2004) Modulation of notch processing by γ-secretase inhibitors causes intestinal goblet cell metaplasia and induction of genes known to specify gut secretory lineage differentiation. *Toxicol. Sci.* **82,** 341–358 CrossRef Medline
8. Hayward, P., Kalmar, T., and Arias, A. M. (2008) Wnt/Notch signalling and information processing during development. *Development* **135,** 411–424 CrossRef Medline
9. Zhao, Y., Katzman, R. B., Delmolino, L. M., Bhat, I., Zhang, Y., Gurumurthy, C. B., Germaniuk-Kurowska, A., Reddi, H. V., Solomon, A., Zeng, M. S., Kung, A., Ma, H., Gao, Q., Dimri, G., Stanculescu, A., *et al.* (2007) The notch regulator MAML1 interacts with p53 and functions as a coactivator. *J. Biol. Chem.* **282,** 11969–11981 CrossRef Medline
10. Del Bianco, C., Aster, J. C., and Blacklow, S. C. (2008) Mutational and energetic studies of Notch 1 transcription complexes. *J. Mol. Biol.* **376,** 131–140 CrossRef Medline
11. Liu, Z. J., Xiao, M., Balint, K., Soma, A., Pinnix, C. C., Capobianco, A. J., Velazquez, O. C., and Herlyn, M. (2006) Inhibition of endothelial cell proliferation by Notch1 signaling is mediated by repressing MAPK and PI3K/Akt pathways and requires MAML1. *FASEB J.* **20,** 1009–1011 CrossRef
12. McCright, B. (2003) Notch signaling in kidney development. *Curr. Opin. Nephrol. Hypertens.* **12,** 5–10 CrossRef Medline
13. Vooijs, M., Ong, C. T., Hadland, B., Huppert, S., Liu, Z., Korving, J., van den Born, M., Stappenbeck, T., Wu, Y., Clevers, H., and Kopan, R. (2007) Mapping the consequence of Notch1 proteolysis in vivo with NIP-CRE. *Development* **134,** 535–544 Medline
14. Niranjan, T., Bielesz, B., Gruenwald, A., Ponda, M. P., Kopp, J. B., Thomas, D. B., and Susztak, K. (2008) The Notch pathway in podocytes plays a role in the development of glomerular disease. *Nat. Med.* **14,** 290–298 CrossRef Medline
15. Waters, A. M., Wu, M. Y., Onay, T., Scutaru, J., Liu, J., Lobe, C. G., Quaggin, S. E., and Piscione, T. D. (2008) Ectopic notch activation in developing podocytes causes glomerulosclerosis. *J. Am. Soc. Nephrol.* **19,** 1139–1157 CrossRef Medline
16. Bielesz, B., Sirin, Y., Si, H., Niranjan, T., Gruenwald, A., Ahn, S., Kato, H., Pullman, J., Gessler, M., Haase, V. H., and Susztak, K. (2010) Epithelial Notch signaling regulates interstitial fibrosis development in the kidneys of mice and humans. *J. Clin. Invest.* **120,** 4040–4054 CrossRef Medline
17. Murea, M., Park, J. K., Sharma, S., Kato, H., Gruenwald, A., Niranjan, T., Si, H., Thomas, D. B., Pullman, J. M., Melamed, M. L., and Susztak, K. (2010) Expression of Notch pathway proteins correlates with albuminuria, glomerulosclerosis, and renal function. *Kidney Int.* **78,** 514–522 CrossRef Medline
18. Walsh, D. W., Roxburgh, S. A., McGettigan, P., Berthier, C. C., Higgins, D. G., Kretzler, M., Cohen, C. D., Mezzano, S., Brazil, D. P., and Martin, F. (2008) Co-regulation of Gremlin and Notch signalling in diabetic nephropathy. *Biochim. Biophys. Acta* **1782,** 10–21 CrossRef Medline

19. Niranjan, T., Murea, M., and Susztak, K. (2009) The pathogenic role of Notch activation in podocytes. *Nephron Exp. Nephrol.* **111,** e73–79 CrossRef Medline
20. Pasupulati, A. K., and Menon, R. K. (2019) Growth hormone and chronic kidney disease. *Curr. Opin. Nephrol. Hypertens.* **28,** 10–15 CrossRef Medline
21. Mukhi, D., Nishad, R., Menon, R. K., and Pasupulati, A. K. (2017) Novel actions of growth hormone in podocytes: implications for diabetic nephropathy. *Front. Med.* **4,** 102 CrossRef Medline
22. Kumar, P. A., Brosius F. C., 3rd, Menon, R. K. (2011) The glomerular podocyte as a target of growth hormone action: implications for the pathogenesis of diabetic nephropathy. *Curr. Diabetes Rev.* **7,** 50–55 CrossRef Medline
23. Chitra, P. S., Swathi, T., Sahay, R., Reddy, G. B., Menon, R. K., and Kumar, P. A. (2015) Growth hormone induces transforming growth factor-β-induced protein in podocytes: implications for podocyte depletion and proteinuria. *J. Cell. Biochem.* **116,** 1947–1956 CrossRef Medline
24. Kumar, P. A., Kotlyarevska, K., Dejkhmaron, P., Reddy, G. R., Lu, C., Bhojani, M. S., and Menon, R. K. (2010) Growth hormone (GH)-dependent expression of a natural antisense transcript induces zinc finger E-box-binding homeobox 2 (ZEB2) in the glomerular podocyte: a novel action of GH with implications for the pathogenesis of diabetic nephropathy. *J. Biol. Chem.* **285,** 31148–31156 CrossRef Medline
25. Beel, A. J., and Sanders, C. R. (2008) Substrate specificity of γ-secretase and other intramembrane proteases. *Cell. Mol. Life Sci.* **65,** 1311–1334 CrossRef Medline
26. Haynes, J., Srivastava, J., Madson, N., Wittmann, T., and Barber, D. L. (2011) Dynamic actin remodeling during epithelial-mesenchymal transition depends on increased moesin expression. *Mol. Biol. Cell* **22,** 4750–4764 CrossRef Medline
27. Whitney, J. L., Bilkan, C. M., Sandberg, K., Myers, A. K., and Mulroney, S. E. (2013) Growth hormone exacerbates diabetic renal damage in male but not female rats. *Biol. Sex Differ.* **4,** 12 CrossRef Medline
28. Song, K., Fu, J., Song, J., Herzog, B. H., Bergstrom, K., Kondo, Y., McDaniel, J. M., McGee, S., Silasi-Mansat, R., Lupu, F., Chen, H., Bagavant, H., and Xia, L. (2017) Loss of mucin-type *O*-glycans impairs the integrity of the glomerular filtration barrier in the mouse kidney. *J. Biol. Chem.* **292,** 16491–16497 CrossRef Medline
29. Cheng, H. T., and Kopan, R. (2005) The role of Notch signaling in specification of podocyte and proximal tubules within the developing mouse kidney. *Kidney Int.* **68,** 1951–1952 CrossRef Medline
30. Asanuma, K., Oliva Trejo, J. A., and Tanaka, E. (2017) The role of Notch signaling in kidney podocytes. *Clin. Exp. Nephrol.* **21,** 1–6 CrossRef Medline
31. Lasagni, L., Ballerini, L., Angelotti, M. L., Parente, E., Sagrinati, C., Mazzinghi, B., Peired, A., Ronconi, E., Becherucci, F., Bani, D., Gacci, M., Carini, M., Lazzeri, E., and Romagnani, P. (2010) Notch activation differentially regulates renal progenitors proliferation and differentiation toward the podocyte lineage in glomerular disorders. *Stem Cells (Dayton, OH)* **28,** 1674–1685 CrossRef Medline
32. Sweetwyne, M. T., Gruenwald, A., Niranjan, T., Nishinakamura, R., Strobl, L. J., and Susztak, K. (2015) Notch1 and Notch2 in podocytes play differential roles during diabetic nephropathy development. *Diabetes* **64,** 4099–4111 CrossRef Medline
33. Press, M., Tamborlane, W. V., and Sherwin, R. S. (1984) Importance of raised growth hormone levels in mediating the metabolic derangements of diabetes. *New Engl. J. Med.* **310,** 810–815 CrossRef Medline
34. Ying, Q., and Wu, G. (2017) Molecular mechanisms involved in podocyte EMT and concomitant diabetic kidney diseases: an update. *Ren. Fail.* **39,** 474–483 CrossRef Medline
35. Ahn, S. H., and Susztak, K. (2010) Getting a notch closer to understanding diabetic kidney disease. *Diabetes* **59,** 1865–1867 CrossRef Medline
36. Lin, C. L., Wang, F. S., Hsu, Y. C., Chen, C. N., Tseng, M. J., Saleem, M. A., Chang, P. J., and Wang, J. Y. (2010) Modulation of notch-1 signaling alleviates vascular endothelial growth factor-mediated diabetic nephropathy. *Diabetes* **59,** 1915–1925 CrossRef Medline
37. Wang, Y., and Zhou, B. P. (2011) Epithelial-mesenchymal transition in breast cancer progression and metastasis. *Chin. J. Cancer* **30,** 603–611 CrossRef Medline
38. Collu, G. M., and Brennan, K. (2007) Cooperation between Wnt and Notch signalling in human breast cancer. *Breast Cancer Res.* **9,** 105 CrossRef Medline
39. Leong, K. G., Niessen, K., Kulic, I., Raouf, A., Eaves, C., Pollet, I., and Karsan, A. (2007) Jagged1-mediated Notch activation induces epithelial-to-mesenchymal transition through Slug-induced repression of E-cadherin. *J. Exp. Med.* **204,** 2935–2948 CrossRef Medline
40. Nakuluri, K., Mukhi, D., Nishad, R., Saleem, M. A., Mungamuri, S. K., Menon, R. K., and Pasupulati, A. K. (2019) Hypoxia induces ZEB2 in podocytes: Implications in the pathogenesis of proteinuria. *J. Cell. Physiol.* **234,** 6503–6518 CrossRef Medline
41. Hills, C. E., and Squires, P. E. (2011) The role of TGF-beta and epithelial-to mesenchymal transition in diabetic nephropathy. *Cytokine Growth Factor Rev.* **22,** 131–139 Medline
42. Sutariya, B., Jhonsa, D., and Saraf, M. N. (2016) TGF-β: the connecting link between nephropathy and fibrosis. *Immunopharmacol. Immunotoxicol.* **38,** 39–49 CrossRef Medline
43. Zavadil, J., Cermak, L., Soto-Nieves, N., and Böttinger, E. P. (2004) Integration of TGF-β/Smad and Jagged1/Notch signalling in epithelial-to-mesenchymal transition. *EMBO J.* **23,** 1155–1165 CrossRef Medline
44. Geling, A., Steiner, H., Willem, M., Bally-Cuif, L., and Haass, C. (2002) A gamma-secretase inhibitor blocks Notch signaling *in vivo* and causes a severe neurogenic phenotype in zebrafish. *EMBO Rep.* **3,** 688–694 CrossRef Medline
45. Nakuluri, K., Mukhi, D., Mungamuri, S. K., and Pasupulati, A. K. (2018) Stabilization of hypoxia-inducible factor 1α by cobalt chloride impairs podocyte morphology and slit-diaphragm function. *J. Cell. Biochem.* 10.1002/jcb.28041 CrossRef
46. Katsuya, K., Yaoita, E., Yoshida, Y., Yamamoto, Y., and Yamamoto, T. (2006) An improved method for primary culture of rat podocytes. *Kidney Int.* **69,** 2101–2106 CrossRef Medline
47. Das, D., Barnes, M. A., and Nagy, L. E. (2014) Anaphylatoxin C5a modulates hepatic stellate cell migration. *Fibrogenesis Tissue Repair* **7,** 9 CrossRef Medline
48. Zhou, H., Tian, X., Tufro, A., Moeckel, G., Ishibe, S., and Goodwin, J. (2017) Loss of the podocyte glucocorticoid receptor exacerbates proteinuria after injury. *Sci. Rep.* **7,** 9833 CrossRef Medline

Indian Journal of Research in Pharmacy and Biotechnology (IJRPB)
ISSN: 2321-5674 (Print), 2320-3471 (Online)

CrossRef DOI: https://doi.org/10.31426/ijrpb **Indexed in CAS and CABI, Impact Factor: 0.64**

A Validated Reversed Phase HPLC Method Development for the Assay of Ciprofloxacin in Oral Suspension

Bathula Sivannarayana[1], Modugula Jyosthna[1], Dr Dasi Jeevan Mani Babu[1], Mekala Sunil[1], Choppavarapu Dorcas Anand[2], Dr M. Manoranjani[3]

[1]St.Xavier Institute of Pharmacy, Phirangipuram, Guntur. A.P., India
[2]SRR & CVR Govt. (A) Degree College, Vijayawada, A.P., India
[3]Dept. of Chemistry, PB Siddartha College of Arts and Sciences, Vijayawada, A.P., India

E-Mail: drjeevanbabu@gmail.com

Keywords:
Ciprofloxacin, RP-HPLC

ABSTRACT

A simple Reverse phase liquid chromatographic method has been developed and subsequently validated for the determination of Ciprofloxacin in oral suspension. The separation was carried out using a mobile phase consisting of buffer of pH 2.0 and Acetonitrile in the ratio of 87: 13. The column used was Inertsil ODS-3 4.6×250mm, 5µ. with a flow rate of 1.5 ml / min by detection at 278 nm. The described method was linear over a concentration range of 25-150%. The retention time of Ciprofloxacinwas found to be 9.4min. Results of analysis were validated statistically and by recovery studies. The results of the study showed that the proposed RP-HPLC method is simple, rapid, precise and accurate, which is useful for the routine determination of Ciprofloxacinin its pharmaceutical dosage forms.

1. INTRODUCTION

Ciprofloxacin is a broad-spectrum antimicrobial carboxyfluoroquinoline. The bactericidal action of ciprofloxacin results from inhibition of the enzymes topoisomerase II (DNA gyrase) and topoisomerase IV, which are required for bacterial DNA replication, transcription, repair, strand supercooling repair, and recombination. [1]

Indian Journal of Research in Pharmacy and Biotechnology (IJRPB)
ISSN: 2321-5674 (Print), 2320-3471 (Online)

CrossRef DOI: https://doi.org/10.31426/ijrpb **Indexed in CAS and CABI, Impact Factor: 0.64**

Ciprofloxacin is a broad-spectrum anti-infective agent of the fluoroquinolone class. Ciprofloxacin has in vitro activity against a wide range of gram-negative and gram-positive microorganisms. The mechanism of action of quinolones, including ciprofloxacin, is different from that of other antimicrobial agents such as beta-lactams, macrolides, tetracyclines, or aminoglycosides; therefore, organisms resistant to these drugs may be susceptible to ciprofloxacin. There is no known cross-resistance between ciprofloxacin and other classes of antimicrobials. Notably the drug has 100 times higher affinity for bacterial DNA gyrase than for mammalian. The bactericidal action of ciprofloxacin results from inhibition of the enzymes topoisomerase II (DNA gyrase) and topoisomerase IV, which are required for bacterial DNA replication, transcription, repair, strand supercooling repair, and recombination.

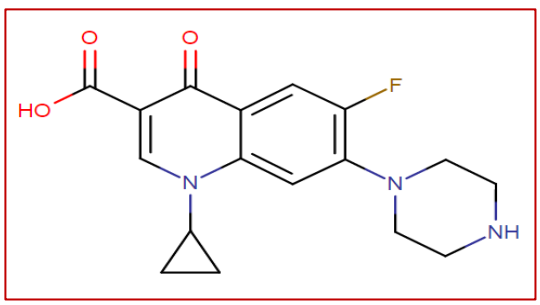

Figure. 1. Molecular structure of Ciprofloxacin

2. Materials and Methods:

2.1 Chemicals and Reagents:

Standard bulk drug sample Ciprofloxacin was provided by Chandra labs, Hyderabad. All the chemicals used were of analytical and HPLC grade procured from Qualigens, India Ltd. The chemicals used for this study were Acetonitrile (HPLC grade), Methanol (HPLC grade), Water (HPLC grade), Ortho phosphoric acid (Analytical grade). Waters HPLC 2695with UV detector was used for the analysis.

2.2. Preparation of Mobile Phase:

Mobile phase-A: (Buffer) Pipette out 10ml of Methanol in to 1000ml of and mix. Adjust to pH 2.0 with Orthophosphoric acid, then filter through 0.45µ filter paper and sonicate for 2minutes.

Mobile phase-B: Acetonitrile

Preparation of Mobile Phase:

Mix the mobile phase-A and mobile phase-B in the ratio in the ratio 87:13%v/v.

Indian Journal of Research in Pharmacy and Biotechnology (IJRPB)
ISSN: 2321-5674 (Print), 2320-3471 (Online)

CrossRef DOI: https://doi.org/10.31426/ijrpb **Indexed in CAS and CABI, Impact Factor: 0.64**

2.3. Preparation of Stock and Standard Solutions:

Preparation of Standard solution:

Weigh and transfer 25mg ciprofloxacin working standard into a 50mL volumetric flask. Add 7ml of acetonitrile andsonicate for 2minutes then add 30ml of pH2.00buffer, sonicate for 10minutes then make up to the mark with diluent. Further pipette out 5ml of the above solution in to 20ml volumetric flask, add 2.8ml of acetonitrile mix well, then add 12ml of pH2.00 buffer, then make up to the mark with diluent.

Preparation of Test Solution:

Shake the bottle 10minutes immediately prior to sampling in order to accomplish homogeneity of suspension. Weigh and transfer 5.5g ciprofloxacin suspension into a 500mL volumetric flask. Add 70ml of acetonitrile sonicate for 10 minutes, then add 250ml of pH 2.00 buffer, sonicate for 20minutes then make up to the mark with diluent. Further pipette out 5ml of the above solution in to 20ml volumetric flask, add 2.8ml of acetonitrile mix well, then add 12ml of pH2.00 buffer, then make up to the mark with diluent.

2.4. Optimized Chromatographic Conditions:

Column: Inertsil ODS-3 4.6×250mm, 5µ.

Flow rate : 1.5 mL /min.

Wavelength : 278 nm

Column temperature : 40°C

Injection Volume : 10 µL

Run Time : 15 minutes

Retention time: Ciprofloxacin, RT about 9.4min

3. Method Validation Parameters:

Linearity:

A series of Ciprofloxacin solutions were prepared in the concentration ranging from 25% to 150% of specification level and injected into the HPLC system as per the test method. The square of the correlation coefficient, intercept and residual sum of squares were calculated.

Indian Journal of Research in Pharmacy and Biotechnology (IJRPB)
ISSN: 2321-5674 (Print), 2320-3471 (Online)

CrossRef DOI: https://doi.org/10.31426/ijrpb **Indexed in CAS and CABI, Impact Factor: 0.64**

Accuracy:

A series of solutionswereprepared in triplicatetest preparation at the specification limit in the range of about 25%to 150% of test concentration and injected into HPLC system and analyzed as per the test method. Individual % recovery, mean % recovery, %RSD and linearity of the testmethodwere calculated at each level.

Intermediate Precision:

To evaluate the intermediate precision for assay method, six samples were prepared and analyzed as per test method by using different column, by different analysts on different days. Intermediate precision was calculated and found to be within the acceptable limits. The overall % RSD of six samples in method precision, intermediate precision (n=6 and n=12) were calculated.

Filter Validation:

A study was conducted to evaluate the filter suitability by using two different types of filters namely0. 45 µm PVDF and 0.45µm Nylon filters. Standard solution was prepared in single and test solution was prepared in duplicate as per the test method. Portion of standard and test solutions were filtered through 0.45 µm PVDF, 0.45 µm nylon filter and some portion of standard and sample solutions were centrifuged and analyzed as per test method.

Robustness:

Flow Rate Variation:

A study was conducted to determine the effect of variation in flow rate. Blank, Standard and sample (at the specification level) were prepared as per the test method and injected into the HPLC system with flow rates of 1.4ml/minute and 1.6ml/minute. The system suitability parameters sample was evaluated and found to be within the specified limits as per test method.

Column Oven Temperature Variation:

A study was conducted to determine the effect of variation in Column oven Temperature. Standard and test preparations (at the specification level) were prepared as per the test method and injected into the HPLC system with a column oven temperature of 35°C and 45°C. System suitability parameters and sample were evaluated and found to be within the specified limits as per test method.

Indian Journal of Research in Pharmacy and Biotechnology (IJRPB)
ISSN: 2321-5674 (Print), 2320-3471 (Online)
CrossRef DOI: https://doi.org/10.31426/ijrpb **Indexed in CAS and CABI, Impact Factor: 0.64**

Effect of Variation In Mobile Phase Composition:

A study was conducted to determine the effect of variation in mobile phase composition. Two different mobile phases of Buffer and Acetonitrile were prepared in the ratio of 855:145%v/v and 885:115%v/v as per the test method. Standard and test preparations with specification level were prepared as per the test method and injected into the HPLC system.

Effect of pH Variation in Mobile Phase:

A study was conducted to determine the effect of variation in pH in the mobile phase. Two mobile phases of pH 2.80 and 3.20 were prepared as per the test method. Blank, Standard and test preparations were prepared as per the test method and injected into the HPLC system with System suitability parameters and sample were evaluated and found to be within the specified limits as per test method.

The Effect of Wavelength Variation:

A study was conducted to determine the effect of variation in wavelength. Standard and test preparations (at the specification level) were prepared as per the test method and injected into the HPLC system with wavelength of -Ciprofloxacin280nm and 276nm.System suitability parameters and sample were evaluated and found to be within the specified limits as per test method.

4. Results and Discussion:

The solution of Ciprofloxacin was scanned in the range of 200-400nm and 278nm was selected as detection wavelength by RP-HPLC method with an isocratic elution technique. The optimization was done by changing the composition of the mobile phase, ratio and flow rate. Finally the mobile phase with buffer (pH 2): ACN in the ratio 87:13v/v% was optimized for the estimation of Ciprofloxacin and the column used for separation is Inertsil ODS-3 4.6×250mm,5µ. [2]

The chromatographicparameters of system suitability such as %RSD, standard recovery, Tailing factor, Theoretical plates were found to be satisfactory. The values of these parameters are tabulated in Table-1.

Indian Journal of Research in Pharmacy and Biotechnology (IJRPB)
ISSN: 2321-5674 (Print), 2320-3471 (Online)
CrossRef DOI: https://doi.org/10.31426/ijrpb **Indexed in CAS and CABI, Impact Factor: 0.64**

Table.1. System suitability data for Ciprofloxacin

System suitability parameters for Ciprofloxacin	Method Precision	Intermediate precision	Acceptance Criteria
%RSD	0.3	0.3	Not more than 2.0
Standard recovery (%)	101.4	99.5	Between 98.0 to 102.0
Tailing factor	1.1	1.1	Not more than 2.0
Theoretical plates	9925	9271	Not less than 2000

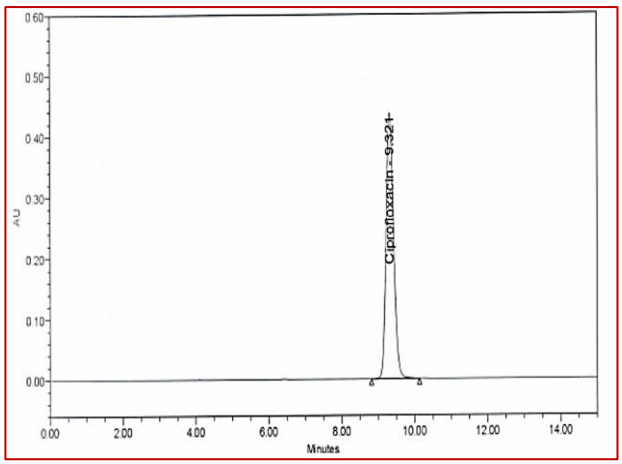

Figure.2.Typical chromatogram of Standard solution

The linearity of the developed method was determined by analyzing different concentrations of the standard solution containing a concentration range from 25% to 150%. The response factor of the standard solutions was calculated. The ratio of peak areas of ciprofloxacin was plotted against the concentration to obtain the calibration graph (Fig. 3) and was found to be linear over the concentration range from 25% to 150%. The data were analyzed by linear regression, least-squares method and the corresponding equation are given by Y = BX + c, where 'Y' is the ratio of the peak areas values of Ciprofloxacin, 'b' is the slope, 'c' is the intercept and 'X' is the concentration of the analyte. Linear regression, least squares fit data are given in (Table 2). [3] The percentage purity was found to be 99.3%. The precision of the method was confirmed by the repeatability of formulation for six times. The accuracy of the method was confirmed by recovery studies and the data was given by (Table 3). [4] Similarity factors were calculated for the filtered standards against unfiltered standard (Centrifuged) and found to be within the specified limit. The difference in the % between unfiltered (centrifuged) and filtered samples were calculated and found to be

Indian Journal of Research in Pharmacy and Biotechnology (IJRPB)
ISSN: 2321-5674 (Print), 2320-3471 (Online)
CrossRef DOI: https://doi.org/10.31426/ijrpb **Indexed in CAS and CABI, Impact Factor: 0.64**

meeting the acceptable limit. Both PVDF and Nylon filters were suitable for the intended purpose.

Table.2.Linearity of detector response for Ciprofloxacin

% Linearity level	Concentration (ppm)	Response	Acceptance criteria
25	31.0875	1536480	Square of Correlation co-efficient should not be less than 0.999
50	62.175	3107355	
75	93.2625	4623963	
100	124.35	6039873	
150	186.525	9110398	
Square of correlation coefficient : 0.999 Slope: 48483.76574 Intercept : 60448.78378 Residual sum of squares: 45710.56736			

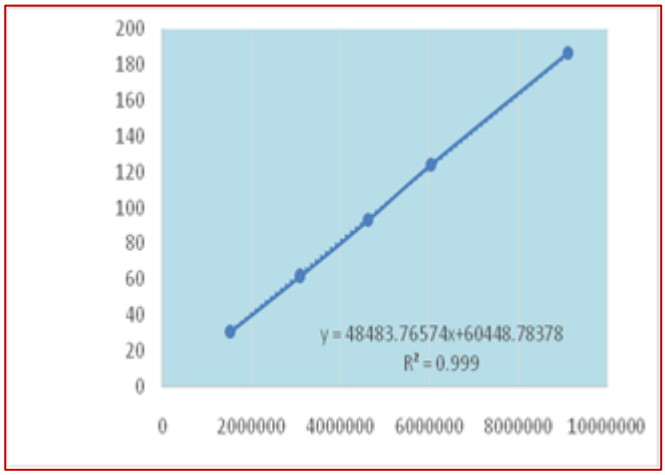

Figure.3.Linearity of detector response graph for Ciprofloxacin.

Indian Journal of Research in Pharmacy and Biotechnology (IJRPB)
ISSN: 2321-5674 (Print), 2320-3471 (Online)
CrossRef DOI: https://doi.org/10.31426/ijrpb **Indexed in CAS and CABI, Impact Factor: 0.64**

Table.3.Accuracy data of Ciprofloxacin

S. No.	% spike level	Amount added (%w/w)	Amount recovered (%w/w)	% Recovery	% Mean recovery	% RSD
1.	25%	62.1229	62.37308	100.4	99.8	0.6
2.		63.0287	62.40228	99.0		
3.		63.0885	62.62924	99.3		
4.		63.1979	62.72669	99.3		
5.		62.2424	62.36469	100.2		
6.		62.3220	62.55297	100.4		
1.	100%	250.8408	247.83270	98.8	99.3	0.4
2.		248.9894	247.87577	99.6		
3.		249.1088	247.78317	99.5		
1.	150%	378.5307	377.14133	99.6	100.6	0.5
2.		374.4894	377.08205	100.7		
3.		374.7781	377.28255	100.7		
4.		373.8921	377.45520	101.0		
5.		373.2252	376.76809	101.0		
6.		374.1609	376.10577	100.5		

Specificity:

Chromatogram of blank and placebo should not show any peak at the retention time of Ciprofloxacin peak and known impurity peaks.

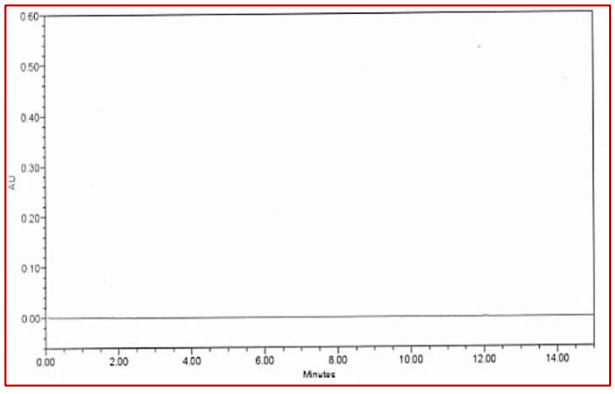

Figure.4.Typical chromatogram of Blank

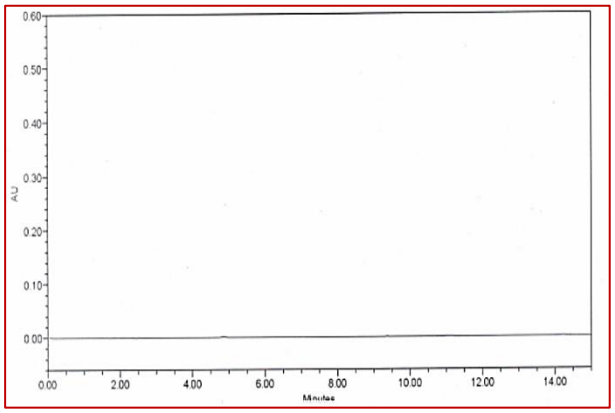

Figure.5.Typical chromatogram of placebo

Indian Journal of Research in Pharmacy and Biotechnology (IJRPB)
ISSN: 2321-5674 (Print), 2320-3471 (Online)

CrossRef DOI: https://doi.org/10.31426/ijrpb **Indexed in CAS and CABI, Impact Factor: 0.64**

Table.4.Method Precision data for Ciprofloxacin

Sample No.	Ciprofloxacin content (%)
1	100.9
2	100.2
3	100.0
4	99.4
5	101.1
6	100.5
Mean	**100.4**
% RSD	**0.6**

5. Conclusion:

This study showed that the antibiotic drug, Ciprofloxacin can be precisely and accurately determined in pure and pharmaceutical dosages. The proposed method is simple and requires less time for analysis. System performance parameters revealed that the method is ideal for the assay ofCiprofloxacin.

Hence, the developed chromatography method was applied for routine analysis and can be used for the intended purpose.

References:

1) Tripathi KD. Essentials of medical pharmacology; sixth edition 2008: 688
2) Abdel-Hay MH, Hassan EM, Gazy AA, Belal TS. Kinetic spectrophotometric analysis and spectrofluorimetric analysis of ciprofloxacin hydrochloride and norfloxacin in pharmaceutical preparations using 4-Chloro-7-nitrobenzo-2-oxa-1,3-diazole (NBD-Cl). J Chin ChemSoc 2008; 55(4): 818-827
3) Gummadi S, Thota D, Varri SV, Vaddi P, Jillella VLNSR. Development and validation of UV spectroscopic methods for simultaneous estimation of ciprofloxacin and tinidazole in tablet formulation.Intcurr Pharm j 2012; 1(10): 317-321
4) El-Brashy AM, El-Sayed MM, El-Sepai FA. Spectrophotometric determination of some fluoroquinoloneantibacterials through charge-transfer and ion-pair complexation reactions. Bul Korean ChemSoc2004; 25(3): 365
5) Safwan A, Mouhammed K. Kinetic Spectrophotometric method for the quantitative analysis of pravastatin sodium (PVS) in pure and pharmaceutical formulations. Arabian J Chem 2012; 4(3): 299-305
6) Chaudhari BG, Patel NM, Shah PB. Determination of simvastatin, pravastatin, rosuvastatin calcium in tablet

Indian Journal of Research in Pharmacy and Biotechnology (IJRPB)
ISSN: 2321-5674 (Print), 2320-3471 (Online)

CrossRef DOI: https://doi.org/10.31426/ijrpb **Indexed in CAS and CABI, Impact Factor: 0.64**

dosage form. Int j pharm sci 2007; 69(10): 130-132

7) Kadikar HK, Shah R. Simultaneous UV spectrophotometry of pravastatin and co-enzyme Q10 in their formulation combined dosage forms and synthetic mixtures. IJPR 2012; 1(4): 112-127
8) D'Silva T, Olivera MA, De'Oliveira RB, Soares CDV. Development and validation of a simple and fast hplc method for determination of lovastatin, pravastatin and simvastatin. J ChromatogrSci2010; 50(9): 831-832
9) Maha F, Abdel-Aziz O, Reham N, Abdel-Fattah L. Validated spectrophotometric methods for determination of some anti-hyperlipidemic drugs. J Med Res 2010; 2(3): 202-211
10) Safwan A, Husni N, Soulafa O. Quantitative determination of pravastatin in pharmaceutical dosage forms by high-performance liquid chromatography with ultraviolet detection. Int J Biomed sci 2011; 4(1): 84-90

Poll Res. 39 (2) : 368-372 (2020)

ISSN 0257–8050

EFFECT OF CARTAP HYDROCHLORIDE (50% SP) ON OXYGEN CONSUMPTION OF FRESH WATER FISH, *CIRRHINUS MRIGALA* (HAMILTON)

G. VANI[1], K. VEERAIAH [2], M. VIJAYA KUMAR [1] AND S.K. PARVEEN [1,]

[1]Department of Zoology, SRR & CVR Government Degree College, (A), Vijayawada 520 004, Krishna District. A.P., India
[2]Department of Zoology and Aquaculture, Acharya Nagarjuna University, Nagarjunanagar 522 510, Guntur, A.P., India

(Received 23 October, 2019; accepted 3 February, 2020)

ABSTRACT

Effect of Cartap hydrochloride on oxygen consumption of the Indian major carp, *Cirrhinus mrigala* was studied. Fingerlings were exposed to sub-lethal (0.0376 mg^{-1}) and lethal (0.376 mg^{-1}) concentrations of Cartap hydrochloride for 24,48,72 and 96hrs. In both sublethal and lethal concentrations for all exposed hours *Cirrhinus mrigala* showed an increased tendency in oxygen consumption during the initial time of exposure and a gradual decrease during the subsequent study period. Alterations in oxygen consumption may be due to respiratory distress as a consequence of impaired oxidative metabolism. Present study showed that Cartap hydrochloride altered respiratory metabolism in *Cirrhinus mrigala* which can be used as bio-indicator for assessing pesticide toxicity to fish.

KEYWORDS: Cartap hydrochloride, *Cirrhinus mrigala,* Oxygen consumption.

INTRODUCTION

Wide and indiscriminate use of pesticides in modern agricultural practices throughout the world has indirectly created problem of pollution of aquatic ecosystems. (Ganeshwade, 2012). These chemicals impair water quality which become unsuitable for all aquatic organisms due to their toxicity, persistence, bioaccumulation, and biomagnification in food chain and ecological balance (Subramani Lavanya *et al.,* 2011). Fish accumulate these pollutants directly or indirectly from polluted waters and food chain (Jabeen *et al*., 2016). In India, Cartap hydrochloride a carbamate pesticide is extensively used in rice and sugarcane crops to control pests. One of the indicators of the health status of a fish is its total oxygen consumption. It helps in evaluating the susceptibility or resistance potential useful to assess the physiological condition of an organism and to correlate the behavior of the animal, which ultimately serve as predictors of functional disruptions of population. Hence the analysis of total oxygen consumption can be used as a biodetectory system to evaluate the basic damage caused to the animal which could either decrease or increase the oxygen uptake (Maharajan *et al.,* 2013). In this viewpoint an attempt was made to study the effect of sublethal and lethal concentrations of Cartap hydrochloride on oxygen consumption of freshwater fish, *Cirrhinus mrigala* exposed for 24,48,72 and 96hrs.

MATERIALS AND METHODS

Experiment on the oxygen consumption of the fish *Cirrhinus mrigala* was carried out in a respiratory apparatus developed by Job (1955). The fingerlings of the test fish *Cirrhinus mrigala* of size 6-8 ± ½ cm and weight 6-7 ± ½ g were procured from local fish hatcheries of Nandivelugu, Tenali mandal, Guntur district, Andhra Pradesh. The fish were acclimated at (28±2 °C) in the laboratory conditions for two

weeks. All the precautions laid down on recommendations of the toxicity tests to aquatic organisms were followed (Annon, 1975). Fish were regularly fed with rice bran and one day prior to the experimentation feeding was stopped. Fish were exposed to sub-lethal ($1/10^{th}$ of 96 h LC_{50} value 0.0376 mg^{-1}) and lethal (96 h LC_{50} value 0.376 mg^{-1}) concentrations of Cartap hydrochloride for 24,48,72 and 96 hrs. The samples for estimation of oxygen consumption were taken from the respiratory chamber, at alternate hours of intervals for 24hours. The amount of dissolved oxygen consumption was calculated per gram body weight per hour. The dissolved oxygen content was estimated by modified Winkler's method as described by Golterman and Clymo (1969). The difference in the dissolved oxygen content between initial and final water samples represents the amount of oxygen consumed by the fish.

Student·s t-test was employed to calculate the significance of the differences between control and experimental means. P values of 0.05 or less were considered statistically significant (Fisher, 1950).

RESULTS

The results of the experimental and control fish values are graphically represented in Figures 1,2,3 and 4 by taking hours of exposure on X axis and the amount of oxygen consumed per gram body weight per hour on Y axis.

In sublethal concentrations of Cartap hydrochloride it was observed that the fish showed increase in oxygen consumption during the initial time of exposure i.e., 0-6 hours in 24 and 48 hour treated fish and 0 to 4 hour in 72 and 96 hour treated fish and a gradual decrease was observed in the subsequent periods of study. The presence of sub

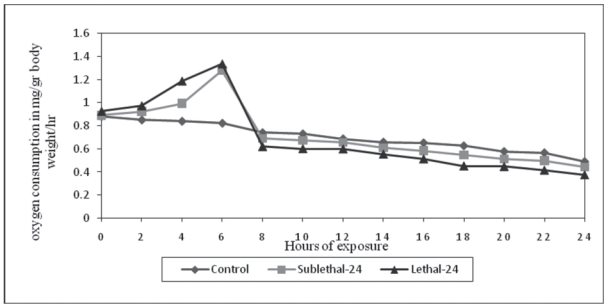

Fig. 1. The amount of oxygen consumed in mg/g body weight/hr of Cirrhinus mrigala exposed to sublethal and lethal concentrations of Cartap hydrochloride for 24 hrs

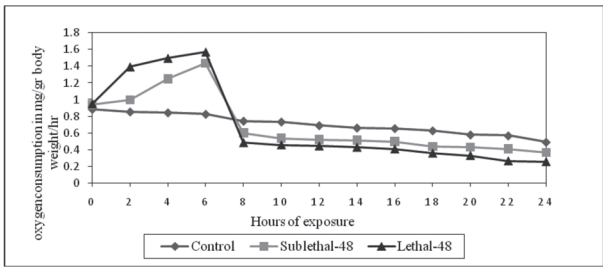

Fig. 2. The amount of oxygen consumed in mg/g body weight/hr of *Cirrhinus mrigala* exposed to sublethal and lethal concentrations of Cartap hydrochloride for 48 hrs.

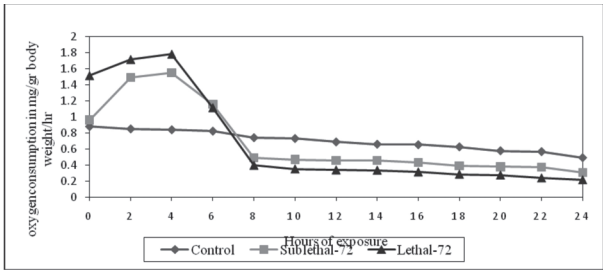

Fig. 3. The amount of oxygen consumed in mg/g body weight/hr of *Cirrhinus mrigala* exposed to sublethal and lethal concentrations of Cartap hydrochloride for 72 hrs.

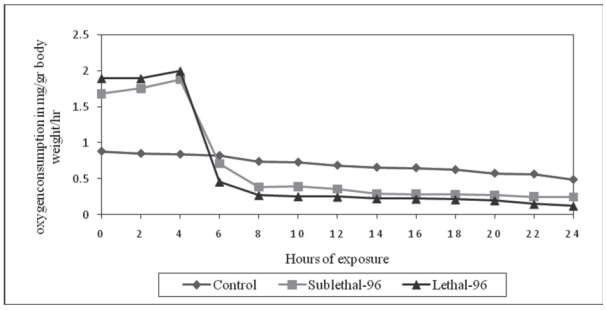

Fig. 4. The amount of oxygen consumed in mg/g body weight/hr of *Cirrhinus mrigala* exposed to sublethal and lethal concentrations of Cartap hydrochloride for 96 hrs.

lethal concentration of toxicants is aquatic environment is inevitable. The toxicant stress on oxygen consumption along with depletion in oxygen in aquaculture practices makes fish less fit and reduces their growth due to lack of proper metabolism (Hyma Ranjani, 2015 and Bantu *et al*., 2017). In lethal concentrations of Cartap hydrochloride it was noticed that a gradual increase in oxygen consumption during the initial time of exposure i.e., 0-6 hours in 24 and 48 hour treated fish and 0 to 4 hour in 72 and 96 hour exposed fish and a gradual decline is observed during the later

periods of study. In control fish the rate of oxygen consumption gradually decreased, and this might be due to starved conditions and the reduced metabolic rates of the starved fish (Anitha, 2015). From the present study it is clear that the Cartap hydrochloride affected oxygen consumption of *Cirrhinus mrigala* under all hours of exposure in both sublethal and lethal concentrations.

DISCUSSION

Several authors reported the effect of carbamate pesticides on the oxygen consumption in fish. Mariya Dasu (2014) observed initial increase in oxygen consumption in *Labeo rohita* exposed to Thiocarb. Anitha (2015) also observed increase in oxygen consumption during the initial time of exposures, i.e. 1 to 6 hours and a gradual decrease was observed during the subsequent period of study in *Labeo rohita* exposed to Pyraclostrobin. In lethal concentrations the rate of oxygen consumption showed a decreasing trend from the beginning to the end. Bantu *et al.,* (2017) observed increase in oxygen consumption during the initial time of exposures i.e., 1 to 4 hours and a gradual decrease during the subsequent ṗeriod in *Labeo rohita* exposed to sublethal concentrations of Indoxacarb for 24hrs and 8 days. Oxygen consumption decreased in *Labeo* during exposure to lethal concentrations of indoxacarb for 24 hours.

The initial increase in oxygen consumption in the present study is in agreement with Neelima *et al.,* (2016) in *Cyprinus carpio* exposed to cypermethrin, Jothinarendiran (2012) in *Channa punctatus* exposed to dimethoate, Bantu *et al.,* (2017) in *Labeo rohita* exposed Indoxacarb, Tilak and Vijaya kumar (2009) in *Channa punctatus* exposed to Quinaphos, Veeraiah (2001) in *Labeo rohita* exposed to Cypermethrin. Hyma Ranjani (2015) in *Catla catla* exposed to Glyphosate. The present work coincides with the report of the same.

The initial increase in oxygen uptake in sublethal concentration might be the reflection of an augmented physiological activity for elimination acting the chemical stress (Tilak and Vijaya kumar, 2009). Due to stress, muscular activity increases which results in an increased demand for oxygen. The increase in activity might boost up oxidative metabolism which results in increased supply of energy to combat the chemical stress (David *et al.,* 2003). Sree Veni and Veeraiah (2014) reported that due to stress there is increased respiratory activity, resulting in increased ventilation and increased uptake of the toxicant in *Cirrhinus mrigala* exposed to cypermethrin.

Several authors (Veenethkumar and David, 2008; Shereena *et al.*, 2009; Logaswamy and Remia, 2009) reported that alteration in whole animal oxygen consumption is due to the disturbance in oxidative metabolism in different species of fish exposed to pesticides. During the initial hours of exposure elevation in the rate of respiration could be explained in terms of acceleration of oxidative metabolism, as a result of sudden response to the toxic stimulus of the pesticide. With the onset of symptoms of poisoning, probably due to acclimatization to the chemical environment the rate decreased in the later periods of exposure. Similar observations were also made by Neelima *et al.,* (2016) and Jothinarendiran (2012). The results of the present study agree with above findings.

As the pesticides stimulate the peripheral nervous system, the activity of fish increases which requires more oxygen to fulfill the energy demand. This could be the reason for initial elevation in the rate of oxygen consumption (Rao, 1989). In sub lethal medium, in the subsequent period of exposure the respiration rate of fish decreased which might be due to acclimatization of the fish in the chemical environment (Rao, 1989 and Neelima *et al.,* 2016). Under toxic conditions, the oxygen in take decreases and a number of poisons become more toxic, so the amount of poison being exposed to the animal also increases. Fish breath more rapidly and the amplitude of respiratory movements will increase (Vakita Venkata Rathnamma and Nagaraju Bantu, 2014). By triggering the process of detoxification, the fish might have overcome the pesticide toxicity.,

In the later period the decrease in oxygen consumption appears to be a protective measure to ensure that there is low intake of the toxic substances which agrees with Tilak and Vijaya Kumar (2009). Subsequent decrease in oxygen consumption may be due to increased entry of Cartap hydrochloride molecules or their accumulation in the body of fish as a function of time. In sub lethal concentrations of the Cartap hydrochloride the decrease in oxygen consumption appears to be mainly due to lowering down of energy requirements which can be considered as adaptive and even strategic which is in accordance with findings of Tilak and Vardhan, (2002). Depletion in the oxygen consumption is due to disorganization of the respiratory action caused by

rupture in the respiratory epithelium of the gill tissue and also secretion of mucus over the gill curtails the diffusion of oxygen (Neelima *et al*., 2016).

Decreased oxygen consumption was observed by Maharajan *et al.,* (2013) in *Catla catla* exposed to Profenofos, by Vakita Venkata Rathnamma and Nagaraju Bantu (2014) in *Labeo rohita* exposed to Chlorantraniliprole, by Jipsa *et al.,* (2014) in *Tilapia mossambica* exposed to Cypermethrin, by Anthony reddy (2015) in *Labeo rohita* exposed to Spinosad. Joshi and Kulkarni (2007) reported that *Garramullya* (Skyes) when exposed to Cypermethrin and Fenevelerate, oxygen consumption increased in the initial period in both lethal and sublethal concentrations and thereafter decreased. They concluded that alteration in oxygen consumption increased and later decreased which is a bioindicator for assessing the pesticide toxicity, which can be correlated with the present study.

From the above results and discussion, it can be concluded that decrease in oxygen consumption in fish in response to the toxic stress is the cumulative effect of several stages at which the toxicant act. From the results obtained, it is clearly evident that Cartap hydrochloride affect the oxygen consumption of *Cirrhinus mrigala* in all exposed concentrations.

CONCLUSION

In conclusion, the analysis of data from the present investigation demonstrated that Cartap hydrochloride had a profound impact on respiration in *Cirrhinus mrigala* in both sublethal and lethal concentrations. Variation in the oxygen consumption in Cartap hydrochloride exposed fish was probably due to impaired oxidative metabolism and pesticide induced stress. Changes in gill architecture under Cartap hydrochloride stress would alter the diffusing capacity of gill with consequent hypoxic or anoxic conditions thus, respiration may become a problematic task for the fish. These results suggest that the altered rates of respiration in *Cirrhinus mrigala* may also serve as a rapid biological monitor to assess the impact of pesticides such as Cartap hydrochloride on other biotic communities in the water body. This study also stresses the diligent use of pesticides to prevent environmental pollution.

ACKNOWLEDGEMENTS

The authors are thankful to the UGC SAP-DRS-III for extending the infrastructure facilities to carry out the present work in the laboratories of the Dept. of Zoology & Aquaculture and also thank the Head, Department of Zoology and Aquaculture for permitting to do the work.

REFERENCES

Anon. 1975. Committee on methods of toxicity tests with fish macro invertebrates and amphibians. EPA, Oregon, 61.

Anitha, A. 2015. Pyraclostrobin (20% WG) induced toxicity and biochemical aspects of freshwater fish *Labeo rohita* (Hamilton) Ph.D. Thesis, Acharya Nagarjuna University. Nagarjuna Nagar, Guntur, A.P, India.

Anthony Reddy, P. 2015. *Impact of Spinosad (45% SC, Tracer) a biopesticide compound on freshwater fish, Labeo rohita* (*Hamilton*) Ph.D. Thesis, Acharya Nagarjuna University, Nagarjuna Nagar, Guntur, A.P, India.

Bantu, N., Hagos, Z., Krishna, C., Goplakrishnan, Abaynew, Rathnamma and Ravibabu, 2017. Acute toxicity and respiratory responses in freshwater fish, *Labeo rohita* exposed to an agrochemical Indoxacarb. *Algerian Journal of Environmental Science and Technology*. 3(3-B) : 595-603.

David, M., Shivakumar, H.B., Shivakumar, R. Mushigeri, S.B. and Ganti, B.H. 2003. Toxicity evaluation of cypermethrin and its effect on oxygen consumption of the freshwater fish , *Tilapia mossambica*, *Indian J. of Environ. Toxicol.*13: 99-102.

Fisher, R.A. 1950. *Statistical Methods for Research Workers,* 11th edition, (Edinburgh UK: Oliver and Boyd Ltd.).

Ganeshwade, R.M. 2012. Histopathological changes in the gills of *Puntius Ticto* (Ham) under dimethoate toxicity. *The BioScan*. 7(3) : 423-426.

Golterman, H. and Clymo, 1969. *Methods for Chemical Analysis of Fresh Water.* Black well Scientific Publication, 166.

Hyma Ranjani, G. 2015. *Glyphosate (Glycil 41% SL) a systemic herbicide impact on biochemical and histopathological changes in the freshwater fish Catla catla (Hamilton)*. Ph. D. Thesis, Acharya Nagarjuna University. Nagarjuna Nagar, Guntur, A.P, India.

Jabeen, F., Chaudhry, A.S., Manzoor, S. and Shaheen, T. 2016. Carbamates and neonicotenoids in Fish, water and sediments from the Indus River for potential health risks. *Environ. Monit. Assess*. 187 (2): 29.

Jipsa, J.R., Kalavathi, R., Dhanya, P.Y. and Logaswamy, S. 2014. Studies on the impact of a Cypermethrin insecticide on oxygen consumption and certain biochemical constituents of a fish *Tilapia mossambica. International Journal of Fisheries and*

Aquatic Studies. 1(5) : 93-97.

Job, S.V. 1955. The oxygen consumption of *Salvelinus fontinalis*. Univ. Toronto Biol. Ser. No. 61; *Ont. Fish. Res. Lab. Publ*. 73 : 1-39.

Joshi, P.P. and Kulkarni, G.K. 2007. Change in the oxygen consumption of a freshwater fish *Garra mulya* (Sykes) exposed to cypermethrin and fenvalerate. *Himalayan J. Environ. Zool.* 21(1): 7-13.

Jothinarendiran, N. 2012. Effect of dimethoate pesticide on oxygen consumption and gill histology of the fish, *Channa punctatus*. *Current Biotica*. 5 (4) : 500-507.

Logaswamy, S. and Remia. K.M. 2009. Impact of Cypermethrin and Ekalux on respiratory and some biochemical activities of a freshwater fish. *Tilapia Mossambica*. *Current Biotica*. 3 : 65-73.

Maharajan.A., Usha, R., Paru Ruckmani, P.S., Vijaykumar, B.S., Ganapiriya, V. and Kumarasamy, P.2013. Sublethal effect of Profenofos on oxygen consumption and gill histopathology of the Indian major carp, *Catla catla* (Hamilton). *Int. J. Pure Appl. Zool*. 1 (1) : 196-204.

Mariya Dasu, P. 2014. Thiodicarb 75 percentage wp a carbamate insecticide induced toxicity biochemical and histopathological changes in the freshwater Indian major carp *Labeo rohita* Hamilton, Ph.D. Thesis, Açharya Nagarjuna University, Nagarjuna Nagar, Guntur, A.P, India.

Neelima, P., Gopala Rao, N., Srinivasa Rao, G. and Chandra Sekhara Rao, J. 2016. A study on oxygen consumption in a freshwater fish *Cyprinus carpio* exposed to lethal and sublethal concentrations of cypermethrin (25% EC). *Int. J. Curr. Microbiol. App. Sci*. 5 (4) : 338-346.

Rao, D.M.R. 1989. Studies on the relative toxicity of Endosulphan to the Indian major carps *Catla catla* with special reference to some biochemical changes induced by the pesticide. *Pest. Biol. Phy*. 33 : 220-229.

Sree Veni, S.M. and Veeraiah, K. 2014. Effect of Cypermethrin (10%EC) on Oxygen Consumption and Histopathology of Freshwater Fish *Cirrhinus mrigala* (Hamilton). *IOSR J. Environ. Sci., Toxicol. Food Technol*. 8(10): 12-20.

Shereena, K.M., Logaswamy, S. and Sunitha, P. 2009. Effect of an organo phosphorous pesticides (Dimethoate) on oxygen consumption of the fish *Tilapia Mossambica*. *Recent Res. Sci. Technol*. 1: 4-7.

Subramani Lavanya, Mathan Ramesh, Chokkalingam Kavitha and Annamalai Malarvizhi, 2011. Hematological, biochemical and ion regulatory responses of Indian major carp *Catla catla*during chronic sublethal exposure to inorganic arsenic. *Chemosphere*. 82 : 977-985.

Tilak, K.S. and Vardhan, S.K. 2002. Effect of fenvalerate on oxygen consumption and hematological parameters in the fish. *Channa punctatus* (Bloch). *J. Aquatic Biol*. 17 : 81-86.

Tilak, K. S. and Vijaya Kumar, M. 2009. Effect of Quinaphos technical grade and commercial grade (25%EC) formulations on oxygen consumption in freshwater fish *Channa punctatus* (Bloch). *ANU Journal of Natural Sciences*: 39-45.

Vakita Venkata Rathnamma and Nagaraju Bantu. 2014. The effect of Chlorantraniliprole on the oxygen consumption of the freshwater fish *Labeo rohita* (Hamilton). *Frontiers of Biological and Life Sciences*. 5-7.

Veeraiah, K. and Durga Prasad, M. K. 2001. Studies on ventilatory patterns of fish under normal and stressed conditions using indigenously designed electronic recording instrument. *Proc. Intern. Conf. ICIPACT* -2001.

Vineetkumar, K. Patil and David, M. 2008. Behavior and respiratory dysfunction as an index of Malathion toxicity in the freshwater fish. *Labeo rohita* (Hamilton). *Turkish Journal of Fisheries and Aquatic Sciences*. 8 : 233-237.

Eco. Env. & Cons. 26 (August Suppl. Issue) : 2020; pp. (S127-S131)

ISSN 0971–765X

Effect of Cartap hydrochloride (50% SP) insecticide on gill histology of the fish, *Cirrhinus mrigala* (Hamilton)

G. Vani[1]*, K. Veeraiah [2], M. Vijaya Kumar[1] and S.K. Parveen[1]

[1]Department of Zoology, SRR & CVR Government Degree College (A), Vijayawada 520 004, Krishna District, A.P., India
[2]Department of Zoology and Aquaculture, Acharya Nagarjuna University, Nagarjunanagar 522 510, Guntur, A.P., India

Received 26 October, 2019; accepted 3 February, 2020)

ABSTRACT

The fish, *Cirrhinus mrigala,* Indian major carp was exposed to Cartap hydrochloride and the static LC_{50}values for 24,48,72 and 96 hours were found to be 0.436, 0.419, 0.394 and 0.376 mg^{-1} and 0.399, 0.371, 0.361 and 0.339 mg^{-1} in Continuous flow-through system. The gills which are the primary organs to get exposed to foreign contaminants and pesticides were studied for histological changes. The following histological changes like epithelial lifting, degeneration of primary and secondary gill lamellae, curling of secondary gill filaments, atrophy of secondary gill lamellae, congestion of secondary lamellae, fusion of secondary gill filaments were observed. The results obtained were discussed at length with the available literature. By studying the histological deformities, it was concluded that the pesticide caused enough damage to the gills of the fish and can influence on the survival of the fish

Key words : *Cartap hydrochloride, Cirrhinus mrigala, Gill histopathology*

Introduction

Indiscriminate and extensive use of pesticides in modern agricultural practices globally for achieving increased food production is one of the major sources of water pollution. Presence of pesticide in aquatic bodies is largely due to outfall from pesticide manufacturing factories and the runoff from agricultural fields (Ganeshwade, 2012). Pesticides are not highly selective but are generally toxic to macrophytes, non-target organisms such as fish (Ayoola, 2008 and Franklin *et al*., 2010).

Fish accumulate these pollutants directly or indirectly from polluted waters and food chain (Jabeen *et al*., 2016). In India, Cartap hydrochloride, a carbamate pesticide is extensively used in rice, sugarcane cabbage and cauliflower crops to control pests. In fish, the gill is the major organ for respiration, excretion and osmotic regulation. Gills are appropriate for the assessment of environmental impact as they are considered as a good tissue indicator of the water quality (Fanta, 2003). Histopathological analysis is a very sensitive parameter and is helpful in determining cellular damage that may occur in target organs (Altinok and Capkin, 2007). In this viewpoint an attempt was made to study the effect of sublethal and lethal concentrations of Cartap hydrochloride on gill histopathology of freshwater fish, *Cirrhinus mrigala* exposed for 24 and 96 hours.

Materials and Methods

The fingerlings of the test fish *Cirrhinus mrigala* of size 6-8 ± ½ cm and weight 6-7 ± ½ gm were pro-

cured from local fish hatcheries of Nandivelugu, Tenali mandal, Guntur district, Andhra Pradesh. The fish were acclimated at (28±2°C)) in the laboratory conditions for two weeks. All the precautions laid down on recommendations of the toxicity tests to aquatic organisms were followed (Annon, 1975). Fish were regularly fed with rice bran and one day prior to the experimentation feeding was stopped. Fingerlings were exposed to sub-lethal ($1/10^{th}$ of 96 h LC_{50} value 0.0376 mg^{-1}) and lethal (96 hours LC_{50} value 0.376 mg^{-1}) concentrations of Cartap hydrochloride for 24 and 96 hrs.

Gills were processed in laboratory for routine histological characterization by the double staining method using Haematoxylene and Eosin. All samples were fixed in 10% phosphate- buffered formalin for about 24 hrs. The specimens were dehydrated in a series of graded ethanol (50%, 70% and 90%) and then after embedded in paraffin. Five-micron sections were cut using an ultramicrotome (Leica, Japan) and deparaffinized by means of xylol. The sections were dehydrated in 90%, 70% and 50% ethanol followed by a 10 min wash in water and further stained with Hematoxylin and Eosin (HE). Sections were observed in digital microscope (Intel Play QX3) at 400 x magnification.

Results

The transverse section of gill tissue of normal fish shows branches from the central axis called the primary gill lamellae. Each of the primary gill lamella further divides into secondary gill lamellae or filaments. Within each division of the gills are the adjacent afferent vessels and efferent vessels with hemocytes. A thin septum separates the primary and secondary gill filaments. The secondary non branching filament lamella possesses epithelial pillar cells separated by large lacunae Fig. 1.

Cartap hydrochloride has induced marked pathological changes in gills of fish *Cirrhinus mrigala*. In the current study, it was observed that with the increase in the time of exposure the histopathological alterations increased in the gills of fish, *Cirrhinus mrigala*.

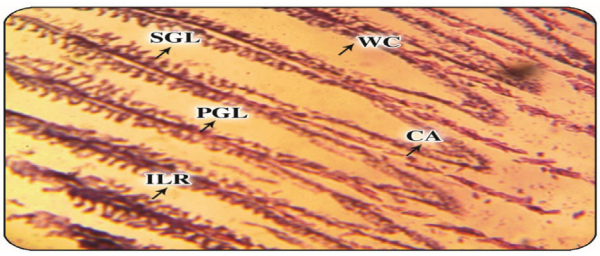

Fig. 1. Normal Gill tissue of *Cirrhinus mrigala*, H.E x 400

CA-Central Axis, PGL-Primary gill lamellae, SGL-Secondary gill lamellae, ILR-Inter lamellar space, WC-Water channel, FSG-Fusion of secondary lamellae, CSG-Curling of secondary lamellae, DPGL-Degenerated primary gill lamellae, DSGL-Degenerated secondary gill lamellae, BC-Blood congestion, EL-Epithelial lifting, LF-Lamellar fusion, ASL-Atrophy of secondary lamellae.

In the control group, no pathological changes were observed in the gills (Fig.1). After treatment with cartap hydrochloride for 24hrs at sublethal concentrationsepithelial lifting,curling of secondary gill filaments,fusion of secondary lamellae and degeneration of secondary gill lamellaestarted to appear (Fig. 2). Degenerative changes like lamellar fusion, epithelial lifting, degenerative secondary gill lamellae and curling of secondary gill filaments were observed after exposure to lethal concentration for 24hrs (Fig. 3). Similar more pronounced degenerative changes like curling of secondary gill filaments, epithelial lifting, degenerative primary and secondary gill lamellae, blood congestion, atrophy of secondary lamellae, mucous secretionwere no-

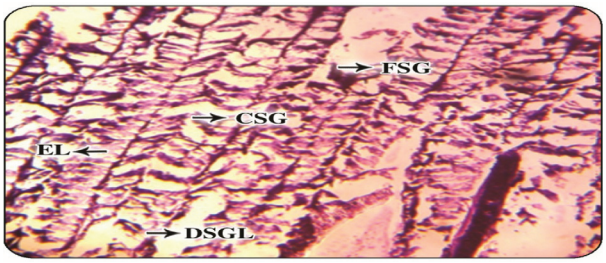

Fig. 2. Gill tissue of *Cirrhinus mrigala*exposed to sublethal concentration of Cartap hydrochloride for 24 hours, H.E x 400

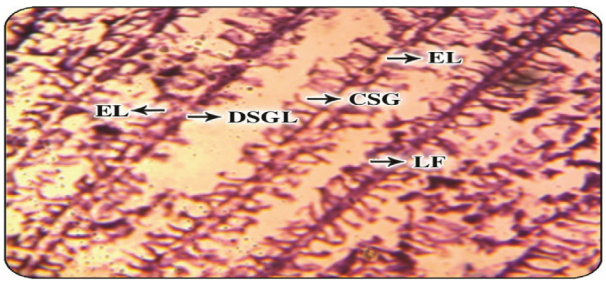

Fig. 3. Gill tissue of *Cirrhinus mrigala* exposed to lethal concentration of Cartap hydrochloride for 24 hours, H.E x 400

ticed in gill exposed to sublethal concentration of cartap hydrochloride for 96 hrs (Fig. 4). Damage in the gills exposed to lethal concentration of cartap hydrochloride for 96 hrs was much extensive with severe degeneration in primary and secondary gill lamellae, hemorrhage between gill filaments, separation of epithelial cells from the basement membrane, collapsed pillar cell, fusion of secondary gill lamellae, lamellar disorganization, atrophy of secondary lamellae, necrosis, blood congestion, mucous secretion, hyperplasia and epithelial lifting (Fig. 5). Thus, the lethal concentration of Cartap hydrochloride has produced significant histopathological changes in comparison to sublethal concentration in *Cirrhinus mrigala*.

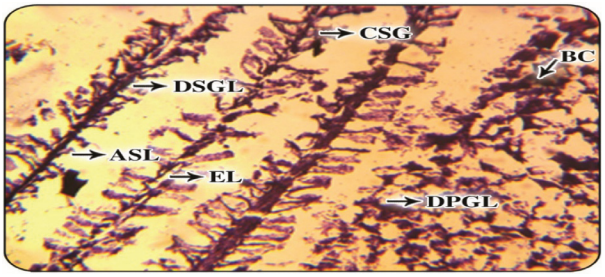

Fig. 4. Gill tissue of *Cirrhinus mrigala* exposed to sublethal concentration of cartap hydrochloride for 96 hours, H.E x 400

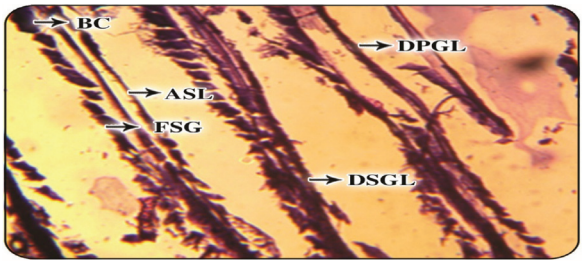

Fig. 5. Gill tissue of *Cirrhinus mrigala* exposed to lethal concentration of cartap hydrochloride for 96 hours, H.E x 400

Discussion

Several authors observed similar degenerative changes in gill when exposed to carbamate pesticides. Vivek *et al.*, (2016) observed fusion of primary and secondary lamellae, epithelial hyperplasia, curling of secondary lamellae, degeneration of lamellae in gills of *Labeo rohita* exposed to sublethal concentrations of cartap hydrochloride for 24,48,72 and 96hrs. Mariya dasu (2014) observed bulging of tips of primary gill filaments, curling of secondary gill filaments, necrosis, fusion of secondary gill lamellae, hyperplasia, hypertrophy of nuclei, pyknotic nuclei, lifting of epithelium in *Labeo rohita* exposed to Thiocarb, a thiocarbamate pesticide in both sublethal and lethal concentrations. Anitha (2015) observed necrosis, curling and fusion of secondary gill filaments, atrophy, degeneration of primary and secondary gill lamella, blood conjunction, epithelial hyperplasia, lamellar telangiectesis, in gills of *Labeo rohita* exposed to sublethal concentrations of Pyraclostrobin for 24 hrs, 5 days and 10 days and to lethal concentration for 24 hrs. Ali Taheri Mirghaed *et al*., (2018) noticed edema, lamellar curling, hyperplasia, lamellar fusion in the gill of *Cyprinus carpio* treated with 0.75 mg/L, 1.5 mg/L, and 3 mg/Lof indoxacarb for 7, 14 and 21 days. The histopathological changes observed in the present study were in accordance with the above studies.

Similar histopathological changes in gills were reported in *Channa punctatus* exposed to Imidacloprid (Pawara *et al.,* 2019), in *Labeo rohita* exposed to phenol (Butchiram *et al.,* 2013), in *Labeo rohita* exposed to cadmium (Saravanan *et al*., 2019), in *Oreochromis niloticus*exposed to heavy metals (Shameem Rani, 2018), in *Labeo rohita* exposed to tannery industrial effluent (Diana Handa and Gurinder Kaur Walia, 2019), in *Puntius sophore* treated with Acephate (Gavit and Patil, 2019), *in Cirrhinus mrigala* exposed to cement factory effluent (Juginu and Sujila, 2019) in *Cirrhinus mrigala*exposed to lead arsenate (Vanitha *et al.,* 2017), in *Labeo rohita* exposed to dimethoate (Dey and Saha, 2014), In *Cirrhinus mrigala* exposed to cypermythrin (Sree Veni and Veeraiah, 2014).

In fish, gill is the major organ for respiration, excretion and osmotic regulation. Gills are appropriate for the assessment of environmental impact as they are considered as a good tissue indicator of the water quality (Fanta, 2003). The lifting of lamellar epithelium in the present studymay be induced by the incidence of severe Oedema (Pane *et al.,* 2004). Swelling in gill epithelium leads to decreased efficiency of gases exchange and oxygen consumption. (Sudhasaravanan and Binukumari, 2015).

The first line of defense to metal/ toxicant exposure in the gills is mucus secretion and by fusion of lamellae it can temporarily protect the underlying epithelium from injury (Handy and Maunder, 2009). Pronounced secretion of mucus layer over the gill lamellae curtails the diffusion of oxygen (David *et al.*, 2002 and Rudragouda Marigoudar *et al*., 2009) which may ultimately reduce the oxygen consump-

tion by the animal (Kalavathy *et al*., 2001). All metabolic pathways depend upon the efficiency of the gills for their energy supply as gills are the major respiratory organs and damage to these vital organs lead to respiratory distress. The present histological studies clearly indicate that the damage in gills of *Cirrhinus mrigala* decreases the uptake of oxygen which results in histotoxic anoxia. Due to this the gill tissue suffers from oxygen debt and losses the capacity to remove CO_2 from blood which is in accordance with (Sathivel *et al*., 1991).

In the present study the observed alterations such as partial fusion of secondary lamellae, lifting of epithelial cells and proliferation of the epithelial cells, act as defense mechanisms towards toxicants. These alterations increase the distance between the external environment and the blood in the gills which serves as a barrier for the entry of contaminants. (Fernandes and Mazon, 2003 and Mallatt, 1985). When any type of toxicants meets gills, lamellar fusion in gills occur which is a protective measure as it diminishes the amount of vulnerable gill surface area in fish (Mallatt, 1985). when gills come in contact withany types of toxicants oedema appears to be a common feature of the gill pathology. Due to disturbance in branchial Na+, K+-ATPase pump by toxicants, solute accumulation in the epithelial cells occur and disturb the osmotic influx of water. This exchange protects the lamellar epithelial cells and prevents the entry of waterborne pollutants into the bloodstream (Arellano *et al*., 1999).

Conclusion

The results of the present study suggest that the changes in gill histomorphology of *Cirrhinus mrigala* may serve as a rapid biological 7monitor to assess the impact of Cartap hydrochloride on other biotic communities in the water body. The results of the present study also stress on the diligent usage of the pesticide product to prevent the environmental pollution.

Acknowledgements

The authors are thankful to the UGC SAP-DRS-III for extending the infrastructure facilities to carry out the present work in the Laboratories of the Dept. of Zoology & Aquaculture. They also thank the Head, Department of Zoology and Aquaculture for permitting to do the work.

References

Ali Taheri Mirghaed., Melika Ghelichpour., Seyed Saeed Mirzargar., Hamidreza Joshaghani. and Hoseinali Ebrahimzadeh Mousavi, 2018. Toxic effects of indoxacarb on gill and kidney histopathology and biochemical indicators in common carp (*Cyprinus carpio*). *Aquaculture Research*. 49(4) : 616-1627.

Altinok, I. and Capkin, E. 2007. Histopathology of rainbow trout exposed to sublethal concentrations of methiocarb or endosulfan. *Toxicol Pathol*. 35 : 405–10.

Anitha, A. 2015. *Pyraclostrobin (20%WG) induced toxicity and biochemical aspects of freshwater fish Labeo rohita* (Hamilton) Ph.D. Acharya Nagarjuna University. Nagarjuna Nagar, Guntur, A.P, India.

Annon, 1975. Committee on methods of toxicity tests with fish macro invertebrates and amphibians. EPA. Oregon: 61.

Arellano, J. M., Storch, V. and Sarasquete, C. 1999. Histological changes and copper accumulation in liver and gills of the *Senegales sole, Solea senegalensis. Ecotoxicology and Environmental Safety*. 44 : 62-72.

Ayoola, S.O. 2008. Toxicity of glyphosate herbicide on Nile tilapia (*Oreochromis niloticus*) juvenile. *Afr. J. Agric. Res*. 3 (12): 825-834.

Butchiram, M.S., Vijaya Kumar, M. and Tilak, K.S. 2013. Studies on the histopathological changes in selected tissues of fish *Labeo rohita* exposed to phenol. *Journal of Environmental Biology*. 34: 247-51.

David, M., Mushigari, S. B. and Prashanth, M. S. 2002. Toxicity of fenvalerate to the freshwater fish. *Labeo rohita. Geobios*. 29 : 25-28.

Dey Chandrimaand Saha Samir Kumar, 2014. Dimethoate (30% EC) induced toxicities on the tissues of the Indian major carp: *Labeo rohita* (Hamilton). *International Journal of Fisheries and Aquatic Studies*. 1(6) : 232-236.

Diana Handa. and Gurinder Kaur Walia. 2019.Quantitative and Semi-quantitative analysis on Gills of a freshwater fish, *Labeo rohita* (Hamilton-Buchanan, 1822) exposed to Tannery industrial effluent using histopathology as biomarker. *IJRAR*. 6(1): 980-981.

Fanta, E., Rios, F.S., Romao, S., Vianna, A.C.C. and Freiberger, S. 2003. Histopathology of the fish *Corydoras paleatus* contaminated with sublethal levels of organophosphorus in water and food. *Ecotoxicology and Environmental Safety*. 54(2) : 119-130.

Fernandes, M.N. and Mazon, A.F. 2003. Environmental Pollution and Fish Gill Morphology. In: Val, A.L. and Kapoor, B.G., Eds., Fish Adaptation. Science Publishers, Enfield: 203-231.

Franklin R. K., Loo, H. S. and Osumanu, H. A. 2010.Incorporation of Bentazone with Exserohilumrostratum for Controlling *Cyperusiria. Am. J. Agri. Biol. Sci*. 5: 210-214.

Gavit, P. J. and Patil, R. D. 2019. Effect of Acephate (Organophosphate) on Gill Histology of the Fresh Water Fish *Puntius sophore* (Hamilton). *IJRAR*. 6(1): 338-342.

Ganeshwade, R.M. 2012. Histopathological changes in the gills of *Puntius Ticto* (Ham) under dimethoate toxicity. *The BioScan*.7(3) : 423-426.

Handy, R. D. and Maunder, R. J. 2009. The biological roles of mucus: Importance for osmoregulation and osmoregulatory disorders of fish health. In: *Osmoregulation and Ion Transport: Integrating Physiological, Molecular and Environmental Aspects*. Society for Experimental Biology Press, London. I: 203- 235.

Jabeen, F., Chaudhry, A.S., Manzoor, S. and Shaheen, T. 2016. Carbamates and neonicotenoids in Fish, water and sediments from the Indus River for potential health risks. *Environ. Monit. Assess*. 187 (2) : 29.

Juginu, M. S. and Sujila, T. 2019. Histopathological responses of gill, liver and kidney in the freshwater fish, *Cyrrhinus mrigala* exposed to cement factory effluent. *Wjpps*. 8 (8) : 1511-1530.

Kalavathy, K., Siva Kumar, A.A. and Chandran, R. 2001. Toxic effects of the pesticide dimethoate on the fish, *Sarotherodon mossambicus*. *J. Ecol. Res Bio*. 2 : 27-32.

Mallatt, J. 1985. Fish gill structural changes induced by toxicants and other irritants: a statistical review. *Canadian Journal of Fisheries and Aquatic Science*. 42(4): 630-648.

Mariya Dasu, P. 2014. *Thiocarb 75 percentage WP a carbamate insecticide induced toxicity biochemical and histopathological changes in the freshwater Indian major carp Labeo rohita* Hamilton, Ph.D. Thesis, Acharya Nagarjuna University, Nagarjuna Nagar, Guntur, A.P, India.

Pane, E.F., Haque, A. and Wood, C.M. 2004. Mechanistic analysis of acute, induced respiratory toxicity in the rainbow trout, *Oncorhynchus mykiss*: an exclusively branchial phenomenon. *Aquatic Toxicology*. 69 : 11-24.

Pawara., Ravindra, H., Patel Nisar, G. and Sarvade Raju, C. 2019.Study on the effect of Imidacloprid on gill tissue of the fish *Channa punctatus* (Perciformes: Channidae) (Bloch.). *IJRAR*. 6 (1): 372-378.

Rudragouda Marigoudar, S., Nazeer Ahmed, R. and David, M. 2009. Cypermethrin induced respiratory and behavioral responses of the freshwater teleost, *Labeo rohita* (Hamilton). *Veterinarski Arhive*. 79(6): 583-590.

Sakthivel., Sampath, K. and Pandian, T.J. 1991. Sublethal effects of textile dye stuff effluent on selected oxidative enzymes and tissue respiration of *Cyprinus carpio* (Linn). *Indian J. Expt. Biol*. 29 : 979-981.

Saravanan, K., Mohanambal, R. and Iyyappan, A. 2019. Effect of cadmium on the histology of gill, liver and hepatopancreas of freshwater fish *Labeo rohita* (Hamilton, 1822). *IJRAR*. 6 (1) : 1255-1263.

Shameem Rani, K. 2018. Histological studies and heavy metal accumulation in the gills and muscles of tilapia fish from Vellar estuary, South East Coast of India, Tamilnadu. *IJRAR*. 5(3) : 298-304.

Sree Veni, S.M. and Veeraiah, K. 2014. Effect of Cypermethrin (10%EC) on Oxygen Consumption and Histopathology of Freshwater Fish *Cirrhinus mrigala*(Hamilton). *IOSR J. Environ. Sci., Toxicol. Food Technol*. 8(10) : 12–20.

Sudhasaravanan, R. and Binukumari, S. 2015. Effects of different concentartions of detergent on dissolved oxygen consumption in *Lepidocephalichythyes thermalis*. *World Journal of Pharmaceutical Research.* (2): 940-945.

Vanitha, S., Amsath,A., Shanthi,P. and Muthukumaravel, K. 2017. Sublethal effects of lead Arsenate on histology of selected organs of freshwater fish, *Cirrhinus mrigala*. *International Journal of Zoology and Applied Biosciences*. 2(5): 250-257.

Vivek, Ch., Veeraiah, K., Padmavathi, P. Dhilleswara Rao, H. and Bramhachari, P.V. 2016. Acute toxicity and residue analysis of cartap hydrochloride pesticide: Toxicological implications on the fingerlings of freshwater fish *Labeo rohita*. *Biocatalysis and Agricultural Biotechnology*. 7 : 193-201.

Nature Environment and Pollution Technology
An International Quarterly Scientific Journal

p-ISSN: 0972-6268
(Print copies up to 2016)
e-ISSN: 2395-3454

Vol. 19 | No. 5 (Suppl) | pp. 1821-1829 | 2020

Original Research Paper

https://doi.org/10.46488/NEPT.2020.v19i05.005

Open Access Journal

Biochemical Changes Induced by Cartap Hydrochloride (50% SP), Carbamate Insecticide in Freshwater Fish *Cirrhinus mrigala* (Hamilton, 1822)

G. Vani*†, K. Veeraiah, M. Vijaya Kumar*, Sk. Parveen* and G.D.V. Prasad Rao*****

*Department of Zoology, SRR & CVR Government Degree College (A), Vijayawada, Andhra Pradesh, India

**Department of Zoology and Aquaculture, Acharya Nagarjuna University, Nagarjunanagar-522 510, Guntur, Andhra Pradesh, India

***Department of Zoology SGS College, Jaggaiahpet, Andhra Pradesh, India

†Corresponding author: G. Vani; gandhamvanipradeep@gmail.com

Nat. Env. & Poll. Tech.
Website: www.neptjournal.com

Received: 08-11-2019
Revised: 25-11-2019
Accepted: 03-01-2020

Key Words:
Cartap hydrochloride
Cirrhinus mrigala
LC_{50}
Glycogen
Total proteins
Nucleic acids

ABSTRACT

The freshwater fish *Cirrhinus mrigala* was exposed to Cartap hydrochloride (50% SP) for 24, 48, 72 and 96 h. The LC_{50} values were found to be 0.436, 0.419, 0.394 and 0.376 mg^{-1} in static method and 0.399, 0.371, 0.361 and 0.339 $mg.L^{-1}$ in continuous flow-through system. The static LC_{50} values are higher than the continuous flow-through method. The LC_{50} values showed a decreasing trend with an increase in time of exposure in both the methods. The decrease was more in a continuous flow-through method than in the static method. The fish were exposed to sub-lethal ($1/10^{th}$ of 96 h LC_{50} value 0.0376 $mg.L^{-1}$) and lethal (96 h LC_{50} value 0.376 $mg.L^{-1}$) concentrations of the pesticide for 24 and 96 hours to study the alterations in glycogen, total proteins and nucleic acids (DNA & RNA) contents of various tissues viz., gill, brain, liver, kidney and muscle. Glycogen, total proteins and nucleic acids (DNA & RNA) content values decreased in all the tissues of exposed fish and the per cent decrease is more apparent in lethal concentrations than in sub-lethal concentrations. From the present study, it can be concluded that Cartap hydrochloride caused a decline in the glycogen, total protein and nucleic acids (DNA, RNA) content in *Cirrhinus mrigala* and the changes are more pronounced in lethal exposure than in sub-lethal exposure.

INTRODUCTION

Indiscriminate use of pesticides is one of the main reasons for the pollution of aquatic ecosystems. These toxic pesticides are causing deleterious effects on aquatic organisms. They are causing stress to aquatic organisms which are reflected as biochemical changes in their body (Mayers 1977). Fish acts as a bioindicator species and can be used for monitoring of water pollution as they accumulate the contaminants from polluted water and diet (Chaudary & Jabeen 2011, Kafilzadeh et al. 2012). Fish accumulate these pollutants directly or indirectly from polluted waters and food chain (Jabeen et al. 2016, Chaudary & Jabeen 2011). Carbamates are extensively used water-soluble pesticides in agricultural practices. In India, Cartap hydrochloride is a Carbamate pesticide which is considered as nereistoxin analog is extensively used in rice and sugarcane crops to control pests. The present investigation is aimed to study the toxic effects of Cartap hydrochloride in sub-lethal and lethal concentrations at 24 and 96 hours of exposure period on glycogen, total protein, DNA and RNA contents of freshwater fish *Cirrhinus mrigala* (Hamilton 1822).

MATERIALS AND METHODS

The fingerlings of the test fish *Cirrhinus mrigala* size 6-8 ± ½ cm and weight 6-7 ± ½ g were procured from local fish hatcheries of Nandivelugu, Tenali Mandal, Guntur district, Andhra Pradesh. The fish were acclimated at (28 ± 2°C)) in the laboratory conditions for two weeks. All the precautions laid down by APHA et al. (1998) were followed. During the acclimation period, the fish were fed with rice bran and groundnut cake. One day before the experimentation feeding was stopped. Cartap hydrochloride (50% SP) commercial grade was purchased from Mangalagiri, Guntur District. The stock solution was prepared with water as a solvent. The acclimatized fish were exposed to static sub-lethal (0.376 $mg.L^{-1}$) and lethal concentrations (3.76 $mg.L^{-1}$) of Cartap hydrochloride (50% SP) for 24 and 96 h. The hydrographical properties of water were estimated by the modified method followed by Golterman & Claimo (1969) method. Finney's probit analysis (Finney 1971) as reported by Roberts % Boyce (1972) was followed to calculate the LC_{50} value. The 95% confidence limits of the LC_{50} values for each test were also calculated for different time periods

by using SPSS software. At the end of the exposure periods, the tissues like gill, brain, liver, kidney and muscle were taken out from exposed and control fish and processed for the estimation of glycogen, total proteins and nucleic acids (DNA & RNA). Glycogen was estimated by the method of Kemp et al. (1954), total protein by Lowry et al. (1951) and DNA and RNA by the methods of Searchy & Maclinnis (1970a & 1970b).

The data obtained in the present work were expressed as means of four observations ± SD (standard deviation) and were statistically analysed using student "t" test (Pillai & Sinha 1968) to compare means of treated data against their controls and the result was considered significant at ($P < 0.05$) level.

RESULTS AND DISCUSSION

Glycogen, total proteins and nucleic acids (DNA & RNA) decreased in various tissues, viz. gill, brain, liver, kidney and muscle of *Cirrhinus mrigala* exposed to sub-lethal and lethal concentrations of cartap hydrochloride for 24 and 96 hours were graphically represented in Fig. 1 to Fig. 8. In exposed fish per cent decrease is more apparent in lethal concentrations than at sub-lethal concentrations.

Glycogen

The changes in glycogen content observed in the various tissues of *Cirrhinus mrigala* after the Cartap hydrochloride exposure along with the control are graphically represented in Fig .1 and Fig. 2.

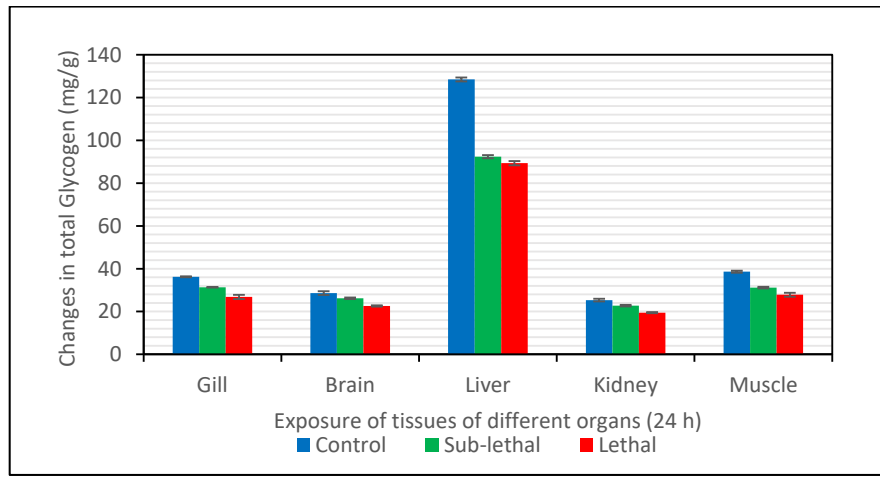

Fig.1: Changes in the glycogen content (mg/g wet weight of the tissue) in the tissue of fish *Cirrhinus mrigala* on exposure to sub-lethal and lethal concentration of Cartap hydrochloride (50%SP) for 24 hours.

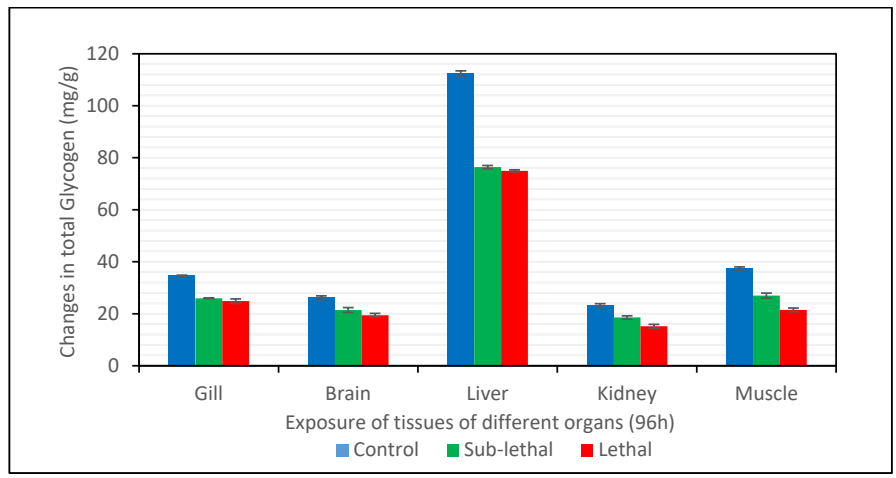

Fig. 2: Changes in the glycogen content (mg/g wet weight of the tissue) in the tissue of fish *Cirrhinus mrigala* on exposure to sub-lethal and lethal concentration of Cartap hydrochloride (50% SP) for 96 hours.

In the tissues of control fish, *Cirrhinus mrigala* glycogen content was in the order of:

Liver > Muscle > Gill > Brain > Kidney

Under exposure to sub-lethal and lethal concentrations of Cartap hydrochloride for 24 and 96 hours, the amount of glycogen was found to decrease in all the tissue of *Cirrhinus mrigala*. The lyotropic gradation series in terms of per cent decrement at 24 h and 96 h exposure was:

Sub-lethal -24 h: Liver > Muscle > Gill > Kidney > Brain

Lethal -24 h: Liver > Muscle > Gill > Kidney > Brain

Sub-lethal 96 h: Liver > Muscle > Gill > Kidney > Brain

Lethal-96 h: Muscle > Kidney > Liver > Gill > Brain

Exposure of *Cirrhinus mrigala* to Cartap hydrochloride for 24 hours caused a maximum decrease of glycogen in the liver (sub-lethal 28.117, lethal 30.453). For 96 h maximum decrease was found in the liver (sub-lethal 32.073) and muscle (lethal 42.570). In the present study under Cartap hydrochloride 24 h sub-lethal and lethal exposure minimum percentage of depletion was in the brain (8.595) and (20.96). For 96 h exposure minimum depletion was found in the brain (sub-lethal 18.056, lethal 25.707).

Srivastava & Singh (2013) observed reduction in glycogen content in different tissues of freshwater fish *Clarius batrachus* exposed to 80% of LC_{50} (22.87 $mg.L^{-1}$) of Mancozeb at different time intervals of 24 and 96 h. Sastry et al. (1982) reported decreased glycogen content of liver and muscles decreased when *Channa punctatus was exposed to* sub-lethal concentration of the carbamate pesticide, Sevin (1.05 $mg.L^{-1}$) for 15, 30 and 60 days. Veeraiah et al. (2013a) observed that exposure to sub-lethal and lethal concentrations of cadmium chloride in the fish *Cirrhinus mrigala* for 96 h caused changes in the total glycogen level which may be attributed to toxic stress, resulting in the disruption of enzymes associated with carbohydrate metabolism. Bantu & Rathnamma (2013) reported that there is a decrease in the amount of glycogen in the fish *Labeo rohita* exposed to sub-lethal and lethal concentrations of Dimethoate for 8 days. Priya et al. (2013) observed depletion of glycogen in the liver of freshwater teleost *Channa punctatus* (Bloch) when exposed to various concentrations of Imidacloprid (0.002 ppm, 0.00 ppm, 0.006 ppm, 0.008 ppm and 0.01 ppm) for 96 h suggesting the possibility of an alter from aerobic to anaerobic mode of energy metabolism of the liver. Dhanalakshmi (2013) noticed decrement in the tissue glycogen concentration in fish *Cirrhinus mrigala* when exposed to 0.25 ppm concentration of the metal chromium sulphate for 24, 48, 72 h and 10, 20 and 30 days which may be due to its enhanced utilization, since glycogen forms the immediate source of energy to meet energy demands under metallic stress caused by test toxicant.

Tataji & Kumar (2016) reported a decline in glycogen content of freshwater fish *Channa punctatus* exposed for 8 days to 1/5th of LC_{50} 96 hours of both Butachlor technical grade and Machete (50% EC), i.e. 32 ppb and 71.2 ppb for both technical and 50% EC respectively. Reduction in glycogen content was also noticed by Naik et al. (2016) in all the tissues of *Labeo rohita* when exposed to sub-lethal concentrations of cypermethrin for 1, 2 and 3 weeks. Exposure of sub-lethal doses (40% and 80 % of LC_{50} of 24 h) of glyphosate for 24 or 96 h against the freshwater non-target fish *Channa punctatus* caused significant ($P < 0.05$) alteration in biochemical parameters in liver and muscle tissues of the fish *Channa punctatus* (Bloch) was reported by Singh et al. (2017). Veeraiah et al. (2018) observed that exposure to lethal and sub-lethal concentrations of cyhalothrin 2.5% EC, in the fish *Ctenopharyngdon idellus* for 24 and 96 hours caused a decrease in glycogen content in all tissues.

According to Dezwaan & Zandee (1973) depletion of glycogen in tissues may be due to direct utilization of the compound for energy generation, a demand caused by pesticide-induced hypoxia. Under hypoxia condition, the fish derives its energy from anaerobic breakdown of glucose which is available to the cell by increased glycogenolysis (Chandravathy & Reddy 1996, Rajamannar & Manohar 1998, Rajamanickam 1992). Reduction in glycogen is probably due to its more rapid break down for energy requirement of fish (Muley et al.1996).

Liver suggested as an organ for detoxification. During exposure to Cartap hydrochloride exposure fishes came under stress condition and need more energy to cope with the toxicants. glycogen serves as reserve material. It is utilized when the body came under stress condition. Depletion of glycogen in liver and tissues may be due to increment in the glycolysis pathway. During stress conditions, the glycogen reserves depleted to meet energy demand (Rawat et al. 2002). Fall in glycogen levels indicates its rapid utilization to meet the enhanced energy demands intoxicant treated animals through glycolysis or hexose monophosphate pathway as observed by Cappon & Nicholas (1975). The above findings support the alterations of glycogen in the present study.

Proteins

The changes in protein content observed in the various tissues of *Cirrhinus mrigala* after Cartap hydrochloride exposure along with the control was graphically represented in Fig. 3 and Fig. 4.

The Protein content in different tissues in control fish *Cirrhinus mrigala* was in the order of:

Muscle > Liver > Brain > Kidney > Gill

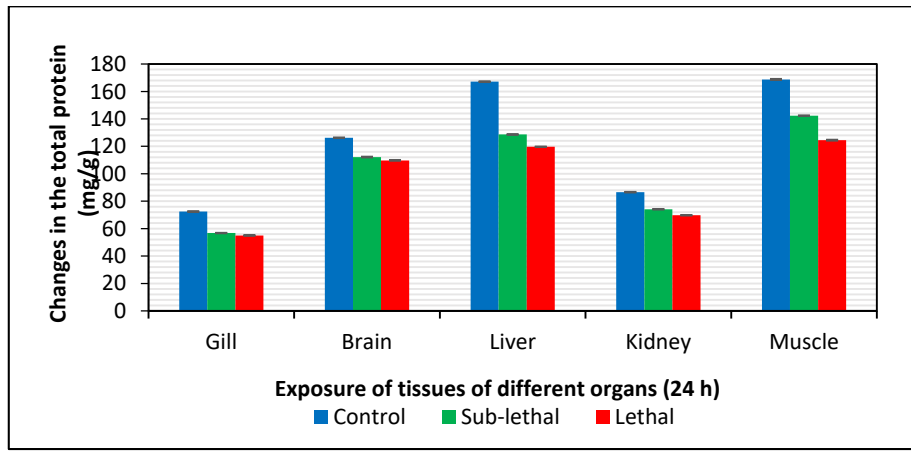

Fig. 3: *Changes* in protein content (mg/g wet wt of the tissue) in different tissues of fish *Cirrhinus mrigala* (Hamilton) on exposure to sub-lethal and lethal concentration of Cartap hydrochloride (50% SP) for 24 hours.

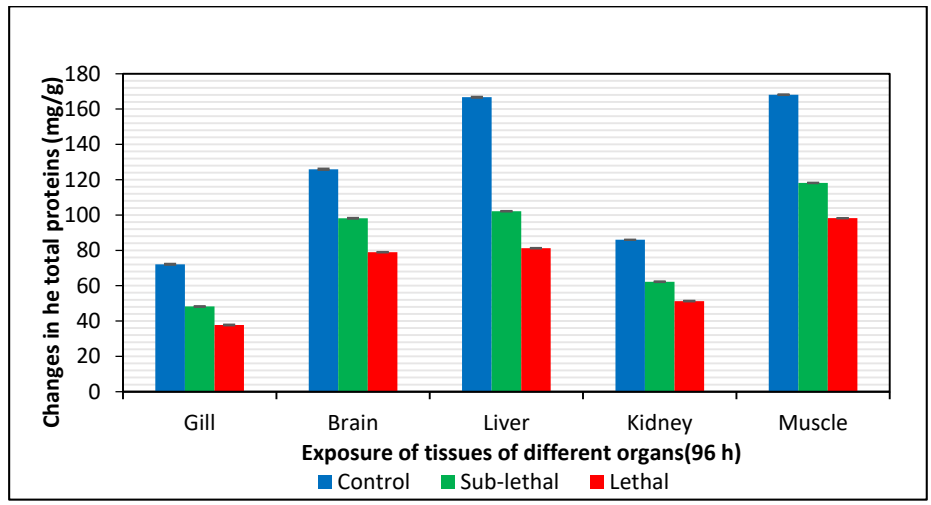

Fig. 4: Changes in protein content (mg/g wet wt of the tissue) in different tissues of fish *Cirrhinus mrigala* (Hamilton) on exposure to sub-lethal and lethal concentration of Cartap hydrochloride (50% SP) for 96hours.

Under exposure of sub-lethal and lethal concentrations of Cartap hydrochloride for 24 h, the amount of protein was found to decrease in all the tissue of *Cirrhinus mrigala.*

The lyotropic gradation series in terms of per cent decrement at 24 h and 96 h exposure was:

Sub-lethal -24 h: Liver > Gill > Muscle > Kidney > Brain

Lethal-24 h- Liver > Muscle > Gill > Kidney > Brain

Sub-lethal -96 h: Liver > Gill > Muscle > Kidney > Brain

Lethal-96 h: Liver > Gill > Muscle > Kidney > Brain

For 24 h exposure maximum per cent of the decrease in total protein was observed in the liver (sub-lethal 23.05, lethal 28.33). For 24 h exposure minimum percentage of depletion of total protein was found in the brain (sub-lethal 11.18, lethal 13.13). For 96 h the percentage of decrease was maximum in the liver (sub-lethal 38.72, lethal 51.27). Similarly, for 96 h minimum percentage of decrease was noticed in the brain (sub-lethal 22.06, lethal 37.30).

Protein is the most primary biochemical ingredient present in large quantities in the body of fish. Liver is rich in protein and centre for various metabolism of the fish. In the present study maximum decrease of total protein in the liver is due to the increased rate of proteolytic activity or repeated break down of protein to yield energy due to stress caused due to pesticide exposure. Anitha & Rathnamma (2016) noticed decreased protein levels in all the tissues like liver, kidney, brain, gill and muscle of *Labeo rohita* exposed to lethal and sub-lethal concentrations of Pyraclostrobin 20%

WG (carbamate) for 24 h and sub-lethal concentrations for 5 and 10 days. A decline in the protein content was noticed by Kumari et al. (2014) in the liver of *Clarias batrachus* when exposed to sub-lethal concentrations (2 and 4 $mg.L^{-1}$) of the Carbaryl for 96 h. A decrease in protein may be due to the impairment of protein synthesis or an increase in the rate of its degradation to amino acids. Exposure to Carbryl for 4 and 24 days, decreased protein content in liver and muscle of fish *Mugil cephalus*, when exposed to the lethal and sub-lethal concentration of Carbaryl for 4 days and 21 days respectively was reported by Shivanagouda et al. (2013). Kumar et al. (2017) reported a reduction in proteins in the liver and kidney of freshwater fish, *Channa punctatus* exposed to different sub-lethal concentrations of pesticide Carbaryl for a period of 15, 30, 45, 60, 75 and up to 90 days. Muddassir (2015) observed significant decrease value in Total protein in the liver of *Channa punctatus* was treated with 0.1 mL Carbofuran and 0.09 mL Malathion pesticides at different time intervals 7, 14, 21 and 28 days. The decrement of total protein may be due to the inhibition of RNA synthesis disturbing the protein metabolism or this may be due to liver damage where most protein synthesis usually occurs, these results agreed with that of Singh & Sharma (1998). The depletion of protein might also be attributed to spontaneous utilization of amino acids in various catabolic reactions inside the organism to combat the stress condition (Borah & Yadav 1996). Wankhedkar & Bhavsar (2015) found that total protein content significantly decreased in foot and hepatopancreas in land snail *C. moussonianus* when treated with Cartap hydrochloride and Imidacloprid at lowest concentration i.e. LC_{50} 0.41ppm and LC_{50} 0.54 ppm respectively. Veeraiah et al. (2018) observed a decrease in protein content in all tissues exposed to lethal and sub-lethal concentrations of cyhalothrin 2.5% EC, in the fish *Ctenopharyngdon idellus* for 24 and 96 h.

Proteins are important organic constituents of the animal cells. Understanding the protein components of the cell becomes necessary in the light of the radical changes taking place in protein profiles during pesticide intoxication (Anitha & Rathnamma 2016). The decreased trend of the protein content as observed in the present study in most of the fish tissues may be due to metabolic utilization of the ketoacids through gluconeogenesis pathway for the synthesis of glucose or due to the directing of free amino acids for the synthesis of necessary proteins, or for the maintenance of osmotic and ionic regulation (Schmidt Neilson 1975).

Nucleic Acids (DNA & RNA)

The changes in DNA content observed in the various tissues of *Cirrhinus mrigala* after the Cartap hydrochloride exposure along with the control was graphically represented in Fig. 5 and Fig. 6.

In control fish, DNA content present in different organs was in the order of:

Muscle > Gill > Brain > Liver > Kidney.

Under exposure to sub-lethal and lethal concentrations of Cartap hydrochloride, for 24 h the amount of DNA was found to decrease in all the tissue of *Cirrhinus mrigala.* The lyotropic gradation series in terms of per cent decrement at 24 h and 96 h exposure was:

Sub-lethal -24 h: Gill > Liver > Muscle > Brain > Kidney

Lethal-24 h-Gill > Liver > Muscle > Brain > Kidney

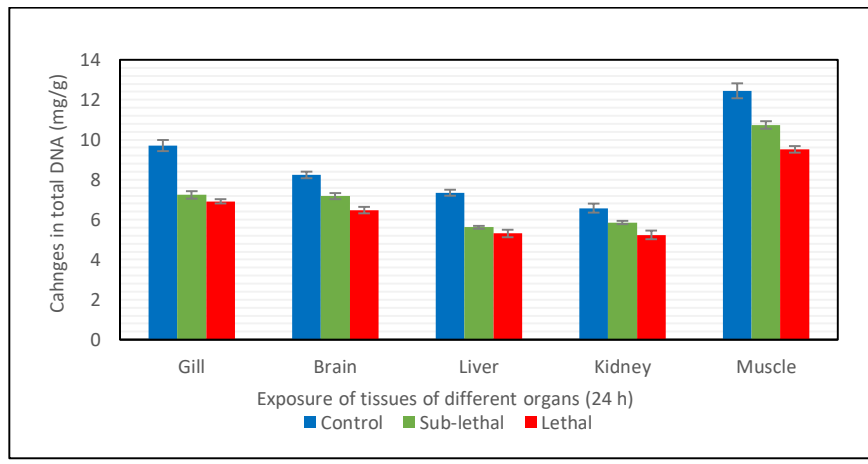

Fig. 5: Changes in the amount of deoxyribonucleic acid (DNA) (mg/g wet weight of the tissue) in different tissues of the fish, *Cirrhinus mrigala* on exposure to sub-lethal and lethal concentration of Cartap hydrochloride (50% SP) for 24 h.

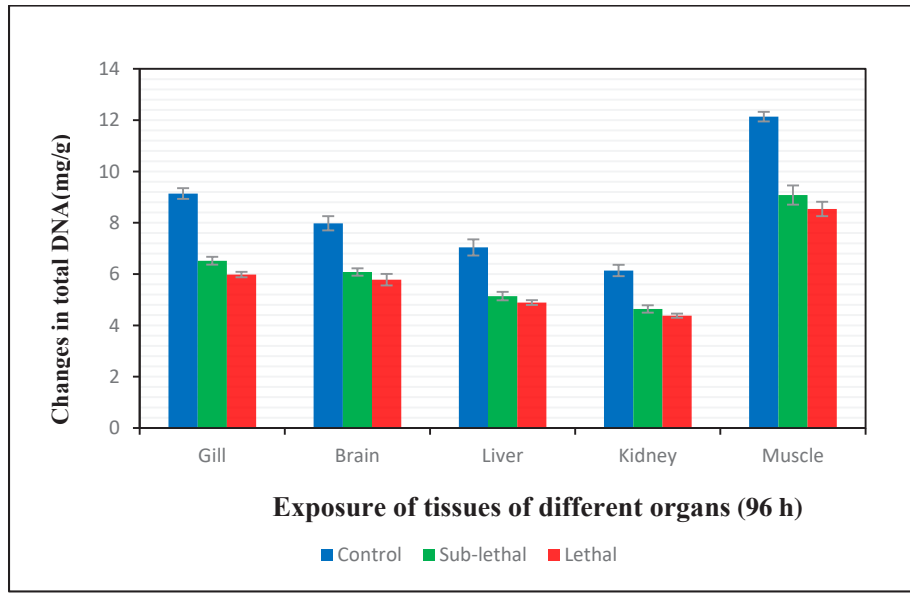

Fig. 6: Changes in the amount of deoxyribonucleic acid (DNA) (mg/g wet wt of the tissue) in different tissues of the fish *Cirrhinus mrigala* on exposure to sub-lethal and lethal concentration of Cartap hydrochloride (50% SP) for 96 h.

Sub-lethal-96 h: Gill > Liver > Muscle > Kidney > Brain

Lethal-96 h: Gill > Liver > Muscle > Kidney > Brain

In the present study under Cartap hydrochloride exposure for 24 h, maximum percentage of depletion in amount of DNA was noticed in Gill (sub-lethal 25.44, lethal 28.74). Minimum percentage of depletion was exhibited in the Kidney (sub-lethal 10.95, lethal 20.37). Under exposure to sub-lethal and lethal concentrations of Cartap hydrochloride for 96 h, maximum percentage of depletion was seen in Gill (sub-lethal 28.67, lethal 34.58) and minimum percentage of depletion was noticed in the brain (sub-lethal 23.81, lethal 27.57).

The changes in RNA content observed in the various tissues of *Cirrhinus mrigala* after Cartap hydrochloride exposure along with the control was graphically represented in Fig. 7 and Fig. 8.

The RNA content in different tissues in control fish *Cirrhinus mrigala* was in the order of:

Muscle > Brain > Gill > Liver > Kidney.

Under exposure to lethal and sub-lethal concentrations of Cartap hydrochloride, for 24 and 96 h, the amount of RNA was found to decrease in all the tissues. The lyotropic gradation series in terms of per cent decrement at 24 h and 96 h exposure was:

Sub-lethal -24h: Muscle > Gill > Kidney > Brain > Liver

Lethal-24h: Muscle > Gill > Kidney > Liver > Brain

Sub-lethal -96h: Gill > Muscle > Kidney > Liver > Brain

Lethal-96h: Gil l > Muscle > Liver > Kidney > Brain

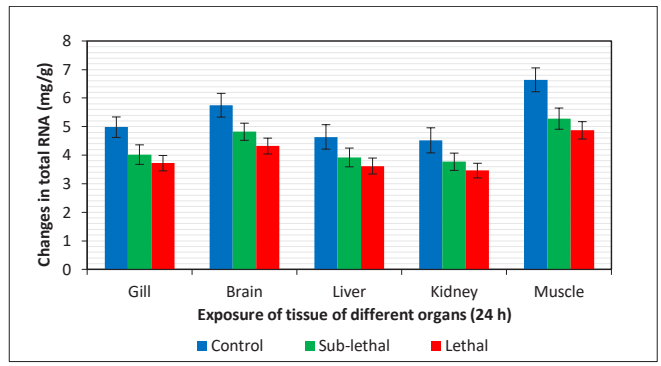

Fig. 7: Changes in the amount of ribonucleic acid (RNA) (mg/g wet wt of the tissue) in different tissues of the fish, *Cirrhinus mrigala* on exposure to sub-lethal and lethal concentration of Cartap hydrochloride (50% SP) for 24 h.

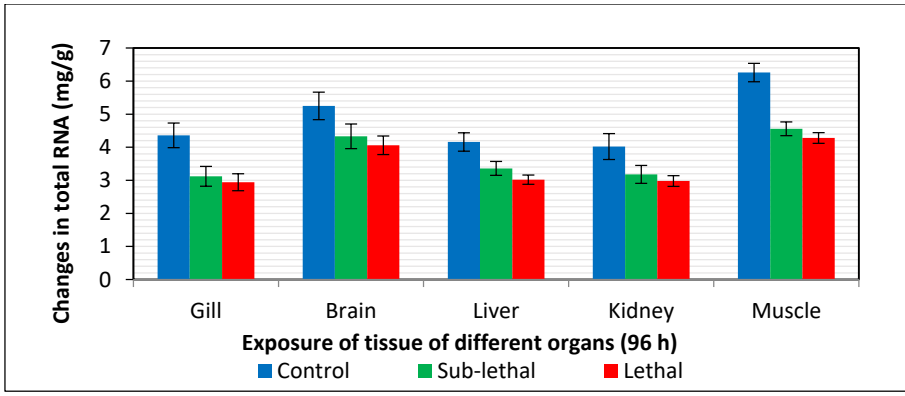

Fig. 8: Changes in the amount of ribonucleic acid (RNA) (mg/gm wet wt of the tissue) in different tissues of the fish, *Cirrhinus mrigala* on exposure to sub-lethal and lethal concentration of Cartap hydrochloride (50% SP) for 96 h.

After 24 h of exposure maximum percentage of decrease in the amount of RNA was found in muscle (sub-lethal 20.48, lethal 26.65). Minimum per cent of the decrease in RNA was found in the liver (15.51) in sub-lethal concentration and brain (19.65) in lethal concentration. After 96h of exposure maximum percentage of decrease in the amount of RNA was found in Gill (sub-lethal 28.44, lethal 32.56). Minimum percentage of decrease in RNA was found in brain(sub-lethal 17.52, lethal 22.66).

The results indicated that the DNA and RNA content in all the tissues of test fish were decreased compared to controls and the decreasing trend was more pronounced in lethal concentrations than in sub-lethal concentrations. In maintaining the physiological configuration of the fish Nucleic acids play a vital role. As Nucleic acid and protein play the main role in regulating different activities of cells they are regarded as important biomarkers of the metabolic potential of cells (Veeriah et al 2013a).

The decrease in nucleic acid content in the present study was in accordance with Vivek (2015) in fingerlings of *Labeo rohita* exposed to sub-lethal concentrations of Cartap hydrochloride for 24, 48, 72 and 96 h. Similar results were also found by Dasu (2014) in fingerlings of *Labeo rohita* were exposed to Thiocarb (Larvin 75% WP) a thiocarbamate pesticide. Anitha & Rathnamma (2016) noticed decreased DNA and RNA levels in all the tissues like liver, kidney, brain, gill and muscle of *Labeo rohita* exposed to lethal and sub-lethal concentrations of Pyraclostrobin 20%WG (carbamate) for 24 h and sub-lethal concentrations for 5 and 10 days.

Tilak et al. (2009) noticed a decreased level of DNA and RNA content in Alachlor treated freshwater fish, *Channa punctatus* (Bloch). The decrease of RNA may be due to inhibiting the function of RNA polymerase or due to interference in the incorporation of precursor in the nucleic acid synthesis. The alterations in DNA levels may be due to disturbances in DNA synthesis and its turnover rate besides degenerative changes caused by pesticides.

From the present study, it can be concluded that exposure of *Cirrhinus mrigala* to Cartap hydrochloride caused a decline in the glycogen, total protein and Nucleic acids (DNA, RNA) content which is more pronounced in lethal exposure than in sub-lethal exposure. The alterations caused during pesticide exposure may be due to the decreased catabolism of the biomolecules to meet the energy demand of test organism under stress or their reduced synthesis due to impaired tissue function. Therefore, the results of this study suggest a serious concern towards the potential danger of Cartap hydrochloride for the aquatic environment and organisms suggesting judicious and careful use of this pesticide in the agricultural area.

ACKNOWLEDGEMENTS

The authors are thankful to the UGC SAP-DRS-III for extending the infrastructure facilities to carry out the present work in the Laboratories of the Deptt. of Zoology & Aquaculture and thank the Head, Department of Zoology and Aquaculture for permitting to do the work.

REFERENCES

Anitha, A. and Rathnamma, V.V. 2016. Toxicity Evaluation and Protein Levels of Fish Labeo rohita Exposed to Pyraclostrobin 20% Wg (Carbamate). International Journal of Advanced Research, 4(3): 967-974.

APHA 1998. Standard Method for the Examination of Water and Wastewater, A.D. Eaton, L.S. Clesceri and A.E. Greenberg (Eds.), 20th edition. American Public Health Association, AWWA and WEF, Washington D.C.

Bantu, N. and Rathnamma Vakita 2013. Effect of dimethoate on mortality and biochemical changes of freshwater fish *Labeo rohita* (Hamilton). Journal of Biology and Today's World, 2(10): 456-470.

Borah, S. and Yadav, R.N.S. 1996. Effect of Rogor (30% w/w dimethoate) on the activity of lactate dehydrogenase, acid and alkaline phosphatase in muscle and gill of a freshwater fish, *Heteropneustes fossilis*. Journal of Environmental Biology, 17(4): 279-283.

Cappon, I.D. and Nicholls, D.M. 1975. Factors involved in increased protein synthesis in liver Microsomes after administration of DDT. Pestic. Biochem. Physiol., 5: 109-118.

Chandravathy, V.M. and Reddy, S.L.N. 1996. Lead nitrate exposure changes in carbohydrate metabolism of freshwater fish. Journal of Environmental Biology, 17: 75-79.

Chaudhry, A.S. and Jabeen, F. 2011. Assessing metal, protein, and DNA profiles in *Labeo rohita* from the Indus River in Mianwali, Pakistan. Environ. Monit. Assess., 174(1-4): 665-679.

Dasu, P.M. 2014. Thiocarb 75 % wp a carbamate insecticide induced toxicity biochemical and histopathological changes in the freshwater Indian major carp *Labeo rohita* Hamilton, Ph.D. Thesis, Acharya Nagarjuna University, Nagarjuna Nagar, Guntur, A.P, India

Dezwaan, A. and Zandee, D.I. 1973. Body distribution and seasonal changes in glycogen content of the common sea mussel, *Mytilus edulis*. Comp. Biochem. Physiol., 43: 53-55.

Dhanalakshmi, B. 2013. Acute and chronic toxicity of chromium on biochemical composition of the freshwater major carp *Cirrhinus mrigala* (Hamilton). Asian J. Sci. Technol., 4: 021-026.

Finney, D.J. 1971. Probit Analysis, 3rd edition. Cambridge University Press.

Golterman, H. and Claimo, R.S. 1969. Methods for Chemical Analysis of Freshwater. Blackwell Sci. Pub., 166 pp.

Jabeen, F., Chaudhry, A.S., Manzoor, S. and Shaheen, T. 2016. Carbamates and neonicotenoids in fish, water and sediments from the Indus River for potential health risks. Environ. Monit. Assess., 187(2): 29.

Kafilzadeh, F., Shiva, A.H., Malekpour, R. and Azad, H.N. 2012. Determination of organochlorine pesticide residues in water, sediments and fish from Lake Parishan, Iran. World J. Fish. Mar. Sci., 4(2): 150-154.

Kemp, A. and and Van Heijningen, A.J.K. 1954. A colorimetric method for the determination of glycogen in tissues. Bio. Chem. J., 56: 646-648.

Kumar, A., Singh, S. and Sharma, H.N. 2017. Changes in total protein in Liver and Kidney of freshwater fish, *Channa punctatus* (Bloch.) after intoxication of Carbaryl. Journal of Advanced Laboratory Research in Biology, 8(2): 41-43.

Kumari, A., Srivastava, A. and Jha, M.M. 2014. Carbaryl Induced alteration in histology and certain biochemical parameter in liver of *Clarias batrachus*. Global Journal of Bioscience and Biotechnology, 3(3): 259-263.

Lowry, O.H., Rosebrough, N.J., Farr, A.L. and Randall, R.J.1951. Protein measurement with the Folin Phenol Reagent. J. boil. Chem., 193: 265-275

Mayers, P. A. 1977. In: Review of Physiological Chemistry, 16th edition. Eds: Harper H A. Rodwell U V and Mayers P.A. Large Medical Publications, California.

Muddassir, A.T. 2015. Comparative study of biochemical alterations induced by carbofuran and malathion on *Channa punctatus* (Bloch.). International Research Journal of Biological Sciences, 4(9): 61-65.

Muley, D.V., Kamble, G.B. and Gaikwad, P.T. 1996. Endosulfan toxicity in the freshwater fish *Tilapia mossambica*. Journal of Aquatic Biology, 11: 61-66.

Naik, B. R., Rao, G. N. and Neelima, P. 2016. Sub-lethal toxicity of cyperkill (a synthetic pyrethroid pesticide) on glycogen content in the tissues of *Labeo rohita.* Int. J. Curr. Res. Aca. Rev., 4(12): 127-134.

Pillai, S.K. and Sinha, H.C.1968. Statistical Methods for Biological Works. Ramprasad and Sons, Agra.

Prasada Rao, G. D. V., Veeraiah, K., Krishna, Ch., Rajeswari, A. and Sindhoori, E. 2018. Cyhalothrin induced bio-chemical alterations in the grass carp *Ctenopharyngodon idellus* (Valenciennes). European Journal of Biomedical and Pharmaceutical Sciences, 5(9): 525-536.

Priya, B.P. and Maruthi, Y.A. 2013. Imidacloprid toxicity on biochemical constituents in liver tissue of fresh water teleost *Channa punctatus*. International Journal of Pharma and Bio Sciences, 4(4b): 50-54.

Rajamanickam, C. 1992. Effects of Heavy Metal Copper on the Biochemical Contents, Bioaccumulation and Histology of the Selected Organs in the Freshwater Fish, *Mystus Vittatus* (Bloch). Ph.D. Thesis, Annamalai University, India.

Rajamannar, K. and Manohar, L. 1998. Sublethal toxicity of certain pesticides on carbohydrates, proteins and amino acids in *Labeo rohita*. J. Ecobiol., 10(3): 185-191.

Rawat, D.K., Bais, V.S. and Agrawal, N.C. 2002. A correlative study on liver glycogen and endosulfan toxicity in *Heterpneustes fossilis*. J. Environ. Biol., 23: 205-207.

Roberts, M. and Boyce, C.B.C. 1972. In Methods in Microbiology. 7-A Edition. (eds: J.R. Norris and D.W. Ribbows). Academic Press, New York, pp 479.

Sastry, K.V. and Abad A Siddiqui. 1982. Chronic toxic effects of the carbamate pesticide Sevin on carbohydrate metabolism in a freshwater snakehead fish, *Channa punctatus*. Toxicology Letters, 14(1-2): 123-130.

Schmidt Nielson, B. 1975. Osmoregulation: Effect of salinity and heavy metal. Fed. Proc., 33: 2137-2146.

Searchy, D.G. and MacLennis, A.J. 1970a. Determination of DNA by the Barton Diphenylanine technique. In: Experiments and Techniques in Parasitology. (eds: A.J. Mac Lnnis and M. Voge) W.H. Freeman and Co, San-Franscisco, 190-191 pp.

Searchy, D.G. and MacLennis, A.J. 1970b. Determination of RNA by Dische orcinol technique. In: Experiments and Techniques in Parasitology. (eds: A.J. Mac Lennis and M. Voge). W.H. Freeman and Co, San-Francisco, pp. 189-190.

Shivanagouda, N., Sanagoudra and Bhat, U.G. 2013. Carbaryl induced changes in the protein and cholesterol contents in the liver and muscle of marine benthic fish, *Mugil cephalus*. American Journal of Biochemistry, 3(2): 29-33.

Singh, A. and Singh, A. 2017. Studies on toxicity stress, behavioural alterations and biochemical changes induced by glyphosate herbicide on the freshwater fish, *Channa punctatus* (Bloch). Int. J. Food Agricul. Veter. Sci., 7(3): 39-48.

Singh, R.K. and Sharma B. 1998. Carbofuran induced biochemical changes in *Clarias batrachus*. J. Pestic. Sci., 53: 285-290.

Srivastava, P. and Singh, A. 2013. In vivo study of effects of dithiocarbamates fungicide (mancozeb) and its metabolite ethylene thiourea (ETU) on freshwater fish *Clarius batrachus*. Journal of Biology and Earth Sciences, 3(2): B228-B235.

Tataji, P.B. and Kumar, M.V. 2016. Biochemical changes induced by Butachlor and Machete 50% EC to the freshwater fish *Channa punctata* (Bloch). International Journal of Science and Research, 5: 2048-2052.

Tilak, K.S., Raju, P.W. and Butchiram, M.S. 2009. Effects of alachlor on biochemical parameters of the freshwater fish, *Channa punctatus* (Bloch). J. Environ. Biol., 30(3): 421-426.

Veeraiah, K., Venkatrao, G., Vivek, Ch. and Hymaranjani, G. 2013a. Heavy metal, cadmium chloride induced biochemical changes in the Indian major *Cirrhinus mrigala* (Hamilton). Int. J. Bioassays, 2(07): 1028-1033.

Veeraiah, K., Vivek, Ch., Srinivas Rao, P. and Venkatrao, G. 2013b. Biochemical changes induced by Cypermethrin (10% EC), a pyrethroid compound in sub-lethal and lethal concentrations to the freshwater fish

Cirrhinus mrigala (Hamilton). J. Atoms and Molecules, 3(6): 625-634.
Vivek, Ch. 2015. Impact of Cartap Hydrochloride (50% SP) on Biochemical, Haematological and Enzymatic Activities of the Freshwater Fish, *Labeo Rohita* (Hamilton). Ph.D. Thesis submitted to Acharya Nagarjuna University, Nagarjuna Nagar, Guntur, A.P, India.
Wankhedkar, P. T. and Bhavsar, S.S. 2015. Effect of Cartap hydrochloride and Imidacloprid on biochemical parameters of *Cerastus moussonianus*. Biolife, 3(1): 125-131.

SRR & CVR GOVERNMENT DEGREE COLLEGE (AUTONOMOUS)
MACHAVARAM, VIJAYAWADA-520004
DEPARTMENT OF ZOOLOGY

Name of the Activity	**Training Programme attended by B.Sc. AT.Z.C Final year and Second year Aquaculture Technology students**
Place	**SIFT State Institute of Fisheries Technology Kakinada**
Date	**26/8/2019 to 31/8/2019**

As per the curriculum students go to SIFT STATE INSTITUTE OF FISHERIES TECHNOLOGY (SIFT) IN KAKINADA A.P and will have Hands on Experience in for one week TRAINING PROGRAMME ON PRINCIPLES OF AQUACULTURE AND DEMONSTRATION OF AQUA LAB PROCEDURES (water and soil analysis, microbiology, feed analysis and PCR) in different parameters and sectors of aquaculture.

In the training period, they are taken to different aquaculture ponds to understand the farming techniques, feeding management, disease identification in the ponds and water quality management in field area. Through these types of training programmes students will be exposed to practical approach in the field areas also.

*****

WORKSHOP

Printed Circuit Board (PCB) Designing

DATE: 13-03-2020

No. of Participants : 44

Instructor: Ch. Veera Arjuna Rao

CMOS Lab, Vijayawada

DEPARTMENT OF PHYSICS & ELECTRONICS

SRR & CVR GOVERNMENT DEGREE COLLEGE(A)

MACHAVARAM, VIJAYAWADA

PCB Circuit Design

Objective:

Training in Printed Circuit Board (PCB) Designing to enhance students' creativity.

This Training also help them to choose a career in PCB Designing.

A workshop on "PCB circuit Design " is arranged to MECs students by Department of Physics & Electronics.

Dr. Velaga Joshi, Principal; RJD, Guntur had chaired this program & mentioned consistently like these training programs are organised by Physics & Electronics department. These will trigger the creativity in students.

PCB Designing is an integral part of any Electronic Gadget or Robotics. A printed circuit board (PCB) mechanically supports and electrically connects electronic components using conductive tracks from copper sheets laminated onto a non-conductive substrate. Capacitors, resistors or active devices are soldered on the PCB.

Hands on experience to design electronic circuit with screen printing technique is demonstrated to students by Trainer from CMOS Lab, Vijayawada, **Ch. Veera Arjuna Rao**. Students prepared PCB & soldered electronic circuits used in their regular Lab's needs.

A total of 44 students from MECs had trained in this 1 Day training program with faculty.

Smt. Sailaja, HoD , Physics & Electronics Department encouraged students to learn PCB design and educated them the career opportunities in it.

Outcome:

Students are well trained in PCB fabrication, Circuit Design, Soldering, Screen Printing.

They got the knowledge of software tools available to build PCB.

They manufactured PCB & soldered electronic circuits used in their regular Lab's needs.

They educated about the further career opportunities available in PCB design.

Student Details who participated in PCB DESIGN workshop

SRR & CVR GOVERNMENT DEGREE COLLEGE(A)

DEPARTMENT OF PHYSICS & ELECTRONICS

Printed Circuit Board Designing Workshop

Dt : 13-03-2020

S.No.	Regd. No.	Name of the Student	Signature
1	19303201	Allacheruvu Brahmaiah	A. Brahmaiah.
2	19303202	Yetuvu Ramesh	Y. Ramesh
3	19303203	Shaik Ejaz	S. Ejaz
4	19303204	Perla Yaswanth Kumar	P. Yaswanth Kumar
5	19303206	Varanasi Hemanth Kumar	V. Hemanth Kumar
6	19303207	Kona Mani Kanth	K. mani Kanth
7	19303208	Shaik Abdul Shail	Shaik. Abdul Shail.
8	19303209	Lingam Subhashini	L. Subhashini
9	19303210	Matta Jaswanth	M. Jaswanth
10	19303211	Vaddipalli Navasimha Naidu	V. N. Naidu
11	19303212	Kollipara Teja	K. Teja
12	19303213	Ila Naga Vamsi	I. Naga Vamsi
13	19303214	Peluri Ramana	P. Ramana

14	19303215	Mattipalli Anantha Sai Krishna	M. A. Sai Krishna
15	19303216	Marangi Paul Diwakar	Marangi Paul Diwakar
16	19303217	Alluri Naga Divya Kalyani	A. N. Divya Kalyani
17	19303218	Chekka Swarna Sri	Chekka Swarna Sri
18	19303219	Jagannadham Avinash	J. Avinash.
19	19303220	Vemula Vijay Kumar	V. Vijay Kumar
20	19303221	Gannavarapu Lokesh Babu	Gannavarapu Lokesh Babu
21	19303224	Shaik Shahanaz	Sk. Shahanaz.
22	19303225	Mahanti Siddhartha	M. siddartha
23	19303228	Saladi Mahalakshmi Sireesha	S.M. Sireesha
24	19303230	Kolaboni Ganesh	K. Ganesh
25	19303231	Meka Bharadwaj Sai Krishna	M. Bharadwaj sai krishna
26	19303232	Kasarelli Veera Bhadra Rao	R. Veera Bhadra
27	19303233	Kosuri Naveen	K. Naveen
28	19303234	Vittanala Josesh	V. Josesh.
29	19303235	Chintra Chaitanya Kumar	C. C. Kumar
30	19303236	Shaik Althaf	G. Sai Teja
31	19303237	Tallapragada Manasa	T. Manasa.
32	19303238	Barlapudi Ajay	B. Ajay
33	19303239	Ramavath Naveen Naik	R. Naveen Naik

34	19303240	Vankadavathu Mantru Naik	Vankadavathu Mantru Naik
35	19303241	Vavilapalli Naga Mani	V. Naga Mani
36	19303242	Namalikanth Ramesh Babu	N. Ramesh Babu
37	19303243	Nadakuditi Ravi Varma	N. Ravi Varma
38	19303246	Gundala Venkata Ajay Kumar	G. Venkata Ajay Kumar
39	19303247	Ravada Sreedhar	Ravada Sreedhar
40	19303249	Shaik Duran	Shaik Duran
41	19303251	Kuthada Naga Venkateswara Rao	K.N. Venkateswara Rao
42	19303253	Pakkurthi Sai Ram	P. Sai Ram
43	19303254	Challari Venkata Mahesh	C. Venkata Mahesh
44	19303256	Mopidevi Venkata Vamsi Krishna	M. Venkata Vamsi Krishna

సాంకేతిక పరిజ్ఞానాన్ని పెంపొందించుకోవాలి

మధురానగర్: విద్యార్థులు ఎప్పటికప్పుడు మారుతున్న సాంకేతిక పరిజ్ఞానాన్ని పెంపొందించుకోవాలని అప్పుడే నిర్దేశించుకున్న లక్ష్యాలు సులభంగా చేరుకోగలమని ఆర్జేడీ డాక్టర్ వెలగా జోషి సూచించారు. స్థానిక మాచవరం ఎస్ఆర్ఆర్ అండ్ సీవీఆర్ ప్రభుత్వ డిగ్రీ కళాశాలలో శుక్రవారం ఫిజిక్స్, ఎలక్ట్రానిక్స్ విభాగం ఆధ్వర్యంలో ప్రింటెడ్ సర్క్యూట్ బోర్డ్ డిజైనింగ్ వర్క్‌షాప్ జరిగింది. కార్యక్రమంలో ఆయన ముఖ్య అతిథిగా పాల్గొని వర్క్‌షాప్‌ను ప్రారంభించారు. ఈ సందర్భంగా ఆయన మాట్లాడుతూ విద్యార్థుల్లోని సృజనాత్మకతను వెలికితీయటానికి ఇటువంటి వర్క్‌షాప్‌లు దోహదపడతాయన్నారు. విద్యార్థులు పరిశోధనకు ప్రాధాన్యత ఇవ్వాలని సూచించారు. అనంతరం రిసోర్స్ పర్సన్‌లు సీఎంఓఎస్ రీసెర్చ్ ల్యాబ్ విజయవాడ నుంచి సీహెచ్ వీర అర్జునరావు ప్రింటెడ్ సర్క్యూట్ బోర్డ్ డిజైనింగ్, షోల్డరింగ్, సర్క్యూట్ తయారీ, స్క్రీన్ ప్రింటింగ్ తదితర అంశాలను వివరించారు. కార్యక్రమాలను ఫిజిక్స్ అండ్ ఎలక్ట్రానిక్స్ విభాగాధిపతి పి. శైలజ పర్యవేక్షించగా, అధ్యాపకులు నయోమి, కనకాల సాయిబలరామ్ సమన్వయపరిచారు.

కాలానుగుణంగా విద్యాబోధన మారాలి

మధురానగర్: మారుతున్నకాలం, పరిస్థితులకు నుగుణంగా విద్యాబోధన చేసి విద్యార్థులను ఉన్నత పౌరులుగా తీర్చిదిద్దాల్సిన బాధ్యత అధ్యాపకులపై ఉందని ఆర్జేడీ, కళాశాల ప్రిన్సిపల్ డాక్టర్ వెలగా జోషి అన్నారు. స్థానిక

ప్రింటెడ్ సర్క్యూట్ బోర్డ్ డిజైనింగ్ వర్క్‌షాప్‌లో ప్రయోగాలు చేస్తున్న విద్యార్థులు

మాట్లాడుతున్న ప్రిన్సిపల్ డాక్టర్ వెలగా జోషి

మాచవరం ఎస్ఆర్ఆర్ అండ్ సీవీఆర్ ప్రభుత్వ డిగ్రీ కళాశాలలో శుక్రవారం ఇంటర్నల్ క్వాలిటీ ఎష్యూరెన్స్ సెల్ ఆధ్వర్యంలో ఇన్ఫర్మేషన్ అండ్ కమ్యునికేషన్ టెక్నాలజీ టీచింగ్ మెథడాలజీపై ఫ్యాకల్టీ డెవలప్‌మెంట్ వర్క్‌షాప్ జరిగింది. కార్యక్రమంలో పాల్గొన్న ఆయన మాట్లాడుతూ బోధనా పద్ధతుల్లోని మెలకువలను తెలియజేసేందుకు జిల్లాలోని వివిధ డిగ్రీ కళాశాల అధ్యాపకులకు వర్క్‌షాప్‌ను నిర్వహిస్తున్నట్లు తెలిపారు.

సాక్షి Sat, 14 March 2020
https://epaper.sakshi.com/c/49928543

సాంకేతిక పరిజ్ఞానాన్ని పెంపొందించుకోవాలి

ప్రింటెడ్ సర్క్యూట్ బోర్డ్ డిజైనింగ్ వర్క్‌షాప్‌లో ప్రయోగాలు చేస్తున్న విద్యార్థులు; మాట్లాడుతున్న ప్రిన్సిపల్ డాక్టర్ వెలగా జోషి

మధురానగర్: విద్యార్థులు ఎప్పటికప్పుడు మారుతున్న సాంకేతిక పరిజ్ఞానాన్ని పెంపొందించుకోవాలని అప్పుడే నిర్దేశించుకున్న లక్ష్యాలు సులభంగా చేరుకోగలమని ఆర్జేడీ డాక్టర్ వెలగా జోషి సూచించారు. స్థానిక మాచవరం ఎస్ఆర్ఆర్ అండ్ సీవీఆర్ ప్రభుత్వ డిగ్రీ కళాశాలలో శుక్రవారం ఫిజిక్స్, ఎలక్ట్రానిక్స్ విభాగం ఆధ్వర్యంలో ప్రింటెడ్ సర్క్యూట్ బోర్డ్ డిజైనింగ్ వర్క్‌షాప్ జరిగింది. కార్యక్రమంలో ఆయన ముఖ్య అతిథిగా పాల్గొని వర్క్‌షాప్‌ను ప్రారంభించారు. ఈ సందర్భంగా ఆయన మాట్లాడుతూ విద్యార్థుల్లోని సృజనాత్మకతను వెలికితీయటానికి ఇటువంటి వర్క్‌షాప్‌లు దోహదపడతాయన్నారు. విద్యార్థులు పరిశోధనకు ప్రాధాన్యత ఇవ్వాలని సూచించారు. అనంతరం రిసోర్స్ పర్సన్‌లు సీఎంఓఎస్ రీసెర్చ్ ల్యాబ్ విజయవాడ నుంచి సీహెచ్ వీర అర్జునరావు ప్రింటెడ్ సర్క్యూట్ బోర్డ్ డిజైనింగ్, షోల్డరింగ్, సర్క్యూట్ తయారీ, స్క్రీన్ ప్రింటింగ్ అంశాలను వివరించారు. కార్యక్రమాలను ఫిజిక్స్ అండ్ ఎలక్ట్రానిక్స్ విభాగాధిపతి పి. శైలజ పర్యవేక్షించగా, అధ్యాపకులు నయోమి, కనకాల సాయిబలరామ్ సమన్వయపరిచారు.

కాలానుగుణంగా విద్యాబోధన మారాలి

మధురానగర్: మారుతున్నకాలం, పరిస్థితులకు నుగుణంగా విద్యాబోధన చేసి విద్యార్థులను ఉన్నత పౌరులుగా తీర్చిదిద్దాల్సిన బాధ్యత అధ్యాపకులపై ఉందని ఆర్జేడీ, కళాశాల ప్రిన్సిపల్ డాక్టర్ వెలగా జోషి అన్నారు. స్థానిక మాచవరం ఎస్ఆర్ఆర్ అండ్ సీవీఆర్ ప్రభుత్వ డిగ్రీ కళాశాలలో శుక్రవారం ఇంటర్నల్ క్వాలిటీ ఎష్యూరెన్స్ సెల్ ఆధ్వర్యంలో ఇన్ఫర్మేషన్ అండ్ కమ్యునికేషన్ టెక్నాలజీ టీచింగ్ మెథడాలజీపై ఫ్యాకల్టీ డెవలప్‌మెంట్ వర్క్‌షాప్ జరిగింది. కార్యక్రమంలో పాల్గొన్న ఆయన మాట్లాడుతూ బోధనా పద్ధతుల్లోని మెలకువలను తెలియజేసేందుకు జిల్లాలోని వివిధ డిగ్రీ కళాశాల అధ్యాపకులకు వర్క్‌షాప్‌ను నిర్వహిస్తున్నట్లు తెలిపారు. అనంతపూర్ ప్రభుత్వ కళాశాల జువాలజీ అసోసియేట్ ప్రొఫెసర్ డాక్టర్ జి. రాజశేఖర్ రిసోర్స్ పర్సన్‌గా వ్యవహరించారు. కార్యక్రమంలో వర్క్‌షాప్ కోఆర్డినేటర్ ఎం. శ్యాంబాబు పాల్గొన్నారు.

సాక్షి Sat, 14 March 2020
https://epaper.sakshi.com/c/49928596

WORKSHOP

NANO MATERIALS PREPARATION

DATE: 12-12-2019

RESOURCE PERSON : **Dr.G.GIRIDHAR**

Asst. Professor, Department of Nano Technology

Acharya Nagarjuna University, Nagarjuna Nagar

No of Students Participated: **40**

DEPARTMENT OF PHYSICS & ELECTRONICS

SRR & CVR GOVERNMENT DEGREE COLLEGE (AUTONOMOUS),

Machavaram, Vijayawada - 520 004

NANO MATERIALS PREPARATION

The Department of Physics & Electronics had conducted a one day workshop on "Preparation of NanoMaterials" in Collaboration with NanoTechnology Department Acharya Nagarjuna University , Nagarjuna Nagar , Guntur.

Objectives of Workshop

- To create interest in students on research in Material Science & enrich their knowledge on new technologies.
- To acknowledge students about Easy & low cost equipment methods to prepare nanoparticles in UG labs.
- Students are able to do Nano particle preparation as their future Project work.

S.R.R. & C.V.R. GOVT. DEGREE COLLEGE
(Autonomous)
NAAC accredited with 'B+' Grade
Machavaram, VIJAYAWADA - 520 004. Krishna District.
Cell : 94922 34488 Ph : 0866-2430060, Fax : 0866-2441092, www.srrcvr.org, srrandcvr@gmail.com

Dr. Velaga Joshi, Principal
M.A. (Phil.), M.A. (His.), M.A., (M.C.J.), B.L., M.Phil., Ph.D.,

Date 11 DEC 2019

To,
Dr. G. Giridhar,
Assistant Professor,
Dept. of Nano Technology,
Acharya Nagarjuna University,
Nagarjuna Nagar,
Guntur District.

Respected Sir,

Sub: Invitation to conduct Workshop on Preparation of Nano Materials For Final B.Sc., Students of SRR & CVR Govt. Degree College (A), Vijayawada on 12th December, 2019 – Regarding.

* * *

The Department of Physics/Electronics, SRR & CVR Govt. Degree College (A), Vijayawad is going to conduct Workshop on preparation of Nano Materials for Final B.Sc., Students on 12th December, 2019.

Hence, I request you sir, kindly come and conduct the workshop as a resource person on 12th December, 2019 in our college for which we are grateful to you sir.

Thanking You Sir,

Yours Sincerely,

Dr. Velaga Joshi, Principal
Principal
SRR & CVR Govt. COLLEGE
VIJAYAWADA.

As per the request forwarded by The Department of Physics & Electronics, SRR & CVR GDC(A), Vijayawada, Dr. G. Giridhar , Assistant Professor , Nanotechnology arranged a workshop at Physics Lab , SRR & CVR GDC(A) on Dt. 12-12-2019.

Dr. Giridhar demonstrated the experimental procedure to synthesise Zinc, manganese, Silver nanoparticles in a lab using chemicals and magnetic stirrer.

He discussed the precautions that should be taken to prepare superior metal nanoparticles.

He explained the various other methods, characterization techniques & applications of these Nanoparticles.

Students interacted with the resource person & refined their knowledge on nano materials.

Dr. Velaga Joshi , Principal , RJD(FAC), Guntur felicitated Dr. Giridhar & appreciated both staff , students of Physics & Electronics Department.

Dr. Joshi said such workshops are arranged by Physics & Electronics Department from time to time to inculcate & develop new technologies to students.

Profile of Resource Person : Dr.G.GIRIDHAR

Dr. Giridhar Published 30 (international)+ 2 (national) journal Publication in various research topics of material sciences.

He also guided 11 students for CSIR-SRTP-2020 . Under his guidance 1 Ph.D & 1 M. Phil. is successfully awarded.

Outcomes

Students had hands on experience on nano particles preparation which is the part of their Curriculum in Modern Physics.

It enhanced their knowledge about the application of nano particles of normal metals they use in their daily life.

Few students got much interest to continue their higher studies in Physics & nano Technology.


Zn Nano Particle
Mn - Nano Particle
Cu - Nano Particle

COLLEGE ACTIVITY REGISTER

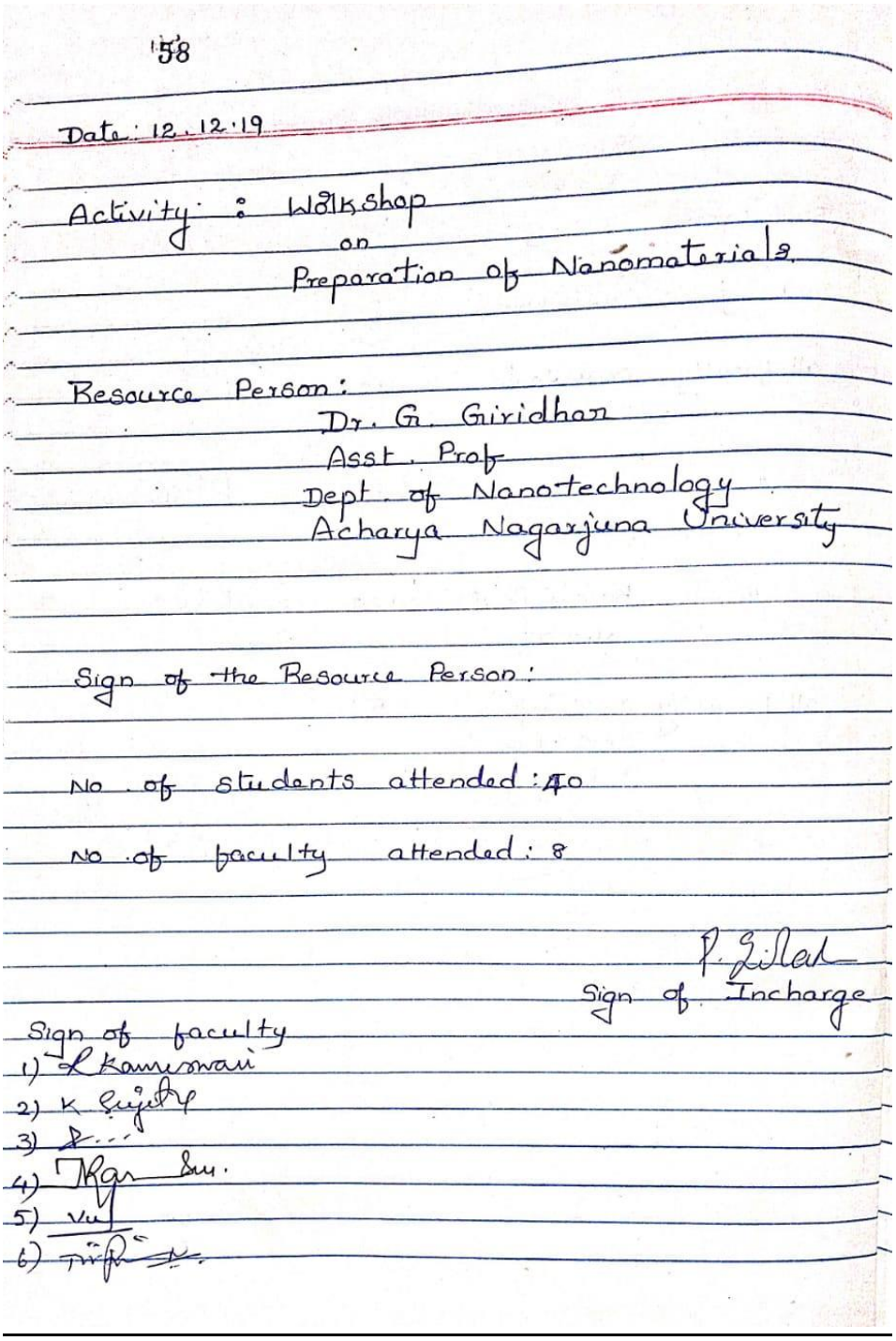

158

Date: 12.12.19

Activity : Workshop
on
Preparation of Nanomaterials

Resource Person:
Dr. G. Giridhar
Asst. Prof
Dept. of Nanotechnology
Acharya Nagarjuna University

Sign of the Resource Person:

No. of students attended: 40

No. of faculty attended: 8

P. Lillah
Sign of Incharge

Sign of faculty
1) K Kameswari
2) K Sujatha
3) ...
4) Rgr Sw.
5) Vu
6) ...

STUDENTS ATTENDANCE

S.R.R. & C.V.R. GOVT. DEGRE COLLEGE (A)

Machavaram, Vijayawada – 520004, Krishna District, A.P.

DEPARTMENT OF PHYSICS

All the B.Sc final year Students attended the WORK-SHOP On "Preparation of Nano Materials" on 12th December 2019 in final year B.Sc Physics lab from 10 A.M to 5 P.M. Dr.G.Giridhar, Asist. Professor in Nano Technology, Acharya Nagarjuna University, Guntur is a Resource Person.

Student Attendance

Sl.No	Name of the Students	Signature of the students
1.	A.Pedda Anantha Raju.	A.P.A. Raju.
2.	M. Prabhukiran	M. Prabhu Kiran.
3.	M. Venkaiah	M. Venkaiah
4.	SHABANA FATHIMA	Shabana Fathima
5.	V. VAISHNAVI	V. Vaishnavi
6	M. Siva	M. Siva
7.	T. Durga Vasi	T. Vasi
8.	B. Kranthi Koti	B. Kranthi Koti
9.	L. Thaubi	L. Thoubi
10.	D. Purnachandra Rao	D. Purna.
11.	T. Bhargav	T. Bhargav
12.	B. sudheer	B. Sudheer
13.	G. naveen kumar	Gnaveen
14.	M. venkaiah	
15.	A. Kondalu	A. Kondalu
16.	K.V. Krishna Reddy	K.V. Reddy
17	K. Mounika	K. Mounika
18	K. Prasanna Gopal	K. Prasanna Gopal
19.	V. Samatha	V. Samatha
20	Sk. Nazma	Sk. Nazma
21	G. Prathima	G. Prathima.
22	P. Vinod kumar	P. Vinod kumar

Sl.No	Name of the Students	Signature of the students
23	R. Vijaya Kumar	R Vijaya Kumar
24.	G. Rama Kalyan	G. Ramakalyan
25	P. Aravind	P. Aravind
26.	K. Antaryami	K. Antaryami Rao
27.	L. Uday Kiran	Udaykiran
28.	V. Narasimha	V. Narasimha Rao
29.	K. Jagadish	K. Jagadesh
30.	~~Subramanyam~~	
31.	A. Subrahmanyam	A. Subrahmanyam
32.	M. Gopi Chandana	M. Gopi Chandana C.
33.	V. Uma Maheswari	V. Uma Maheswari
34.	P Sarathi	P Sarathi
35.	T. Sai S.V.D Jyothi	T. Sai S.V.D Jyothi
36.	T. Damayanthi	T. Damayanthi
37.	P. Rohini	P. Rohini
38.	D. Renuka	D. Renuka
39.	K. Shamitha	K. Shamitha
40.	B. Shanmukha Sai	B. Shanmukha Sai
	B. Nagaraju	B. Nagaraju

PAPER CLIPPINGS

'ఎస్ఆర్ఆర్'లో నానో టెక్నాలజీపై వర్క్‌షాప్

మధురానగర్: మాచవరం ఎస్ఆర్ఆర్ అండ్ సీవీఆర్ ప్రభుత్వ డిగ్రీ కళాశాలలో కళాశాల భౌతిక శాస్త్రం, ఎలక్ట్రానిక్స్ విభాగం ఆధ్వర్యంలో నానో టెక్నాలజీ రంగంలోని నానో మెటీరియల్స్, నానో పదార్థాల తయారీపై గురువారం వర్క్‌షాప్ జరిగింది. ఆచార్య నాగార్జున యూనివర్సిటీ అసిస్టెంట్ ప్రొఫెసర్ డాక్టర్ జి.గిరిధర్ నానో టెక్నాలజీ గురించి విద్యార్థులకు వివరించారు. జింక్, కాపర్, మెగ్నీషియం పదార్థాలను వినియోగించి నానో పదార్థాల తయారీని ప్రయోగాత్మకంగా విద్యార్థుల చేత చేయించారు. ఈ సందర్భంగా విద్యార్థులు అడిగిన పలు ప్రశ్నలకు ఆయన సమాధానం ఇచ్చారు. విద్యార్థులు వర్క్‌షాప్‌ను సద్వినియోగం చేసుకుని నైపుణ్యాలను మెరుగు పరుచుకోవాలని సూచించారు. ఆర్జేడీ డాక్టర్ వెలగా జోషి మాట్లాడుతూ విద్యార్థులలో నైపుణ్యాలను, సాంకేతికతను పెంపొందించేందుకు తాము వర్క్‌షాప్‌లు ఏర్పాటు చేస్తున్నట్లు తెలిపారు. అనంతరం డాక్టర్ గిరిధర్‌ను ఘనంగా సత్కరించారు. కార్యక్రమాలను వర్క్‌షాప్ కో-ఆర్డినేటర్ డాక్టర్ ఆర్.కామేశ్వరి, విభాగాధిపతి పి.శైలజ, అధ్యాపకులు కె.సుజాత, ఉమాలక్ష్మి, టీవీ రాంబాబు, కె.సాయిబలరామ్, ఎండీ ఇక్బాల్ పాష, రాజశేఖర్ తదితరులు పర్యవేక్షించారు.

సాక్షి Fri, 13 December 2019
https://epaper.sakshi.com/c/46802066

ఈనాడు అమరావతి

శుక్రవారం 13 డిసెంబరు 2019 20 పేజీలు

నానో పదార్థాల తయారీపై కార్యశాల

విద్యార్థులకు అవగాహన కల్పిస్తున్న డాక్టర్ గిరిధర్

మాచవరం, న్యూస్‌టుడే : స్థానిక ఎస్సార్ అండ్ సీవీఆర్ ప్రభుత్వ డిగ్రీ కళాశాల భౌతికశాస్త్రం, ఎలక్ట్రానిక్స్ విభాగాల సంయుక్త ఆధ్వర్యంలో గురువారం నానో సాంకేతిక రంగంలోని నానో పదార్థాల తయారీపై కార్యశాల నిర్వహించారు. ఆచార్య నాగార్జున విశ్వవిద్యాలయం సహాయ ఆచార్యుడు డాక్టర్ జి.గిరిధర్ హాజరై నానో టెక్నాలజీపై అవగాహన కల్పించారు. జింక్, కాపర్ (రాగి), మెగ్నీషియం పదార్థాలను ఉపయోగించి విద్యార్థులతో నానో పదార్థాలను తయారు చేయించారు. డాక్టర్ ఆర్.కామేశ్వరి సమన్వయకర్తగా వ్యవహరించారు. భౌతికశాస్త్ర విభాగాధిపతి పి.శైలజ, డాక్టర్ కె.సుజాత, యు.ఉమాలక్ష్మి, డిగ్రీ, పీజీ విద్యార్థులు పాల్గొన్నారు.